EXPLOITING TRANSMIT CHANNEL SIDE INFORMATION IN MIMO WIRELESS SYSTEMS

A DISSERTATION
SUBMITTED TO THE DEPARTMENT OF ELECTRICAL ENGINEERING
AND THE COMMITTEE ON GRADUATE STUDIES
OF STANFORD UNIVERSITY
IN PARTIAL FULFILLMENT OF THE REQUIREMENTS
FOR THE DEGREE OF
DOCTOR OF PHILOSOPHY

Mai Hong Vu

July 2006

I certify that I have read this dissertation and that, in my opinion, it is fully adequate in scope and quality as a dissertation for the degree of Doctor of Philosophy.

Arogyaswami J. Paulraj (Principal Adviser)

I certify that I have read this dissertation and that, in my opinion, it is fully adequate in scope and quality as a dissertation for the degree of Doctor of Philosophy.

Stephen P. Boyd

I certify that I have read this dissertation and that, in my opinion, it is fully adequate in scope and quality as a dissertation for the degree of Doctor of Philosophy.

John M. Cioffi

Approved for the University Committee on Graduate Studies.

Abstract

Transmit channel side information (CSIT) is information about the channel available to the transmitter. In multiple-input multiple-output (MIMO) wireless, CSIT can significantly improve system performance by increasing the transmission rate and enhancing reliability. The time-varying nature of the wireless channel, however, often results in partial CSIT. Partial information poses challenges to signal design to exploit the CSIT and to performance analysis of the resulting system.

This thesis focuses on exploiting partial CSIT in a single-user MIMO wireless system, assuming perfect channel knowledge at the receiver. The thesis approaches this problem in three steps: building a dynamic CSIT model, deriving the capacity gains with CSIT, and designing optimal precoding schemes to exploit the CSIT. The results are applicable to practical MIMO wireless systems.

Due to inherent delays in CSIT acquisition, CSIT modeling must account for channel temporal variation. A dynamic CSIT model is accordingly constructed, using an initial channel measurement, the delay, and the channel statistics. The CSIT consists of a channel estimate and its error covariance, which function as an effective channel mean and covariance, respectively. Both parameters depend on the channel temporal correlation factor, indicating the CSIT quality. Parameterizing by this factor, dynamic CSIT covers the range from perfect channel estimate at zero delay to the actual channel mean and covariance as the delay grows.

Dynamic CSIT multiplicatively increases the capacity at low signal-to-noise ratios (SNRs) for all multi-input systems. The optimal input signal then is typically simple single-mode beamforming. At high SNRs, dynamic CSIT can additively increase the

capacity for systems with more transmit than receive antennas. The optimal signal can drop modes at high SNRs, depending on the CSIT. Furthermore, a convex optimization program is developed to find the MIMO capacity given a dynamic CSIT. Using this program, a simple, analytical capacity lower-bound, based on the Jensen-optimal input, is shown to be tight in many cases.

Linear precoders can optimally exploit CSIT. A linear precoder functions as a multi-mode beamformer, spatially directing signal and allocating power based on the CSIT. A precoder is designed to exploit a dynamic CSIT in systems employing a space-time block code. The design relies on a dynamic water-filling algorithm, in which both the beam direction and power evolve with each water-filling iteration. The precoder achieves a range of significant SNR gain and is robust to changing CSIT quality. Another precoder is designed for high-K channels, given the CSIT as the channel amplitudes and the channel phase-shift distribution. This CSIT helps simplify the precoder to single-mode beamforming, with per-antenna power allocation dependent on the phase-shift distribution.

Acknowledgments

My PhD study at Stanford University has been a journey of discovery and professional growth. Having arrived where I am today, I owe thanks to many people.

First, I thank my advisor, Professor Arogyaswami J. Paulraj, for his guidance and support throughout the years I worked with him. His engineering insights and technical depth in wireless, together with the critical ability to connect theory to practice, have been a source of inspiration. I am thankful for the opportunity to work with him and for the cultivating time during my PhD.

Thanks to Professors Stephen Boyd for his stimulating classes, and for the masterfully-written and easy-to-understand book on convex optimization. From them, I have learned convex optimization theory and applied it extensively in my research.

Thanks to Professor John Cioffi for the challenging, yet essential, digital communication classes. I am grateful for his taking the time and providing valuable advices on occasions I spoke to him. I am also thankful for his kindly letting me attend his weekly group meetings during the last year, which I enjoyed and learned a lot from.

Thanks to Professor George Papanicolaous for being particularly supportive, and for the stimulating discussions during the time-reversal and smart-antenna groups meetings over the last couple of years. His mathematical insights and curiosity have always been encouraging.

I thank Professor Mark Horowitz for his mentoring and unwavering support during my first few years at Stanford. It had been a privilege working with him.

I enjoyed the intellectual environment Stanford harbors and appreciate the interactions with other students and researchers. To this aspect, I must thank SARG members

for being dynamic colleagues and for creating a stimulating research environment.

During my time at Stanford, I have also had the opportunities to know and interact with many other people, who have enriched and made unique my experience. Thanks especially to the friendly administrative staff who helped make things go smoothly: Kathleen Kimpo, Dennis Murphy, Pat Oshiro, Kelly Yilmaz, and Diane Shankle.

I would like to acknowledge the financial support of the Electrical Engineering Diversity PhD Fellowship, the Rambus Stanford Graduate Fellowship, and the Intel Foundation PhD Fellowship. These fellowships have enabled my PhD education and allowed me the opportunities to explore and define my research areas.

Last but not least, I thank my family for their constant support and encouragements. My journey so far would not have been possible without their love and support.

Contents

List of Figures

Chapter 1

INTRODUCTION

During the last decade, wireless communication has enjoyed tremendous growth in both voice and data appliances. Cell phones and laptops with wireless capability are becoming increasingly common. Not only the voice quality of cell phones has been improving, the data rate of wireless LANs has also reached unprecedented levels of hundreds of megabits per seconds [1, 2], allowing seamless connectivity. New capabilities are being realized, such as providing broadband voice and data on a single unit [3], video broadcasting on cell phones [4], and replacing cables with high-speed wireless connectors [5].

One of the technological enablers of such advances, and a breakthrough in wireless technology, is the use of multiple antennas at both the transmitter and the receiver. Multiple-input multiple-output (MIMO) systems allow a growth in transmission rate linear in the minimum of the numbers of antennas at each end [6]. They also enhance link reliability and improve coverage [7]. MIMO is now entering next generation cellular and wireless LAN products [2, 3, 8], with the promise of widespread adoption in the near future.

While the benefits of MIMO are realizable when the receiver alone knows the communication channel, these are further enhanced when the transmitter also knows the channel. The value of transmit channel knowledge can be significant. For example, in a 4-transmit 2-receive antenna system, transmit channel knowledge can more than double the capacity at -5dB SNR and add 1.5bps/Hz to the capacity at 5dB SNR. Such SNR ranges are common in practical wireless systems. Therefore, exploiting transmit channel

side information (CSIT) in MIMO wireless is of great practical interest.

The random time-varying wireless medium, however, makes it difficult and often expensive to obtain perfect CSIT. In closed-loop methods, CSIT is degraded by the limited feedback resources, associated feedback delays, and scheduling lags, especially for mobile users with a small channel coherence time [9]. In open-loop methods, antenna calibration errors and turn-around time lags again limit CSIT accuracy [10]. Therefore, the transmitter often only has partial channel information. Schemes exploiting partial CSIT thus are both important and necessary.

This thesis focuses on modeling partial CSIT, analyzing capacity benefits of the CSIT, and designing schemes to exploit it. A major challenge in modeling CSIT is capturing the channel time-variation. Due to delays in acquiring channel information, this time-variation directly affects the CSIT quality and results in partial information. Nevertheless, partial CSIT can still increase the channel capacity significantly. The capacity gain from CSIT is subsequently quantified. To realize this gain, a transmit processing technique called precoding, which operates on the signal before transmitting from the antennas, can be used. For many common forms of partial CSIT, a linear precoder is optimal from an information theoretic viewpoint [11, 12, 13]. A linear precoder functions as a multi-mode beamformer, which optimally matches the input signal on one side to the channel on the other side. It decouples the transmit signal into orthogonal spatial eigen-beams and sends higher power along the beams where the channel is strong, but reduced or no power along the weak, thus enhancing system performance.

In this introduction, the benefits of transmit channel side information are first discussed with concrete examples. A review follows on the information-theoretic foundation for exploiting CSIT, establishing the optimality of linear precoders. The function of a linear precoder is then analyzed. These discussions form the foundation on which this thesis is built. The thesis contribution is then concisely described. The last section outlines the focus of each chapter in the thesis.

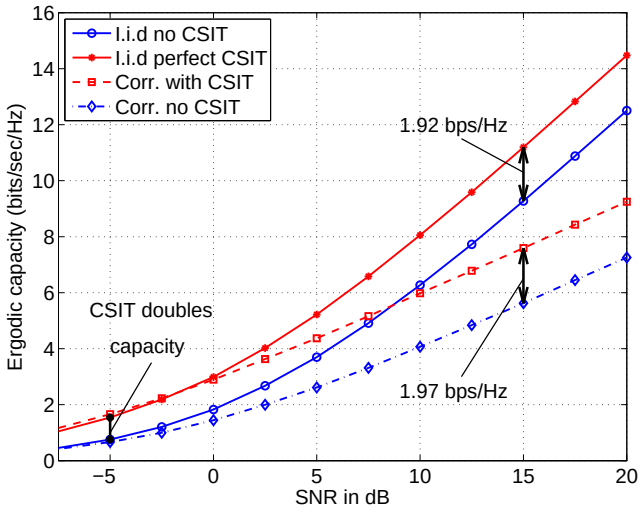

Figure 1.1: Capacity of 4×2 channels with and without CSIT.

1.1 Benefits of transmit channel side information

A wireless channel exhibits time, frequency, and space selective variations, known as fading. This fading arises due to Doppler, delay, and angle spreads in the scattering environment [14, 15, 7]. This thesis focuses on the time-varying channel, assuming frequency flat and negligible angle spread. A frequency-flat solution, however, can be applied per sub-carrier in a frequency-selective channel deploying orthogonal frequency-division modulation (OFDM).

In a frequency-flat MIMO system, channel information can contain two dimensions: temporal and spatial. Temporal CSIT – channel information across multiple time instances – provides negligible capacity gain at medium-to-high SNRs [16]. Spatial CSIT, which is channel information across antennas, on the other hand, offers potentially significant increase in channel capacity at all SNRs. Figure 1.1 provides an example of this capacity increase for two 4×2 channels. For the i.i.d channel, capacities with perfect CSIT and without are plotted. For the correlated channel with rank-one transmit covariance, capacities with the covariance knowledge and without are shown. The capacity gain from CSIT at high SNRs here is significant, reaching almost 2 bps/Hz at 15 dB SNR. At lower SNRs, although the absolute gain is not as high, the relative gain is much more pronounced. For both channels, CSIT helps to double the capacity at -5 dB SNR.

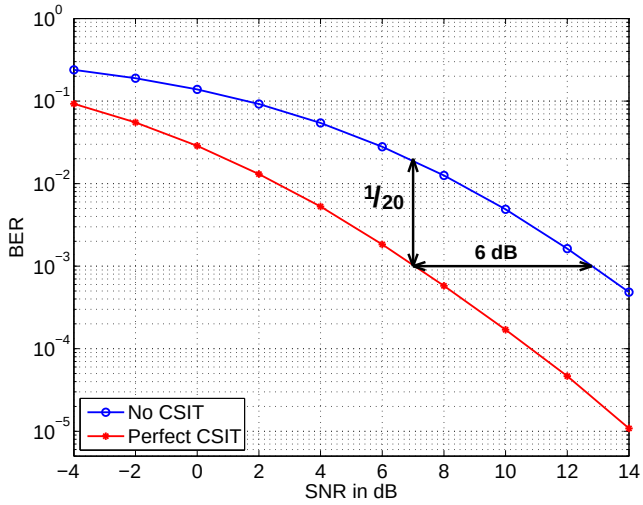

Figure 1.2: Error performance of a 4×1 system with and without CSIT.

Spatial CSIT helps to not only increase capacity but also enhance system reliability and reduce receiver complexity. Reliability can be measured by the system error performance at a fixed transmission rate. By exploiting spatial CSIT, the error rate can significantly decrease at the same SNR. Viewing it another way, the system can achieve the same reliability with less transmit power. Figure 1.2 provides an example of such an SNR gain in a 4×1 system using QPSK. Without CSIT, the system employs an orthogonal space-time block code [17], while with perfect CSIT, it performs beamforming. At 10^{-3} bit error probability, the CSIT provides 6dB gain in SNR, implying reduced transmit power by a factor of 4. Alternatively, at 7dB received SNR, the CSIT helps lower the error probability 20 times. The next section explores the foundation for optimal processing to exploit CSIT.

1.2 Foundation for exploiting CSIT

This section reviews the information theory background for a fading channel with causal side information. The theory can be established by first examining a scalar channel [11]. Consider a frequency-flat time-varying channel $h(s)$ with causal channel-state information U_s at the transmitter and perfect at the receiver, where s denotes the state. Given the current CSIT U_s, the channel $h(s)$ is assumed to be independent of the past $U_1^{s-1} =$

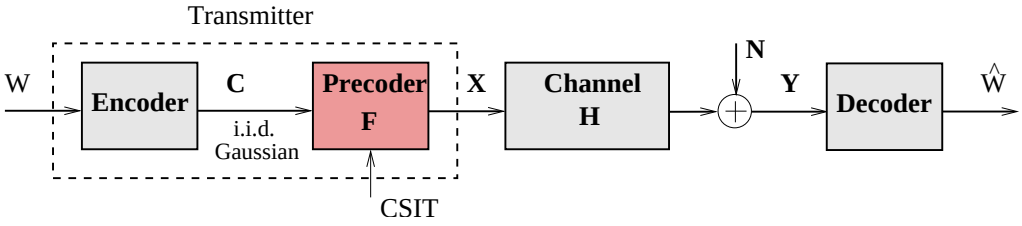

Figure 1.3: An optimal configuration for exploiting CSIT in a MIMO fading channel.

$\{U_1,\, U_2,\, \ldots\, U_{s-1}\}$:

$$\Pr\left(h(s)|U_1^s\right) = \Pr\left(h(s)|U_s\right)\ . \tag{1.1}$$

This condition enables the channel capacity to be a stationary function of the CSIT and not depend on the entire CSIT history. The receiver is assumed to know how the CSIT is used. The channel capacity with an average input power constraint $E[|X_s|^2] \leq P$ is then

$$C = \max_f E\left[\frac{1}{2}\log\Big(1 + hf(U)\Big)\right]\ , \tag{1.2}$$

where the expectation is over the joint distribution of h and U, and $f(U)$ is a power allocation function satisfying the constraint $E[f(U)] \leq P$.

This result implies that it is capacity-optimal to separate channel coding and the CSIT-exploiting function. The capacity of a channel with CSIT can be achieved by a single Gaussian codebook designed for the channel without CSIT, provided that the code-symbol power is dynamically scaled by an appropriate CSIT-dependent function $f(U)$. The combination of this CSIT-dependent function and the channel creates an effective channel, outside of which coding can be applied as if the transmitter had no channel side-information. This insight, in fact, can be traced back to Shannon [12]. For the scalar fading channel, the CSIT-exploiting function is simply dynamic power-allocation.

Subsequently, the result has been extended to the MIMO fading channel [13]. The channel state $\mathbf{H}(s)$ is now a matrix, and the optimal CSIT-exploiting function becomes a weighting matrix – a linear precoder. Specifically, the capacity-optimal input can now be decomposed as

$$\mathbf{X} = \mathbf{F}(U_s)\mathbf{C}\,. \tag{1.3}$$

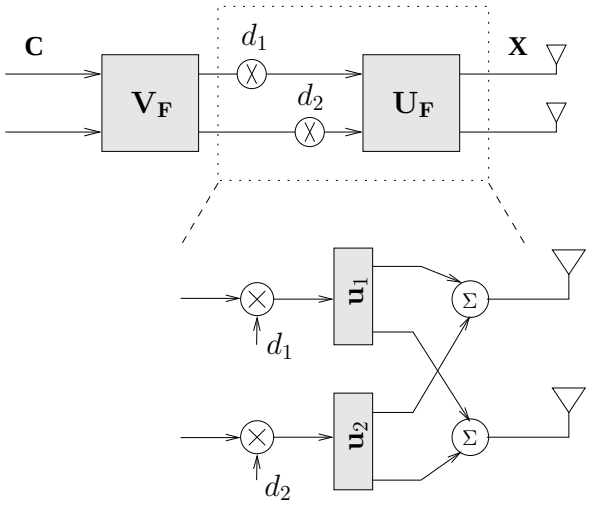

Figure 1.4: A linear precoder as a beamformer.

Here, $\mathbf{C}$ is a codeword optimal for an i.i.d Rayleigh-fading MIMO channel without CSIT, generated from a complex Gaussian distribution with zero-mean and an appropriate covariance $\tilde{P}\mathbf{I}$. The CSIT-exploiting function $\mathbf{F}(U_s)$ is a weighting matrix, which directs signal and allocates power spatially. In other words, the capacity-achieving signal is zero-mean Gaussian-distributed with the covariance $\mathbf{FF}^*$. This optimal input configuration is depicted in Figure 1.3.

These results establish important properties of capacity-optimal signaling for a fading channel with CSIT. First, it is optimal to separate the CSIT-exploiting function and channel coding, the latter designed for the channel without CSIT. Second, a linear precoder is optimal for exploiting CSIT. The separation and linearity properties are the guiding principles for precoder designs in single-user MIMO systems.

1.3 Function of a linear precoder

A linear precoder functions as the combination of an input shaper and a multi-mode beamformer with per-beam power allocation. Consider the singular value decomposition of the precoder matrix

$$\mathbf{F} = \mathbf{U}_F \mathbf{D} \mathbf{V}_F^* \,. \tag{1.4}$$

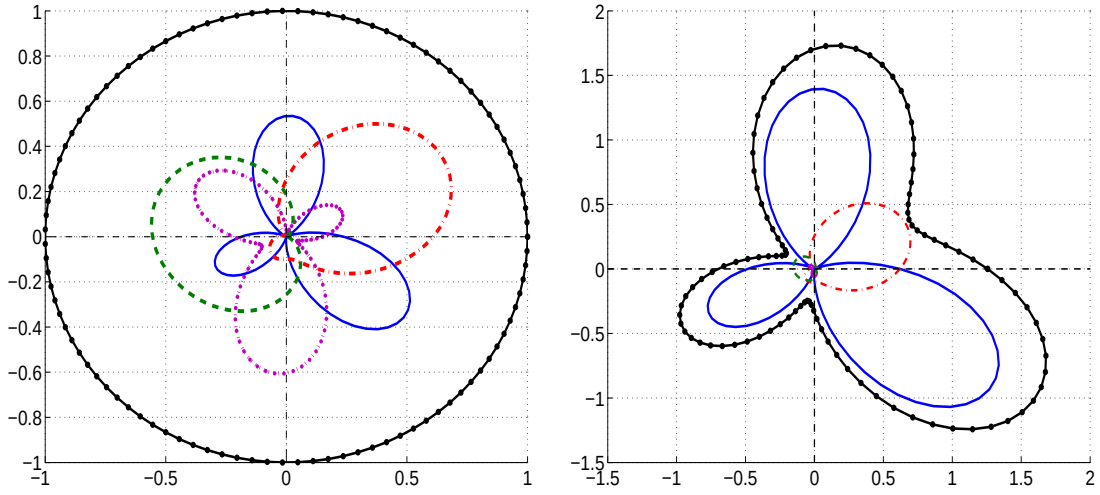

Figure 1.5: Transmit radiation patterns without (a) and with (b) precoding, based on four orthogonal eigen-beams. The outer-most line represents the total radiation pattern, and other lines are the patterns of the four beams.

The orthogonal beam directions (patterns) are the left singular vectors $\mathbf{U}_F$; the beam power-loadings are the squared singular values $\mathbf{D}^2$. The right singular vectors $\mathbf{V}_F$ form the input shaping matrix, combining the input symbols from the encoder to feed into each beam. The structure is shown in Figure 1.4. The beam directions and power-loadings are influenced by the CSIT, the design criterion, and often, the SNR.

To ensure a constant average sum-transmit-power from all antennas, the precoder must satisfy the power constraint

$$\mathrm{tr}(\mathbf{F}\mathbf{F}^*) = 1 \; . \tag{1.5}$$

This condition presumes that the input codeword $\mathbf{C}$ has been normalized for power accordingly.

Essentially, a linear precoder has two effects: decoupling the input signal into orthogonal spatial eigen-beams, and allocating power over these beams, based on the CSIT. If the precoded orthogonal eigen-beams match the channel eigen-directions (the eigenvectors of $\mathbf{H}(s)^*\mathbf{H}(s)$), there will be no interference among signals sent on these beams, creating parallel channels and allowing transmission of independent signal streams. This

effect, however, requires perfect CSIT. With partial CSIT, the precoder performs its best to approximately match its eigen-beams to the channel eigen-directions, reducing the interference among these beams. This is the decoupling effect. Moreover, the precoder allocates power on these beams. For orthogonal eigen-beams, if all the beams have equal power, the radiation pattern of the transmit antenna array is isotropic, as in the example on the left in Figure 1.5. If the beam powers are different, however, the overall transmit radiation pattern will have a specific shape, as shown on the right in Figure 1.5. By allocating power, the precoder effectively creates a radiation pattern matched to the channel, based on the CSIT, so that higher power is sent in the directions where the channel is strong and reduced or no power in the weak. More transmit antennas will increase the transmitter ability to finely shape the radiation pattern and, therefore, are likely to deliver more precoding gain.

1.4 Thesis contribution

This section summarizes the contribution of this thesis. The thesis focuses on studying channel side-information at the transmitter (CSIT), while assuming perfect channel knowledge at the receiver. Its contribution can be divided into 3 parts: characterizing types of channel information and building a dynamic CSIT model; optimizing for the capacity and deriving the capacity gain and optimal input with the CSIT; and designing optimal precoding schemes to realize the gain.

1.4.1 Dynamic CSIT modeling

A major challenge in wireless communication is the time-variation of the channel. This time-variation creates difficulty in obtaining channel information, which is required for best performance. While the channel can be measured directly at the receiver with sufficient accuracy, the transmitter must obtain channel information indirectly, using either reciprocity or feedback. In a time-varying channel, the delay involved in such a process can degrade the information accuracy.

The first contribution is characterizing channel information and constructing a dynamic CSIT model, taking into account channel time-variation. The model relies on stochastic processes and estimation theories. Derived from a potentially outdated channel measurement and the channel statistics, this dynamic CSIT consists of a channel estimate and its error covariance, acting as the effective channel mean and covariance. Both parameters depend on a temporal correlation factor, indicating the CSIT quality. Depending on this quality, the model covers smoothly from perfect to statistical channel information [18, 19]. Dynamic CSIT is applicable to all Gaussian random channels.

In characterizing channel information, the thesis also considers another CSIT model for a channel with high K factor. The K factor measures the ratio of power in the fixed and the random parts of the channel. For this high-K model, the channel amplitude is known perfectly at the transmitter, but the phase is known only in distribution. This model is fundamentally different from dynamic CSIT and can be applied, for example, to channels with a direct line-of-sight between the transmitter and the receiver.

1.4.2 Channel capacity and optimal input with CSIT

The second contribution consists of two parts: asymptotic analyses of the capacity gains and the optimal input given dynamic CSIT, and a numerical convex optimization program to find the capacity. Using function analysis and random matrix theory, the analyses in the first part show that dynamic CSIT often multiplicatively increases the capacity at low SNRs for all MIMO systems. It can additively increase the capacity at high SNRs for systems with more transmit than receive antennas [20, 21]. The optimal input also depends on the SNR. At low SNRs, it typically becomes single-mode beamforming on the dominant eigen-mode of the channel correlation matrix. At high SNRs, the optimal input differs across antenna configurations. For systems with equal or fewer transmit than receive antennas, it approaches equi-power. With more transmit than receive antennas, however, the optimal input is highly dependent on the CSIT and can drop modes for channels with a strong mean or strongly correlated transmit antennas [20].

In the second part, optimizing for the channel capacity given a CSIT is a stochastic convex problem. While convexity allows efficient implementations, the stochastic nature

complicates the problem. Efficient techniques to calculate the gradient, Hessian, and function values required for the optimization are specified [22]. The program is then used to study MIMO capacity with dynamic CSIT and to evaluate a simple capacity lower-bound, derived using the Jensen-optimal input. The bound is tight at all SNRs for systems with equal or fewer transmit than receive antennas, and at low SNRs for others.

1.4.3 Precoding designs exploiting CSIT

The third contribution involves designing linear precoders to exploit CSIT, using convex analysis and matrix algebra. The thesis proposes analytical precoder designs for two CSIT models. The first design exploits dynamic CSIT in the form of a known channel mean and a known transmit covariance. Design criteria are characterized based on fundamental and practical measures. For the fundamental measure, the precoder aims to maximize the capacity of a system with a given input code. The design is then generalized for other criteria with stochastic objective functions [19]. For the practical measure, a precoder operates in a system with a space-time block code and aims to minimize the pair-wise codeword error probability [23]. This precoder is designed using a dynamic water-filling algorithm, in which both the precoding beam directions and power allocation evolve with water-filling iterations. Depending on the CSIT quality, these precoders achieve a range of significant and robust SNR gains [18, 19].

Another design is for a channel with CSIT as the channel amplitude and the phase distribution. This CSIT typically applies to a channel with high K-factor. A channel with 2 transmit and 1 receive antenna is studied specifically. The capacity-optimal transmission scheme is simple single-mode beamforming on the mean of the channel phase-shift, with variable antenna power allocation, depending on the phase knowledge [24]. When the phase is perfectly known, the scheme converges to maximum-ratio-combining transmit beamforming. When the phase is completely unknown, the scheme reduces to single antenna transmission.

1.5 Thesis outline

This thesis consists of 4 main chapters. These chapters follow the contributions outlined above, with the third contribution discussed in two chapters. A brief outline of each chapter is as follows.

Chapter 2 discusses the wireless channel characteristics and modeling, MIMO parameters, and techniques for acquiring channel information at the transmitter. It then establishes models of transmit channel side-information, including dynamic CSIT and a variable-phase model for high-K channels.

Chapter 3 focuses on the channel capacity with dynamic CSIT. The chapter first analyzes asymptotic capacity gains from dynamic CSIT and the optimal input at low and high SNRs. Results are established separately for systems with more transmit than receive antennas, and with fewer or equal. The chapter then establishes a convex optimization program to find the channel capacity. This program is used to study effects on the capacity of antenna configurations, the CSIT quality, and the K factor, and to assess a simple, analytical capacity lower-bound.

Chapter 4 proposes precoding designs to exploit dynamic CSIT. Two design criteria are studied: the pair-wise error probability (PEP) and the system capacity. The chapter establishes a PEP-optimal precoder for a system with a space-time block code, distinguishing between orthogonal and non-orthogonal codes. This precoder is then analyzed in terms of the precoding gain, asymptotic behaviors, and special cases. The chapter also briefly discusses other precoding designs based on the system capacity and generalizes for stochastic objective functions involving an expectation without a closed-form. Comparative precoding performance are discussed.

Chapter 5 examines the capacity-optimal transmission scheme with high-K variable-phase CSIT in a 2×1 system. The optimal scheme is simple beamforming, which is established in terms of the signal phase and amplitude separately. The chapter then discusses benefits of this CSIT, including the capacity gain and the simple transmission scheme.

The last chapter, **Chapter 6**, provides the conclusion. This chapter summarizes the main results of the thesis, discusses the deployment of precoding in emerging wireless standards, and outlines future research directions.

Chapter 2

TRANSMIT CHANNEL SIDE INFORMATION MODELS

The wireless channel is a multipath time-varying channel. The multiple paths arise from signals reflecting off multiple random scatterers in the propagation environment. These paths combine sometimes constructively and sometimes destructively, creating a channel with multi-tap impulse response, in which each tap has a random phase and a time-varying amplitude. The wireless channel is therefore often characterized statistically. The channel amplitude fluctuation is called fading, which occurs in both the time and frequency domains. This chapter first establishes a model for the multipath fading channel, then focuses on the frequency-flat case with single response tap.

Multiple antennas bring an additional spatial dimension. Each tap in the MIMO channel is often represented as a matrix, containing multiple elements from the pairs of transmit and receive antennas. These spatial elements can have different statistical parameters. Their statistics characterize antenna correlation, channel mean, and spatial-temporal auto-correlations. Spatial channel information, either instantaneous or statistical, can bring significant improvement in system performance, such as increasing the transmission rate and enhancing reliability.

Due to random fading, acquiring wireless channel information can be difficult. Channel acquisition at the receiver is usually aided by embedded pilots and therefore produces

accurate information. Acquisition at the transmitter, however, has to rely on channel measurements at a receiver, based on reciprocity or feedback. Both methods induce a delay, causing potential loss in information accuracy. Assuming perfect channel knowledge at the receiver, the chapter discusses transmit channel acquisition and characterizes types of channel side information at the transmitter (CSIT).

This chapter introduces two spatial CSIT models. Dynamic CSIT includes a channel estimate with known error covariance, based on an initial channel measurement and the channel temporal and spatial statistics. This model applies to Gaussian random channels, including both Rayleigh and Rician fading, and covers smoothly from statistical to perfect channel knowledge. High-K variable-phase CSIT includes the channel amplitude and the distribution of the channel phase-shift, applied specifically to 2×1 channels, typically with a line-of-sight propagation path. These two models form the foundation for signal design and system analysis in the subsequent chapters.

The chapter is organized as follows. The next section discusses the multipath fading channel characteristics and establishes statistical channel models. Section 2.2 examines the spatial dimension in MIMO and corresponding channel parameters. Transmit channel acquisition principles and techniques are discussed in Section 2.3. The last two sections present the two CSIT models, dynamic and high-K variable-phase, respectively.

2.1 The wireless channel

A wireless channel is created by wave propagation through multiple paths, arisen from scattering, reflection, refraction, or diffraction of the radiated energy off objects in the environment. The channel is often characterized on two different scales: large and small. Large scale propagation captures path loss and shadowing, which result from signal attenuation with distance and random blockage by large objects, such as hills and buildings. Small scale propagation captures the variation arising from signals of random multiple paths adding constructively and destructively. Such random variations create fading: signal strength fluctuation over all time, frequency, and space dimensions. Signal processing for wireless communication usually exploits the small scale channel variation, also called

multipath fading. Hence, this section focuses on the small-scale channel characteristics and models, leaving the large-scale characteristics to references such as [15].

2.1.1 Multipath fading channel characteristics

Multipath fading arises from the sometimes constructive and sometimes destructive addition of signals arriving from multiple paths. Such fluctuation is caused by the random scatterers in the wireless environment; it is intensified in mobile communications with moving transmitter or receiver (or both). This section constructs the multipath fading-channel impulse-response and studies its characteristics. These will form the basis for establishing channel models in the next section.

The channel impulse response

When an ideal impulse is transmitted over a multipath fading channel, there will be two effects on the received signal. First, since different signal paths may have different lengths and attenuation factors, the received signal may appear as a train of pulses with different delays and magnitudes. Second, due to the random nature of the wireless channel, the multipath is varying with time. Thus the number of arrived pulses, the delay between them, and their magnitudes may vary each time sending the impulse. The impulse response of the channel captures both of these effects, and is constructed as follows [25].

Consider transmitting a modulated signal, generally represented as

$$q(t) = Re\big[x(t)e^{j2\pi f_c t}\big] \tag{2.1}$$

where t is the continuous time, f_c is the carrier frequency, and $x(t)$ is the lowpass information-carrying signal. Assuming that there are multiple propagation paths indexed by k, each with a propagation delay $\tau_k(t)$ and an attenuation factor $\alpha_k(t)$, which are both time-varying, the received bandpass signal without noise may be expressed as

$$r(t) = \sum_{k=1}^{K} \alpha_k(t) q\big(t - \tau_k(t)\big) \tag{2.2}$$

where K is the total number of paths. Substituting $x(t)$ in (2.1) yields

$$r(t) = Re\Big\{ \Big[\sum_{k=1}^{K} \alpha_k(t) e^{-j2\pi f_c \tau_k(t)} x\big(t - \tau_k(t)\big)\Big] e^{j2\pi f_c t} \Big\} .$$

The equivalent lowpass received signal therefore is

$$y(t) = \sum_{k=1}^{K} \alpha_k(t) e^{-j2\pi f_c \tau_k(t)} x\big(t - \tau_k(t)\big) .$$

The equivalent lowpass channel can then be described by the time-varying impulse response [25]

$$h(\tau, t) = \sum_{k=1}^{K} \alpha_k(t) e^{-j2\pi f_c \tau_k(t)} \delta\big(t - \tau_k(t)\big) = \sum_{k=1}^{K} \alpha_k(t) e^{\theta_k(t)} \delta\big(t - \tau_k(t)\big) \qquad (2.3)$$

where $\theta_k(t) = -2\pi f_c \tau_k(t)$ is a time-varying phase sequence.

The impulse response $h(\tau, t)$ represents the response of the channel at time t caused by an impulse applied at time $t - \tau$. The channel is completely characterized by the number of multipath components K and the path variables: amplitude $a_k(t)$, delay $\tau_k(t)$, and phase $\theta_k(t)$. These parameters change unpredictably with time and are often described statistically. The received signal $r(t)$ therefore is also random, and when there are a large number of paths, the central limit theorem applies. This means $r(t)$ may be modeled as a complex-valued Gaussian random process. Thus the channel impulse response $h(\tau, t)$ is a complex-valued Gaussian random process in the t variable. The statistical models are described in more detail in the next section.

Large dynamic changes in the transmitting medium are required for the amplitude $\alpha_k(t)$ to change sufficiently to cause a significant change in the received signal. On the other hand, the phase $\theta_k(t)$ will change by 2π radians whenever the delay $\tau_k(t)$ (or in effect the path length) is changed by $1/f_c$, which is a small amount due to large carrier frequency. Therefore $\theta_k(t)$ can change quite rapidly with relatively small motions of the medium. This time variation of the phases $\{\theta_k(t)\}$ is the primary cause of fading phenomena in a multipath channel. The randomly time-varying phases $\{\theta_k(t)\}$ associated with the vectors

$\{\alpha_k(t)e^{\theta_k(t)}\}$ at times result in the received vectors adding constructively or destructively. This adding causes amplitude variation in the received signal, termed *signal fading*.

Discrete-time channel model

For digital signal processing, the signal is processed in the sampled domain, hence it is convenient and necessary to represent the channel in discrete-time for analysis. The Nyquist sampling frequency at twice the maximum signal bandwidth allows perfect reconstruction of the continuous signal from its samples. In wireless communications, the received signal sometimes needs to be sampled at a slightly higher frequency than Nyquist because of possible bandwidth expansion through the channel. This work will assume that an appropriate sampling frequency has been chosen. A single time-sample of the channel response at a specific delay is called a channel tap. Depending on the sampling resolution, the number of distinguishable channel taps L is often smaller than the number of multipaths ($L \leq K$). From (2.3), a discretized channel can be obtained as $h[n;k]$, representing the channel response at the discrete time n caused by a unit sampled input at time $n-k$:

$$h[n;k] = \sum_{k=1}^{L} a_k[n]e^{\theta_k[n]}\delta\big[n-k\big] = \sum_{k=1}^{L} h_k[n]\delta\big[n-k\big] \ , \tag{2.4}$$

where $h_k[n] = a_k[n]e^{\theta_k[n]}$ is the k^{th} channel response tap, in which $a_k[n]$ and $\theta_k[n]$ are the composite tap amplitude and phase respectively.

Temporal selectivity

A wireless channel can be selective, characterized by a varying channel response, in both the time and frequency domains. The impulse response (2.4) can be used to describe the channel in these domains. The time dimension n relates to the channel temporal selectivity, while the delay dimension k captures the spectral selectivity.

Figure 2.1 provides an example of channel temporal selectivity for two scalar wireless links between two distinct pairs of transmit and receive antennas. Not only these channel amplitudes fluctuate over time, they can do so independently, given sufficient antenna spacing.

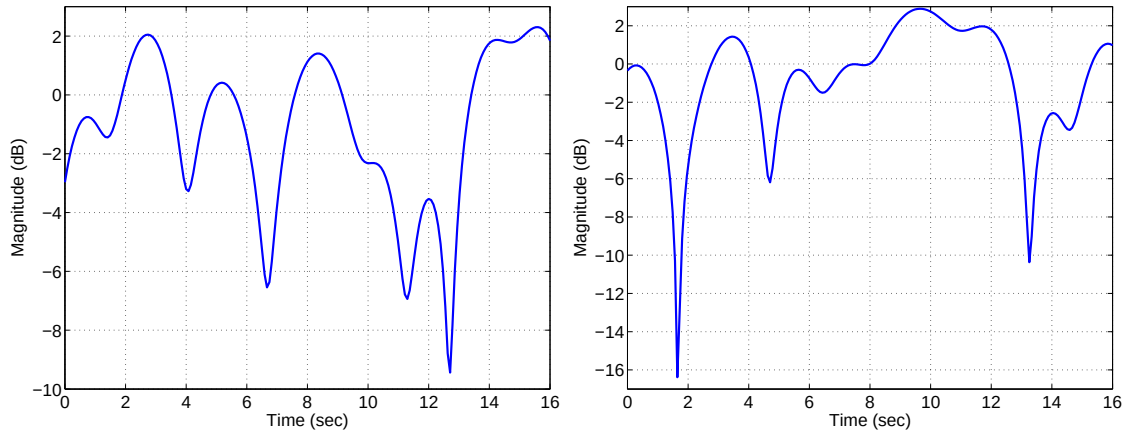

Figure 2.1: Amplitude of the temporal channel response of two different scalar wireless links.

Temporal selectivity is caused by motion of the transmitter, the receiver, or the scatterers in the channel. These motions cause a transmitted single tone to be spread in frequency at the receiver. This effect can be captured in the power spectrum of the channel taps. To simplify the derivation, assume the taps are stationary and statistically independent. The temporal auto-correlation of the k^{th} tap can then be obtained as

$$\rho_k[m] = E\big[h_k[n]h_k[n+m]^*\big] \ , \tag{2.5}$$

which depends only on the time difference m but not the absolute time (here $(.)^*$ denotes complex conjugation). The tap power spectral response is the Fourier transform of this auto-correlation

$$S_k(f) = \sum_m \rho_k[m]e^{-j2\pi fm} \ .$$

The frequency range over which $S_k(f)$ is non-zero indicates the Doppler spread of tap k. The maximum frequency spread among all taps is the channel Doppler spread f_d. The temporal auto-correlation function (2.5), which specifies how fast the channel decorrelates with time, in turn can be expressed in terms of the time interval and the Doppler spread. A popular model for all taps is Clark's spectrum (popularized by Jake [14]), which assumes uniformly distributed scatterers on a circle around the antenna,

$$\rho[m] = J_0(2\pi f_d m\Delta_t) \ , \tag{2.6}$$

where J_0 is the zero$^{\text{th}}$ order Bessel function of the first kind, and Δ_t is the sampling interval. For other propagation environments, the temporal auto-correlation is often obtained empirically.

Higher mobility in a system commonly causes larger Doppler spread and faster channel time variation. In other words, larger Doppler is associated with higher temporal selectivity. A measure of the temporal selectivity is the channel coherence time, defined as the time interval over which the channel remains strongly correlated. The shorter the coherence time, the faster the channel changes with time. Since the coherence time is a statistically defined quantity, an approximate relation to the Doppler is

$$T_c = \frac{1}{f_d} \, . \tag{2.7}$$

In some texts, there exists a constant such as 2, 4, or 8 in front of f_d in this relation; but there no single agreed-number. The important property is the inverse-proportionality between T_c and f_d.

Spectral selectivity

Spectral selectivity, on the other hand, is caused by the presence of multipath, or multiple channel taps indexed by k. It can be captured in the channel frequency response, by taking the Fourier transform of the channel taps as

$$H_k(f) = \sum_n h_k[n] e^{-j2\pi f n} \, .$$

The channel frequency response is the sum of the phase-shifted response of each tap

$$H(f) = \sum_k H_k(f) e^{j2\pi f k} \, . \tag{2.8}$$

Because of these frequency-dependent phase shifts, this sum varies with frequency, causing selectivity. The more taps or equivalently longer multipath delays, the more frequency selective the channel becomes. An indicator of this selectivity is the delay spread, defined

as the range of multipath spread in the channel

$$T_m = \tau_{\max} - \tau_{\min} \ , \tag{2.9}$$

where $\tau_{\max}$ and $\tau_{\min}$ are the maximum and minimum multipath delays, respectively. The channel coherence bandwidth B_c is accordingly defined as

$$B_c = \frac{1}{T_m} \ . \tag{2.10}$$

B_c indicates approximately the frequency separation at which the channel behaves independently. In other words, two transmitted single tones separated by the channel coherence bandwidth or more will be affected by the channel in significantly different ways.

2.1.2 Statistical channel models

Because of the often unpredictable time-varying nature of a wireless channel, the channel is modeled as a random process. The channel at a single time instance therefore is a random variable. Consider a single channel tap $h_k[n]$ of the channel at time n from (2.4), this tap is contributed by a number of multipaths as

$$h_k[n] = a_k[n]e^{j\theta_k[n]} = \sum_{i=1}^{L_k} \alpha_i[n]e^{j\theta_i[n]} \ ,$$

where $\alpha_i[n]$ and $\theta_i[n]$ are the amplitude and phase of path i respectively, and L_k is the total number of contributing paths. The phases of these paths vary rapidly with time and are often modeled as independent uniform random variables in $[0,\ 2\pi]$. The sum of such random-phase components, in which no path has the magnitude dominant compared with all others, can be well approximated as a Gaussian random variable with zero mean [26]. The Gaussian statistics of $h_k[n]$ can also be inferred from applying the central limit theorem to this summation of multiple and statistically similar paths.

Often, the complex channel tap is expressed in terms of its real and imaginary parts

$$h_k[n] = h_{kR}[n] + jh_{kI}[n] \ , \tag{2.11}$$

where both parts are Gaussian random variables with zero mean and equal variance. The channel variance represents the average power gain in the channel. It can be shown then, that the tap amplitude $a_k[n]$ has the Rayleigh distribution and the phase uniform in $[0,\ 2\pi]$ (see [27]). The Rayleigh distribution has been verified empirically to be a good fit for many channels, especially when there are many scatterers in the environment and no direct line-of-sight between the transmitter and the receiver. It also models well the fast fading channel components.

When there is a direct line-of-sight or a cluster of strong paths, the channel may have a non-zero mean (a DC component). The channel then is often modeled as having Rician statistics. The Rician distribution arises from the phase of a constant phasor perturbed by additive, random zero-mean complex Gaussian noise with equal variance on the real and imaginary parts [28]. The channel line-of-sight in this case acts as the constant phasor while the other multipaths contribute to the zero-mean Gaussian part. In a multi-tap channel, the line-of-sight usually affects only one tap. The real and imaginary parts of that tap (2.11) are now non-zero mean Gaussian random variables; their variances are equal but the means need not be. Other channel taps are still zero-mean.

There are yet other statistical models for wireless channels, such as Nakagami, Suzuki, Weibull [26], in addition to empirical models. While these models may be more accurate for some channels, they are also more complicated to work with because of a larger number of parameters. Since the Rayleigh and Rician models can well represent a majority of channels to sufficient detail, subsequent analyses will mainly use these models.

The variance of a zero-mean channel tap represents its power gain. The power gain of a multi-tap channel is captured in the power-delay profile. A common model for this profile is the exponential model, in which the tap power follows an exponential function with the exponent as the negative of the tap delay

$$E\left[|h_k[n]|^2\right] = p_0 e^{-jk\tau_0} \ ,$$

where p_0 and τ_0 are constants. For analysis, the power gain of a scalar channel between a single transmit and a single receive antennas is often normalized to 1, counting all taps. For a frequency-flat channel with single time-response tap, that tap is normalized to have a unit variance.

Another parameter is the distribution of the path delay sequence, which has been modeled less extensively. Existing models include Poison distribution, Gilbert's burst noise, and a pseudo-Markov model [26]. The analysis in this thesis, however, will focus solely on the frequency-flat channel; hence this parameter has no affect and will be omitted.

2.2 MIMO channel parameters

The MIMO wireless channel is created by using multiple antennas at both the transmitter and the receiver. It generalizes the special cases of having a single antenna at only one side: multiple input single output (MISO), and single input multiple output (SIMO). In addition to spanning the temporal and spectral dimensions, a MIMO channel exhibits a new spatial dimension across the antennas. The channel contains multiple elements among the antennas and is often represented in a matrix form. These elements can correlate and can have different mean (line-of-sight) values. Their composite temporal and spectral responses are also more complex than the scalar case.

2.2.1 The spatial dimension

For simplicity, let's first examine the frequency-flat MIMO channel. The channel has only a single tap. This tap, however, contains multiple elements between all pairs of transmit-receive antennas. In a system with N transmit and M receive antennas, the channel can be represented as a matrix $\mathbf{H}$ of size $M \times N$

$$\mathbf{H} = \begin{bmatrix} h_{11} & h_{12} & \cdots & h_{1N} \\ h_{21} & h_{22} & \cdots & h_{2N} \\ \vdots & & & \\ h_{M1} & h_{M2} & \cdots & h_{MN} \end{bmatrix}, \tag{2.12}$$

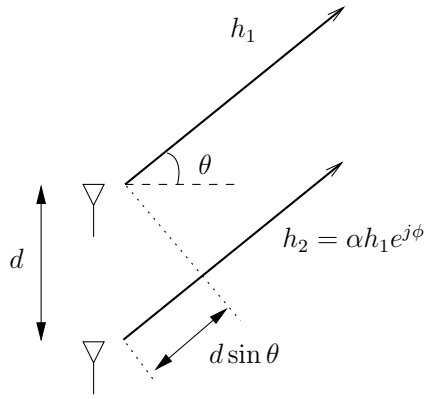

Figure 2.2: Single-path spatial propagation model.

in which h_{ij} is the scalar channel from transmit antenna j to receive antenna i. For brevity, the time-dependent index $[n]$ has been omitted.

Each channel element h_{ij} can have different amplitude and phase, caused by spatial selectivity. The channels at the same time, same frequency but at different locations can experience different fading. To understand the underlying spatial effect, consider a signal arriving at a two-antenna array from a single direction. The corresponding channel, depicted in Figure 2.2, contains two propagation paths to the two antennas, h_1 and h_2, which differ by a gain ratio α and a phase shift ϕ as

$$h_2 = \alpha e^{j\phi} h_1 \ . \tag{2.13}$$

The difference in antenna gains (when $\alpha \neq 1$) is caused by the antenna array structure and the local scattering from the mounting structure (walls, rooftops) near the antennas. Although dependent on the angle of signal arrival, α is much less sensitive to its changes than is the phase shift ϕ. The phase shift results from the difference in distances that the wave propagates to the antennas. It depends on the angle of arrival θ, the distance d between the two antennas, and the carrier frequency f_c, or the wavelength λ_c equivalently, as

$$\phi = 2\pi \frac{d}{\lambda_c} \sin\theta \ . \tag{2.14}$$

Depending on the antenna distance relative to the wavelength, this phase shift can be highly variable in response to a small change in the angle of arrival θ. For example,

at a distance of tens of the wavelength, if θ is uniformly distributed in $[-\pi/3, \pi/3]$, the distribution of ϕ looks almost uniform in $[-\pi, \pi]$. A similar single-path model applies to multiple transmit-antenna channels, in which θ is the angle of departure. A typical MIMO channel has multiple propagation paths from multiple directions. The multipath makes the phase shifts between the channel elements even more sensitive to changes in the angles of arrival or departure, causing the spatial selectivity in the channel.

A frequency-selective MIMO channel contains multiple matrix taps at different delays. Elements of different taps are often assumed to be independent. The tap-delay scalar channel between every transmit-receive antenna pair can have the same power-delay profile, except any difference in the non-zero-mean tap of a Rician channel.

Similar to a scalar channel, each element h_{ij} in a MIMO channel can be modeled as a complex Gaussian random process. These elements, however, can correlate and have different means. Decompose the channel (2.12) into a fixed part and a variable part as

$$\mathbf{H} = \mathbf{H}_m + \tilde{\mathbf{H}}\,, \tag{2.15}$$

where $\mathbf{H}_m$ is the complex channel mean, and $\tilde{\mathbf{H}}$ is a zero-mean complex Gaussian random matrix.

2.2.2 Channel covariance and antenna correlations

The channel covariance captures the spatial correlation among all the transmit and receive antennas. It is defined among all MN channel elements as a $MN \times MN$ matrix

$$\mathbf{R}_0 = E\left[\tilde{\mathbf{h}}\tilde{\mathbf{h}}^*\right]\,, \tag{2.16}$$

where $\tilde{\mathbf{h}} = \text{vec}\left(\tilde{\mathbf{H}}\right)$, and $(.)^*$ denotes a conjugate transpose. $\mathbf{R}_0$ is a positive semi-definite Hermitian matrix. Its diagonal elements represent the power gain of the MN scalar channels, and the off-diagonal elements are the cross-coupling between these scalar channels.

The covariance $\mathbf{R}_0$ is often assumed to have a simplified, separable Kronecker structure [29]. The Kronecker model assumes that the covariance of the scalar channels seen from

all N transmit antennas to a single receive antenna (corresponding to a row of $\mathbf{H}$) is the same for any receive antenna (any row) and equals to $\mathbf{R}_t$ ($N \times N$). Let $\breve{\mathbf{h}}_i^T$ be row i of $\tilde{\mathbf{H}}$, then

$$\mathbf{R}_t = E\left[\breve{\mathbf{h}}_i \breve{\mathbf{h}}_i^*\right]$$

for any i. Similarly, the covariance of the scalar channels seen from a single transmit antenna to all M receive antennas (corresponding to a column of $\mathbf{H}$) is assumed to be the same for any transmit antenna (any column) and equals to $\mathbf{R}_r$ ($M \times M$). That is, let $\tilde{\mathbf{h}}_j$ be column j of $\tilde{\mathbf{H}}$, then

$$\mathbf{R}_r = E\left[\tilde{\mathbf{h}}_j \tilde{\mathbf{h}}_j^*\right]$$

for any j. Both covariance matrices $\mathbf{R}_t$ and $\mathbf{R}_r$ are complex Hermitian positive semi-definite. The channel covariance can now be decomposed as

$$\mathbf{R}_0 = \mathbf{R}_t^T \otimes \mathbf{R}_r \,, \tag{2.17}$$

where $\otimes$ denotes the Kronecker product [30]. The channel (2.15) can then be written as

$$\mathbf{H} = \mathbf{H}_m + \mathbf{R}_r^{1/2} \mathbf{H}_w \mathbf{R}_t^{1/2} \,, \tag{2.18}$$

where $\mathbf{H}_w$ is a $M \times N$ matrix with zero-mean unit-variance i.i.d complex Gaussian entries. Here $\mathbf{R}_t^{1/2}$ is the unique square-root of $\mathbf{R}_t$, such that $\mathbf{R}_t^{1/2}\mathbf{R}_t^{1/2} = \mathbf{R}_t$; similarly for $\mathbf{R}_r^{1/2}$.

The Kronecker correlation model has been experimentally verified in indoor environments for up to 3×3 antenna configurations [31, 32], and in outdoor environments for up to 8×8 configurations [33]. Other more general covariance structures have been proposed in the literature [34, 35], in which the transmit covariances ($\mathbf{R}_t$) corresponding to different reference receive antennas are assumed to have the same eigenvectors, but not necessarily the same eigenvalues; similarly for $\mathbf{R}_r$.

2.2.3 Channel mean and the Rician K factor

The channel mean is the fixed component of the channel, usually corresponding to a line-of-sight propagation path or a cluster of strong paths. The mean of a MIMO channel is

a complex matrix $\mathbf{H}_m$ of size $M \times N$ obtained as

$$\mathbf{H}_m = E[\mathbf{H}] \ . \tag{2.19}$$

The elements of the mean can have different amplitudes and arbitrary phase, caused by the spatial effect analyzed in Section 2.2.1. The strength of a channel mean can be loosely quantified by the Rician K factor. It is defined as the ratio of the power in the channel mean and the average power in the channel variable component as

$$K = \frac{||\mathbf{H}_m||_F^2}{\mathrm{tr}(\mathbf{R}_0)} \ , \tag{2.20}$$

where $||.||_F$ is the matrix Frobenius norm, and tr(.) is the trace of a matrix. The K factor can take any real value between 0 and infinity. When $K = 0$, the channel has the Rayleigh distribution. When $K \to \infty$, the channel becomes deterministic. Measurements of fixed broadband channels have shown that the K factor can have a wide range from 0 to up-to 30dB in practice, and it tends to decrease with increasing distance between the transmitter and the receiver [36].

2.2.4 Channel auto-covariance and the Doppler spread

The channel auto-covariance characterizes how rapidly the channel decorrelates with time. Assuming stationarity, the covariance between two channels samples $\mathbf{H}[n]$ and $\mathbf{H}[n+m]$ (2.15) depends only on the time difference but not the absolute time

$$\mathbf{R}[m] = E\left[\tilde{\mathbf{h}}[n]\tilde{\mathbf{h}}[n+m]^*\right] \ , \tag{2.21}$$

where $\tilde{\mathbf{h}}$ denotes the vectorized version of the corresponding zero-mean part of the channel matrix. When $m = 0$, this auto-covariance coincides with the channel covariance $\mathbf{R}_0$ (2.16); when m becomes large, it eventually decays to zero.

For a MIMO channel, the covariance $\mathbf{R}_0$ captures the spatial correlation among all the transmit and receive antennas, while the auto-covariance at a non-zero delay $\mathbf{R}[m]$ captures both channel spatial and temporal correlations. Based on the premise that the

channel temporal statistics can be the same for all antenna pairs, it may be assumed that the temporal correlation is homogeneous and identical for any channel element. Then, the two correlation effects are separable, and the channel auto-covariance becomes their product as

$$\mathbf{R}[m] = \rho[m]\mathbf{R}_0 \ , \tag{2.22}$$

where $\rho[m]$ is the temporal correlation of a scalar channel (2.5). In other words, all the MN scalar channels between the M transmit and N receive antennas have the same temporal correlation function. This temporal correlation is a function of the time difference m and the channel Doppler spread. Similar assumptions for MIMO temporal correlation have also been used in constructing channel models and verifying measurement data in [32, 35].

2.3 Transmit channel acquisition

In a communication system, the signal enters the channel after leaving the transmitter. Therefore, a transmitter can only acquire channel information indirectly, based on the information at a receiver. The receiver can estimate the channel directly from the channel-modified received-signal, usually based on embedded pilots. The transmitter can then obtain the information in two ways, based on the reciprocity principle and by using feedback.

2.3.1 Reciprocity-based methods

The reciprocity principle in wireless states that the forward channel from an antenna A to another antenna B is identical to the transpose of the reverse channel from B to A. Reciprocity requires the forward and reverse channels to be at the same frequency, the same time, and the same antenna locations. In a full-duplex system, this principle suggests that the transmitter (at A) can obtain the forward channel (A to B) from the reverse channel (B to A), which the receiver (at A) can measure, as illustrated in Figure 2.3.

In real full-duplex communications, however, the forward and reverse links cannot use

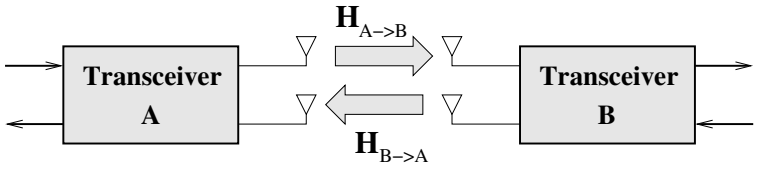

Figure 2.3: Obtaining CSIT using reciprocity.

all identical frequency, time, and space instances. The reciprocity principle may still hold approximately if the difference in any of these dimensions is relatively small, compared to the channel variation across the referenced dimension. In the temporal dimension, this condition implies that any time lag Δ_t between the forward and reverse transmissions must be much smaller than the channel coherence time T_c:

$$\Delta_t \ll T_c \, .$$

Similarly, any frequency offset Δ_f must be much smaller than the channel coherence bandwidth B_c ($\Delta_f \ll B_c$), and the antenna location differences on the two links must be much smaller than the channel coherence distance D_c [7].

Practical channel acquisition based on reciprocity may be applicable in time-division-duplex (TDD) systems. While TDD systems often have identical forward and reverse frequency bands and antennas, there is a turn-around delay between the forward and reverse links. Such delay must be negligible compared to the channel coherence time. In a frequency-division-duplex (FDD) system, the temporal and spatial dimensions may be identical, but the frequency offset between the forward and reverse links is usually much larger than the channel coherence bandwidth, due to high carrier frequency. Therefore, reciprocity is usually not applicable in FDD systems [10].

To reduce the turn-around delay in TDD systems, especially in fast-fading mobile communication, channel sounding is sometimes used. Channel sounding uses a reverse-link transmission specifically for channel measurement, in which the scheduled users send a sounding (pilot) signal to help the base learn their channels. The sounding signals are orthogonal among simultaneously scheduled users. The obtained channel information is used for the very next transmission to those users.

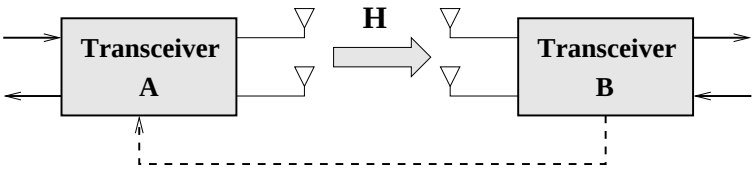

Figure 2.4: Obtaining CSIT using feedback.

A complication in using reciprocity methods is that the principle only applies to the radio channel between the antennas, while in practice, the "channel" is measured and used at the baseband processor. Different transmit and receive RF hardware chains hence become part of the forward and reverse channels. Since these chains have different frequency transfer characteristics, reciprocity requires transmit-receive chain calibration. During calibration, the difference in the frequency response between the two chains are identified [37]. A digital equalizer is then built and incorporated into the baseband section to make the two chains effectively identical. This equalizer usually requires high numerical precision and accuracy. Calibration must be performed periodically to track the slow time variations of the RF chains.

2.3.2 Feedback-based methods

Another method of obtaining channel information at the transmitter is using feedback from the receiver of the forward link, depicted in Figure 2.4. The channel is measured at the receiver at B during the forward transmission (A to B), then the information is sent to the transmitter at A on the reverse link. Feedback is not limited by the reciprocity requirements. However, the feedback delay Δ_t between channel measurement at B and its use by the transmitter at A can be a source of error, unless it is much smaller than the channel coherence time:

$$\Delta_t \ll T_c \, .$$

Feedback can also be used to send channel statistics that change much slower in time compared to the channel itself. In such cases, the delay requirement for valid feedback can be relaxed significantly.

Channel acquisition using feedback can be applied in both TDD and FDD systems,

but is more common in FDD. Although not subjected to transmit-receive calibration, feedback imposes another system overhead by using transmission resources. Therefore, methods of reducing feedback overhead, such as quantizing feedback information, are of practical importance [38, 39, 40]. These methods, however, are not a focus of this thesis.

2.4 A dynamic CSIT model

This section establishes a CSIT model in the form of a channel estimate and its error covariance at the transmit time n. Although CSIT formulation as a noisy channel estimate has been used in the literature [41, 42], this model is an explicit construction, using an initial channel measurement and relevant channel statistics – mean, covariance, and auto-correlation. The model applies to frequency-flat MIMO channels.

With both CSIT acquisition methods outlined in Section 2.3, there exists a delay from when the channel information is measured to when it is used by the transmitter. Because of the channel temporal variation, this delay may affect the reliability of the obtained information, depending on the type of information. Consider instantaneous channel measurements and the channel statistics. Instantaneous measurements are sensitive to the delay, especially in mobile communication, leading to a potential mismatch between the measurement and the channel at the time of use. Channel statistics, including the channel mean (2.19), covariance (2.16) and auto-correlation (2.21), can be obtained by averaging instantaneous measurements over tens of coherence times. They remain valid for tens to hundreds coherence intervals, relatively long compared to a transmission interval. Therefore, these statistics are not affected by channel acquisition delay and can be considered reliable.

A more reliable and complete CSIT can provide more gain in system capacity and performance. This principle suggests combining both instantaneous measurements and the channel statistics to create a CSIT model robust to channel variation, while optimally capturing the potential gain.

2.4.1 MMSE channel estimation at the transmitter

Suppose that the transmitter has an initial channel measurement at time 0 and relevant channel statistics. Consider CSIT at the transmit time n in the form of a channel estimate and its error covariance. The main source of irreducible error in channel estimation is the random channel time-variation. Thus, assume the channel measurement at time 0 error-free, the error in the channel estimate depends only on the delay n between this initial measurement and its use by the transmitter.

Denote $\hat{\mathbf{H}}[n]$ as the channel estimate at time n, and $\mathbf{E}[n]$ as the estimation error with correlation $\mathbf{R}_e[n]$. A CSIT model can then be written as

$$\begin{aligned} \mathbf{H}[n] &= \hat{\mathbf{H}}[n] + \mathbf{E}[n]\,, \\ \mathbf{R}_e[n] &= E\big[\mathbf{e}[n]\mathbf{e}[n]^*\big]\,. \end{aligned} \tag{2.23}$$

where $\mathbf{e}[n] = \mathrm{vec}\big(\mathbf{E}[n]\big)$. Assuming unbiased estimates, $\mathbf{E}[n]$ can be modeled as a stationary zero-mean Gaussian random process. $\mathbf{R}_e[n]$ is then the error covariance dependent on the delay n and the Doppler spread. The CSIT consists of the estimate $\hat{\mathbf{H}}[n]$ and its error covariance $\mathbf{R}_e[n]$. At time zero, $\mathbf{E}[0] = \mathbf{0}$ and $\mathbf{R}_e[0] = \mathbf{0}$, corresponding to perfect CSIT.

Assume that the initial channel measurement $\mathbf{H}[0]$ with the channel statistics $\mathbf{H}_m$, $\mathbf{R}_0$, and $\mathbf{R}[n]$ are available to the transmitter. Then the CSIT at time n follows from the MMSE estimation theory [43] as

$$\begin{aligned} \hat{\mathbf{h}}[n] &= E\big[\mathbf{h}[n]|\mathbf{h}[0]\big] &&= \mathbf{h}_m + \mathbf{R}[n]^*\mathbf{R}_0^{-1}\left(\mathbf{h}[0] - \mathbf{h}_m\right) \\ \mathbf{R}_e[n] &= \mathrm{cov}\big[\mathbf{h}[n]|\mathbf{h}[0]\big] &&= \mathbf{R}_0 - \mathbf{R}[n]^*\mathbf{R}_0^{-1}\mathbf{R}[n]\,, \end{aligned} \tag{2.24}$$

where $\hat{\mathbf{h}}[n] = \mathrm{vec}\big(\hat{\mathbf{H}}[n]\big)$ (note that the lower-case letters $\mathbf{h}$ denote the vectorized version of the corresponding upper-case matrices $\mathbf{H}$). A similar method was used for estimating a scalar time-varying channel from a vector of outdated estimates [44]. The channel estimate with error covariance (2.24) is an explicit construction of the CSIT model as a noisy channel estimate for a MIMO system.

The two quantities $\{\hat{\mathbf{H}}[n], \mathbf{R}_e[n]\}$ constitutes the CSIT. They effectively function as a

channel mean and a channel covariance at a delay n. Thus $\hat{\mathbf{H}}$ and $\mathbf{R}_e$ are also referred to as the effective mean and effective covariance, respectively, and the pair forms an effective statistics.

2.4.2 Dynamic CSIT with homogeneous temporal correlation

Using the homogeneous channel temporal-correlation model (2.22), the channel estimate and its error covariance become

$$\begin{aligned} \hat{\mathbf{H}}[n] &= \rho[n]\mathbf{H}_0 + (1-\rho[n])\,\mathbf{H}_m\,, \\ \mathbf{R}_e[n] &= \left(1-\rho[n]^2\right)\mathbf{R}_0\,. \end{aligned} \tag{2.25}$$

The CSIT can now be simply characterized as a function of $\rho[n]$, the initial channel measurement $\mathbf{H}_0$, and the channel mean $\mathbf{H}_m$ and covariance $\mathbf{R}_0$. The channel estimate becomes a linear combination of the initial measurement and the channel mean. The error covariance is a linear function of the channel covariance alone. With Kronecker antenna correlation (2.17), the estimated channel has the effective antenna correlations as

$$\begin{aligned} \mathbf{R}_{t,e}[n] &= \sqrt{1-\rho[n]^2}\,\mathbf{R}_t\,, \\ \mathbf{R}_{r,e}[n] &= \sqrt{1-\rho[n]^2}\,\mathbf{R}_r\,, \end{aligned} \tag{2.26}$$

which again follow a Kronecker structure. When the antennas at the receiver are uncorrelated, $\mathbf{R}_r = \mathbf{I}$, then the effective receive correlation is assumed to be $\mathbf{R}_{r,e}[n] = \mathbf{I}$, and the effective transmit correlation becomes

$$\mathbf{R}_{t,e}[n] = \left(1-\rho[n]^2\right)\mathbf{R}_t\,. \tag{2.27}$$

In the CSIT models (2.25) and (2.26), $\rho[n]$ acts as a channel estimate quality dependent on the time delay n. For a zero or short delay, ρ is close to 1; the estimate depends heavily on the initial channel measurement, and the error covariance is small. As the delay increases, ρ decreases in magnitude to 0, reducing the impact of the initial measurement. The estimate then moves toward the channel mean $\mathbf{H}_m$, and the error covariance grows toward the channel covariance $\mathbf{R}_0$. Therefore, the CSIT ranges between perfect channel

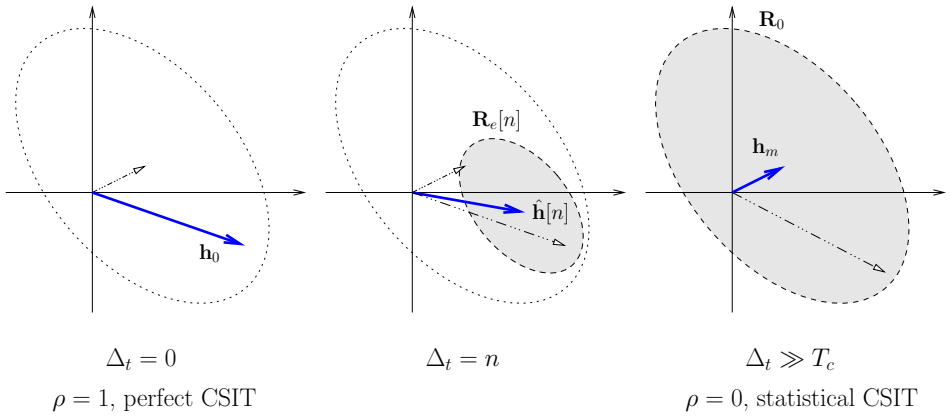

Figure 2.5: Dynamic CSIT model in the form of a delay-dependent channel estimate (bold vector) and its error covariance (shaded ellipse).

knowledge (when $\rho = 1$) and the channel statistics (when $\rho = 0$). By taking into account the channel time variation using ρ, this model optimally captures the available channel information and creates dynamic CSIT. The model is illustrated in Figure 2.5.

2.4.3 Special CSIT cases

Several special cases of dynamic CSIT are of interest. When $\rho = 1$, it is *perfect CSIT*; the error-covariance is zero. For *partial CSIT* at $0 \leq \rho < 1$, the CSIT consists of an effective channel mean and an effective covariance. If either of this mean or covariance is trivial, then the CSIT collapses to a special case. Using $\rho = 0$ as a representative for partial CSIT, these special cases are subsequently described in terms of the original channel statistics.

Assume further that the channel covariance has the Kronecker structure (2.17) and only transmit antennas are correlated, so that $\mathbf{R}_0 = \mathbf{R}_t^T \otimes \mathbf{I}$. The channel (2.18) can now be written as

$$\mathbf{H} = \mathbf{H}_m + \mathbf{H}_w \mathbf{R}_t^{1/2} \,. \tag{2.28}$$

The CSIT including $\mathbf{H}_m$ and $\mathbf{R}_t$ is referred to as *statistical CSIT*. When $\mathbf{R}_t$ is arbitrary but $\mathbf{H}_m = 0$, it is *transmit covariance CSIT* . When $\mathbf{H}_m$ is arbitrary but $\mathbf{R}_t = \mathbf{I}$, it is *mean CSIT*. Finally, the condition when $\rho = 0$, $\mathbf{H}_m = 0$, and $\mathbf{R}_t = \mathbf{I}$ corresponds to an i.i.d Rayleigh fading channel with no channel information at the transmitter.

2.5 A high-K variable-phase CSIT model

Partial CSIT can also be in a parametric form such as the channel distribution parameters, the K factor, or the condition number. This section presents a model for a high-K channel with two transmit and one receive antennas. Such a channel has two elements with a gain factor and a phase shift between them as in (2.13). The channel can represent, for example, the forward link at a base station with direct-path propagation and large spacing (about 10 carrier wavelengths) between the two transmit antennas.

With high K factor, the antenna gains are likely to be stable and can be estimated accurately. Therefore, α and h_1 are assumed to be known perfectly at the transmitter. The phase shift (2.14), however, is highly variable because of the large separation between the antennas, leading to potential errors in the phase estimate. Assume that the probability distribution function (PDF) of ϕ is known but not the exact value of ϕ. This phase-shift distribution is circular between $-\pi$ and π. A Dirac delta distribution function corresponds to exact phase knowledge, whereas a uniform distribution means no phase information. In fast time-varying channels, the phase measurements are more error prone, hence the distribution will tend toward uniform.

The precise shape of the phase-shift PDF depends on the channel characteristics and the measurement method. Assume that the distribution is *symmetric* around a mean ϕ_0. For example, a model candidate is the Rician phase distribution. This distribution arises from the phase of a constant phasor perturbed by random zero-mean complex Gaussian noise with equal variance on the real and imaginary parts [28, 45]. The quality of the phase estimate here can be conveniently described by the Rician factor β. With mean ϕ_0 and quality β, denoting $\tilde{\phi} = \phi - \phi_0$, the PDF of the phase-shift estimate ϕ is

$$f_{\mathbf{\Phi}}(\phi) = \frac{e^{-\beta^2}}{2\pi}\Big\{1 + \sqrt{\pi}\beta\cos\tilde{\phi}e^{\beta^2\cos^2\tilde{\phi}}\big[1 + \mathrm{erf}(\beta\cos\tilde{\phi})\big]\Big\}. \tag{2.29}$$

If $\beta = 0$, the distribution is uniform, corresponding to no phase knowledge. When $\beta \to \infty$, it converges to the Dirac delta function, meaning ϕ_0 is the exact phase-shift. Figure 2.6 provides a plot of the phase distribution with mean $\phi_0 = 0$ at various values of β.

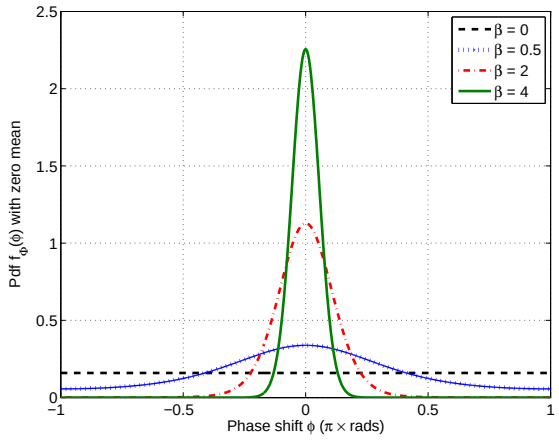

Figure 2.6: The Rician phase distribution.

2.6 Chapter summary

This chapter has characterized and modeled a MIMO wireless channel, discussed channel acquisition at the transmitter, and established CSIT models. The wireless channel is characterized by multipath fading, which causes time and frequency selectivities. In discrete-time, the channel impulse response contains multiple delayed-taps with time-varying amplitude and random phase. The channel is therefore often modeled statistically, each channel response tap as a Gaussian process.

Consider the frequency-flat channel, MIMO brings the additional spatial dimension and creates a channel in which each response tap is a matrix. Each element of this channel matrix is a Gaussian process. Assuming stationary, their covariance captures the correlation among the transmit and receive antennas. Their auto-covariance at a non-zero delay captures both the antenna and channel temporal correlations. Their means can be non-zero, depending on fading, and can be partially characterized by the Rician K factor.

The transmitter can obtain channel information indirectly by reciprocity or feedback. Both methods introduce a delay, potentially affecting the information accuracy because of the channel time-variation. For the information to be useful, this delay usually needs to be much smaller than the channel coherence time.

Dynamic CSIT is a model for transmit channel side information that takes into account channel time-variation. The model consists of a channel estimate and its error covariance,

built on an initial, accurate channel measurement and the channel mean, covariance, and temporal correlation factor ρ. This factor functions as the CSIT quality, with 1 corresponding to perfect, and 0 to statistical information. Parameterized by ρ, the CSIT provides an effective channel mean and an effective covariance. This model can be applied to a general Rician correlated fading MIMO channel.

Another CSIT model is established for a channel with high K. Focusing on the 2×1 channel, the transmitter is assumed to know the amplitudes of the channel elements precisely, but only the distribution of their phase-shift. This model is applicable, for example, to a down link with a line-of-sight from a basestation to a mobile.

With the established CSIT models, the thesis proceeds to examine the capacity impact of CSIT and design precoding schemes exploiting them. Chapter 3 next analyzes the capacity and the optimal input given dynamic CSIT.

Chapter 3

MIMO CAPACITY WITH DYNAMIC CSIT

As seen in Chapter 1, transmit channel side information can significantly increase channel capacity. To establish the capacity with CSIT, it is necessary to find the optimal input signal. For memoryless channel with perfect channel information at the receiver, the optimal input is Gaussian distributed with zero-mean [46]. Therefore, the objective remains to find its optimal covariance. The covariance can be described in terms of precoding: its eigenvectors are the beam directions, and the eigenvalues the beam power allocation.

For dynamic CSIT, involving a non-zero effective channel mean and a non-trivial effective channel covariance, the capacity optimization problem involves evaluating an expectation over the non-central Wishart distribution [47]. A closed-form solution for the optimal input covariance, given such channel statistics, is still an open problem. Partial solutions exist for special cases: covariance CSIT, when the channel covariance is non-trivial but the mean is zero [48, 49], and mean CSIT, when the channel mean is non-zero but the covariance is the identity matrix [50, 51]. In these cases, the optimal beam directions are known analytically, but not the power allocation. Nevertheless, some impacts of the channel mean and transmit antenna correlation on the capacity can be quantified. For example, the capacity is a monotonically increasing function of the singular values of the channel mean [51]. With transmit covariance CSIT, the capacity of a MISO channel

is Schur-convex in the covariance eigenvalues and the capacity gain from the CSIT grows with increasing number of transmit antennas [52]. Transmit antenna correlation, furthermore, has an advantage at low SNRs by reducing the required minimum bit energy [53]. With dynamic CSIT, the impacts on the capacity can also be analyzed.

This chapter first analyzes the capacity with dynamic CSIT asymptotically. It establishes the optimal input covariance and the capacity gain, given dynamic CSIT, at low and high SNRs. At low SNRs, the optimal input typically becomes simple single-mode beamforming, and the capacity gain is multiplicative. At high SNRs, the optimal solution depends on the relative numbers of transmit and receive antennas. For systems with equal or fewer transmit than receive antennas, the optimal input approaches equi-power and the capacity gain diminishes to zero. For systems with more transmit than receive antennas, however, both the optimal input and the capacity gain depend heavily on the CSIT. Contradictory to equi-power, the optimal input here may drop modes at high SNRs. Conditions for mode dropping are established for representative channels with high K factor or strong transmit antenna correlation. These conditions provide intuition to when it is optimal to activate only a fraction of the available eigen-modes at all SNRs, given the CSIT. In such a case, CSIT provides an additive capacity gain at high SNRs.

Fortunately, capacity optimization with dynamic CSIT is a convex problem, hence allowing efficient numerical implementation [54]. The problem, however, is stochastic, posing challenge in evaluating function values. This chapter next develops a convex optimization program using an interior point method. This program inputs the channel statistical parameters – the mean and the transmit covariance – and the SNRs; it outputs the optimal signal covariance and the channel capacity. The program employs efficient techniques for calculating the gradients and the Hessians, using Monte-Carlo to approximate the expectation of stochastic functions. Its runtime is linear in the number of channel samples and quadratic-to-cubic in the number of transmit antennas.

The program is then used to study impacts of the channel mean, the transmit covariance, the CSIT quality, and the K factor on the capacity and the optimal input. It also helps evaluate a lower bound on the capacity, based on the sub-optimal input covariance that maximizes Jensen's bound on capacity, and establish conditions with which

this bound is tight, hence allowing a simple, analytical capacity approximation.

The chapter is organized as follows. Section 3.1 formulates the channel capacity with dynamic CSIT. The chapter then analyzes the capacity asymptotically. Section 3.2 establishes the capacity gains at low and high SNRs, and Section 3.3 characterizes the optimal input. The next part builds a capacity optimization program. Section 3.4 discusses methods for calculating the gradient and Hessian and analyzes the program run-time complexity. Section 3.5 then uses this program to analyze different effects of the CSIT on the capacity and assess a lower bound on the capacity. Finally, Section 3.6 summarizes the chapter.

3.1 Channel ergodic capacity with dynamic CSIT

Consider the ergodic capacity of a MIMO channel with constant sum power across all transmit antennas at every time instance. Assume perfect channel state information at the receiver (CSIR) and dynamic CSIT (2.25), given an estimate quality ρ. With perfect CSIR, the capacity is achieved by a zero-mean complex Gaussian input [46] with covariance dependent on the CSIT.

3.1.1 The ergodic capacity formulation

Given dynamic CSIT, the channel ergodic capacity, together with the optimal input covariance, can be obtained by two-stage averaging. In the first stage, each initial channel measurement $\mathbf{H}_0$ with estimate quality ρ produces CSIT value $\{\hat{\mathbf{H}}, \mathbf{R}_e\}$ (2.25). The channel seen from the transmitter thus effectively has mean $\hat{\mathbf{H}}$ and covariance $\mathbf{R}_e$. Provided zero-mean Gaussian input with covariance $\mathbf{Q}$, the average mutual information across the channel, given $\mathbf{H}_0$, is

$$\mathcal{I}(\mathbf{H}_0, \mathbf{Q}) = E_{\mathbf{H}} \left[\text{logdet}(\mathbf{I} + \gamma \mathbf{H}\mathbf{Q}\mathbf{H}^*) \right] \ .$$

The signal covariance $\mathbf{Q}$ that maximizes $\mathcal{I}(\mathbf{H}_0, \mathbf{Q})$ is the optimizer of the problem

$$\begin{aligned} \mathcal{I}_o(\mathbf{H}_0) \;=\; & \max_{\mathbf{Q}} \quad E_{\mathbf{H}}\big[\mathrm{logdet}(\mathbf{I}+\gamma\mathbf{H}\mathbf{Q}\mathbf{H}^*)\big] \\ & \text{subject to} \quad \begin{aligned} \mathrm{tr}(\mathbf{Q}) &= 1 \\ \mathbf{Q} &\succcurlyeq \mathbf{0}\,, \end{aligned} \end{aligned} \tag{3.1}$$

where γ is the SNR. The equality constraint results from the constant sum transmit power, and the inequality from the positive semi-definite property of a covariance matrix. Note that the expectation is evaluated over the effective channel Gaussian statistics with mean $\hat{\mathbf{H}}$ and covariance $\mathbf{R}_e$, which are functions of $\mathbf{H}_0$ and the actual channel statistics (2.25).

In the second stage, $\mathcal{I}_o(\mathbf{H}_0)$ is averaged over the distribution of $\mathbf{H}_0$ to get the channel ergodic capacity. For a given estimate quality ρ, therefore, the capacity is

$$\mathcal{C} = E_{\mathbf{H}_0}\left[\mathcal{I}_o(\mathbf{H}_0)\right]\,, \tag{3.2}$$

where $\mathbf{H}_0$ is Gaussian distributed with mean $\mathbf{H}_m$ (2.19) and covariance $\mathbf{R}_0$ (2.16), the actual channel statistics.

3.1.2 The optimal input covariance

Establishing the capacity with dynamic CSIT thus essentially requires solving (3.1). This problem is to find the optimal input covariance and the capacity for a channel with statistical CSIT, involving arbitrary channel mean and covariance. The input covariance can be decomposed into its eigenvalues and eigenvectors as

$$\mathbf{Q} = \mathbf{U}_Q\mathbf{\Lambda}_Q\mathbf{U}_Q\,. \tag{3.3}$$

The columns of $\mathbf{U}_Q$ are the orthogonal eigen-beam directions (patterns), and $\mathbf{\Lambda}_Q$ represents the power allocation on these beams. The problem has analytical solution for the eigenvectors $\mathbf{U}_Q$ in special cases of mean CSIT, involving an arbitrary mean but with identity covariance matrix, and covariance CSIT, involving an arbitrary covariance but

with zero mean. The eigenvalues $\mathbf{\Lambda}_Q$, however, requires numerical solution. In the general case of arbitrary mean and covariance matrices, no analytical solution so far exists for either $\mathbf{U}_Q$ or $\mathbf{\Lambda}_Q$. Fortunately, the problem is convex, hence allowing efficient and accurate numerical implementation. Furthermore, the optimal $\mathbf{Q}$ and the capacity with dynamic CSIT, and therefore the capacity gain from CSIT, can be asymptotically quantified at low and high SNRs, as discussed in Section 3.2.

Review of the optimal eigen-beams in special CSIT cases

The optimal eigenvectors $\mathbf{U}_Q$ are known analytically for the mean CSIT and transmit covariance CSIT. With mean CSIT, the transmitter knows the non-zero effective channel mean $\hat{\mathbf{H}}$, while the effective covariance is the identity matrix ($\mathbf{R}_e = \mathbf{I}$). Perform the SVD of the mean as

$$\hat{\mathbf{H}} = \mathbf{U}_{\hat{H}} \mathbf{\Sigma}_{\hat{H}} \mathbf{V}_{\hat{H}}^* \ ,$$

then the optimal input covariance eigenvectors are [50, 51]

$$\mathbf{U}_Q = \mathbf{V}_{\hat{H}} \ . \tag{3.4}$$

The intuitive reason is the identity channel covariance, which implies the random part of the channel has no direction preference. Thus the optimal input eigen-directions align with those of the channel mean.

With covariance CSIT, the transmitter knows the non-identity effective channel covariance $\mathbf{R}_e$, while the mean is zero ($\hat{\mathbf{H}} = \mathbf{0}$). The covariance is further assumed to have the Kronecker structure, so that $\mathbf{R}_e = (1-\rho^2)\mathbf{R}_t^T \otimes \mathbf{R}_r$, where $\mathbf{R}_t$ and $\mathbf{R}_r$ are the transmit and receive antenna correlations, respectively. Perform the EVD of the transmit correlation as

$$\mathbf{R}_t = \mathbf{U}_t \mathbf{\Lambda}_t \mathbf{U}_t^* \ , \tag{3.5}$$

then the optimal input covariance eigenvectors are [48, 49]

$$\mathbf{U}_Q = \mathbf{U}_t \ . \tag{3.6}$$

Since the channel mean is zero, only the direction preference of the random channel part matters. This result holds even when receive correlation exists ($\mathbf{R}_r \neq \mathbf{I}$). The receive correlation only affects the optimal eigenvalues $\mathbf{\Lambda}_Q$, but not the eigenvectors $\mathbf{U}_Q$ [55]. For a non-Kronecker covariance $\mathbf{R}_e$, however, no analytical results for $\mathbf{U}_Q$ so far exist.

3.2 Asymptotic-SNR capacity gains

This section analytically quantifies the capacity gains from dynamic CSIT, asymptotically at low and high SNRs. In particular, the gain at low SNRs is multiplicative and is achieved by single-mode beamforming. The gain at high SNRs is additive and requires multi-mode transmission. These gains also depend on the CSIT.

3.2.1 Low-SNR optimal beamforming and capacity gain

This section first establishes the optimal input at low SNRs with statistical CSIT, as formulated in (3.1), then analyzes the capacity gain.

Low-SNR optimal beamforming

The optimal signal at low SNRs is typically single-mode beamforming with the direction given by the CSIT, as stated in the following theorem.

Theorem 1. *As the SNR $\gamma \to 0$, the optimal input covariance of problem (3.1) converges to a rank-one matrix with a unit eigenvalue and the corresponding eigenvector given by the dominant eigenvector of*

$$\mathbf{G} = E[\mathbf{H}^*\mathbf{H}] \,,$$

provided this dominant eigenvalue is unique. In other words, the optimal input becomes a single-mode beamforming signal along the dominant eigenvector of $\mathbf{G}$. If there are multiple dominant eigenvalues of $\mathbf{G}$, the transmit power can be split arbitrarily among their eigenvector directions.

For the channel model (2.28), $\mathbf{G} = E[\mathbf{H}^*\mathbf{H}] = \hat{\mathbf{H}}^*\hat{\mathbf{H}} + M\mathbf{R}_{t,e}$.

Proof. Using the Taylor series, the function $f = \log\det(I + \gamma\mathbf{A})$, where $\mathbf{A}$ is a positive semi-definite matrix, can be expanded as a polynomial of γ as

$$f = \mathrm{tr}(\mathbf{A})\gamma - \mathrm{tr}(\mathbf{A}^2)\gamma^2 + \mathrm{tr}(\mathbf{A}^3)\gamma^3 - \dots$$

In problem (3.1), denote $\mathcal{I}(\mathbf{Q})$ as the objective function for brevity. Noting that

$$\mathcal{I}(\mathbf{Q}) = E_{\mathbf{H}}\big[\mathrm{logdet}(\mathbf{I} + \gamma\mathbf{H}\mathbf{Q}\mathbf{H}^*)\big] = E_{\mathbf{H}}\big[\mathrm{logdet}(\mathbf{I} + \gamma\mathbf{H}^*\mathbf{H}\mathbf{Q})\big] \ ,$$

and applying the above expansion, at low SNRs ($\gamma \to 0$), the mutual information $\mathcal{I}(\mathbf{Q})$ approaches

$$\mathcal{I}(\mathbf{Q}) \overset{\gamma\to 0}{\approx} E_{\mathbf{H}}\left[\mathrm{tr}(\mathbf{H}^*\mathbf{H}\mathbf{Q})\gamma\right] = \gamma\,\mathrm{tr}\left(E_{\mathbf{H}}[\mathbf{H}^*\mathbf{H}]\mathbf{Q}\right) = \gamma\,\mathrm{tr}\left[\mathbf{G}\mathbf{Q}\right] \ .$$

Maximizing this expression with the constraint $\mathrm{tr}(\mathbf{Q}) = 1$ results in the optimal $\mathbf{Q}$ in Theorem 1. □

In a slightly different context, considering the spectral efficiency in a wideband channel, the optimal input in the special case of $\mathbf{G}$ having multiple dominant eigenvalues is briefly discussed in [56]. Taking into account the wideband slope, it is shown that in order to minimize the required bandwidth, the optimal input should distribute power among the dominant eigen-directions of $\mathbf{G}$ equally. The analysis in this chapter assumes a fixed bandwidth, resulting in arbitrarily distributed input power.

Low-SNR capacity ratio gain with statistical CSIT

Using the optimal input at low SNRs, the capacity gain with statistical CSIT can be quantified precisely. The gain is multiplicative, as stated in the following theorem.

Theorem 2. *As the SNR $\gamma \to 0$, the ratio between the optimal mutual information in (3.1) and the value obtained by equi-power isotropic input approaches*

$$r = \frac{N\lambda_{\max}(\mathbf{G})}{tr(\mathbf{G})} \ . \tag{3.7}$$

This ratio scales linearly with the number of transmit antennas and is related to the condition of the channel correlation matrix $\mathbf{G} = E[\mathbf{H}^*\mathbf{H}]$.

Proof. From the proof of Theorem 1, at low SNRs, the optimal mutual information with CSIT in (3.1) approaches

$$\mathcal{I}^\star \stackrel{\gamma\to 0}{=} \gamma\lambda_{\max}(\mathbf{G}) \; .$$

The mutual information with equi-power allocation, on the other hand, equals

$$\mathcal{I}_0 \stackrel{\gamma\to 0}{=} \frac{\gamma}{N}\mathrm{tr}(\mathbf{G}) \; .$$

Taking the ratio between these two expressions, $r = \mathcal{I}^\star/\mathcal{I}_0$, yields (3.7). □

At low SNRs, the transmitter has little power, and the CSIT allows it to focus all this power on the strongest known direction in the channel, rather than spreading equally everywhere. More transmit antennas will increase the focusing ability and hence the low-SNR capacity gain (3.7). As an extreme example, when $\mathbf{G}$ is rank-one, the ratio equals the number of transmit antennas N.

For dynamic CSIT with a given quality ρ, each initial channel measurement $\mathbf{H}_0$ provides a channel correlation $\mathbf{G}$ based on the effective channel statistics. The capacity gain is then obtained by averaging the ratio (3.7) over the distribution of $\mathbf{H}_0$.

Low-SNR capacity ratio gain with perfect CSIT

Perfect CSIT also multiplicatively increases the capacity at low SNRs. Moreover, the asymptotic gain can be quantified in the limit of a large number of antennas, as stated in the following theorem.

Theorem 3. *As the SNR* $\gamma \to 0$*, the ratio of the ergodic capacity with perfect CSIT to that without CSIT equals*

$$r = \frac{E[\lambda_{\max}(\mathbf{H}^*\mathbf{H})]}{\frac{1}{N}E[tr(\mathbf{H}^*\mathbf{H})]} \; , \tag{3.8}$$

where the expectations are performed over the actual channel distribution.

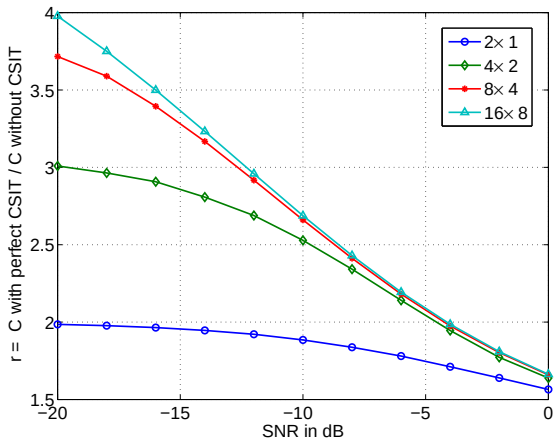

Figure 3.1: Ratio of the capacity of i.i.d. channels with perfect CSIT to that without CSIT. The legend denotes the numbers of transmit and receive antennas. The asymptotic capacity ratio, in the limit of large number of antennas, while keeping the number of transmit antennas twice the receive, is 5.83.

For an i.i.d. Rayleigh fading channel, if the number of antennas increases to infinity, provided the transmit to receive antenna ratio N/M stays constant, this ratio approaches a fixed value as

$$r \overset{N\to\infty}{\longrightarrow} \left(1+\sqrt{\frac{N}{M}}\right)^2 . \tag{3.9}$$

This limit depends on the ratio of the number of transmit to receive antennas and is always greater than 1.

Figure 3.1 shows examples of the capacity ratio (3.8) for 4 channels with twice the number of transmit as receive antennas. The ratio increases as the SNR decreases and as the number of antenna increases. Keeping the same transmit-receive antenna proportion, as the number of antennas increases to infinity, the ratio will approach 5.83. CSIT at low SNRs thus can increase the capacity significantly.

Proof. With perfect CSIT, using the Taylor expansion similar to the proof of Theorem 1, the solution for (3.1) at low SNRs is single-mode beamforming on the dominant eigen-mode of $\mathbf{H}_0^*\mathbf{H}_0$. The optimal mutual information is then $\mathcal{I}_o(\mathbf{H}_0) = \gamma\lambda_{\max}\left(\mathbf{H}_0^*\mathbf{H}_0\right)$. The ergodic capacity (3.2) becomes

$$\mathcal{C} = \gamma E_{\mathbf{H}_0}\left[\lambda_{\max}\left(\mathbf{H}_0^*\mathbf{H}_0\right)\right] ,$$

where $\mathbf{H}_0 \sim \mathcal{N}(\mathbf{H}_m, \mathbf{R}_0)$. Without CSIT, however, the capacity is achieved by equi-power isotropic input [6]. At low SNRs, using the Taylor expansion, the capacity approaches

$$\mathcal{C}_0 = \gamma E_{\mathbf{H}_0}\left[\frac{1}{N}\mathrm{tr}\left(\mathbf{H}_0^*\mathbf{H}_0\right)\right] .$$

Taking the ratio of the above two expressions side-by-side yields (3.8).

For an i.i.d. Rayleigh fading channel, $\mathbf{H}_m = \mathbf{0}$ and $\mathbf{R}_0 = \mathbf{I}$. In the limit of large number of antennas, provided the ratio of the number of transmit to receive antennas stays constant, the maximum eigenvalue of $\mathbf{H}_0^*\mathbf{H}_0$ satisfies [57, 58]

$$\frac{1}{N}\lambda_{\max}\left(\mathbf{H}_0^*\mathbf{H}_0\right) \xrightarrow{\text{a.s.}} \left(1+\sqrt{\frac{M}{N}}\right)^2 .$$

The capacity without CSIT, normalized by γ, on the other hand, equals

$$\frac{1}{N}E\left[\mathrm{tr}\left(\mathbf{H}_0^*\mathbf{H}_0\right)\right] = \frac{1}{N}E\left[||\mathbf{H}_0||_F^2\right] = M .$$

Taking the ratio of the above two expressions side-by-side yields (3.9). □

3.2.2 High-SNR capacity gain

At high SNRs, the optimal input and the capacity gain depend on the channel rank and the relative antenna configuration. For full-rank channels, dynamic CSIT does not increase the capacity at high SNRs for systems with equal or fewer transmit than receive antennas ($N \leq M$), but does for systems with more transmit antennas ($N > M$). For rank-deficient channels with non-full-rank $\mathbf{R}_t$, transmit covariance CSIT helps increase the capacity. Each case is considered next.

Full-rank channels with equal or fewer transmit than receive antennas

When $N \leq M$, asymptotically at high SNRs, problem (3.1) has the optimal input covariance as $\frac{1}{N}\mathbf{I}$. This result is well-known and can be easily shown. For full-rank channel $\mathbf{H}$, the condition $N \leq M$ makes $\mathbf{H}^*\mathbf{H}$ full-rank, hence the mutual information at high SNRs

can be decomposed as

$$\begin{aligned} \mathcal{I}(\mathbf{Q}) &= E_{\mathbf{H}}\left[\mathbf{I}_N + \log\det(\gamma \mathbf{H}^*\mathbf{H}\mathbf{Q})\right] \\ &\overset{\gamma\to\infty}{\approx} E_{\mathbf{H}}\left[\log\det(\gamma \mathbf{H}^*\mathbf{H}\mathbf{Q})\right] \\ &= E_{\mathbf{H}}\left[\log\det(\mathbf{H}^*\mathbf{H})\right] + \log\det(\gamma\mathbf{Q})\,. \end{aligned} \tag{3.10}$$

Maximizing the above expression, subject to $\mathrm{tr}(\mathbf{Q}) = 1$, leads to $\mathbf{Q} = \mathbf{I}/N$. In other words, the optimal input covariance at high SNRs approaches equi-power in all directions, independent of the CSIT. For these systems, the capacity gain from CSIT diminishes to 0 at high SNRs.

Full-rank channels with more transmit than receive antennas

When $N > M$, in contrast, dynamic CSIT can also provide capacity gain at high SNRs. The gain here is additive. Since $\mathbf{H}^*\mathbf{H}$ is rank-deficient in this case, the decomposition (3.10) does not apply. The optimal input covariance of (3.1) at high SNRs depends on the channel statistics, or the CSIT $\{\hat{\mathbf{H}}, \mathbf{R}_e\}$. While an analytical optimal covariance for arbitrary $\hat{\mathbf{H}}$ and $\mathbf{R}_e$ is still unknown, the capacity gain is maximum with perfect CSIT ($\hat{\mathbf{H}} = \mathbf{H}_0,\ \mathbf{R} = \mathbf{0}$, corresponding to $\rho = 1$), in which case, this gain can be accurately quantified [21].

Theorem 4. *For $N > M$, at high SNRs, the incremental capacity gain from perfect CSIT ($\rho = 1$), over the mutual information obtained by equi-power isotropic input, equals*

$$\Delta\mathcal{C} = M\log_2\left(\frac{N}{M}\right) \textit{ bps/Hz}\,. \tag{3.11}$$

This gain scales linearly with the number of receive antennas and depends on the ratio of the number of transmit to receive antennas.

Intuitively, with $N > M$, the channel seen from the transmitter has a null-space. By knowing the channel, the transmitter can avoid sending any power into this null-space and therefore achieve a capacity gain. For example, for systems with twice the number of transmit as receive antennas, the capacity incremental gain approaches the number of

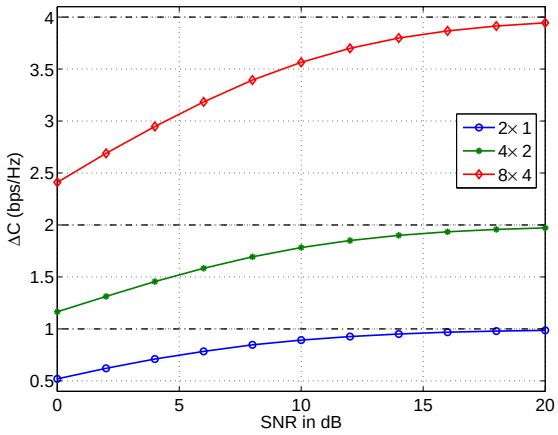

Figure 3.2: Incremental capacity gain from perfect CSIT for i.i.d. channels. The legend denotes the numbers of transmit and receive antennas.

receive antennas in bps/Hz and can be achieved at an SNRs as low as 20dB, as illustrated in Figure 3.2.

Proof. With perfect CSIT, the solution for (3.1) is standard water-filling on $\mathbf{H}_0^*\mathbf{H}_0$ [46]. Let σ_i^2 be the eigenvalues of $\mathbf{H}_0^*\mathbf{H}_0$, then the optimal eigenvalues of $\mathbf{Q}$ are

$$\lambda_i = \left(\mu - \frac{1}{\gamma\sigma_i^2}\right)_+ ,$$

where μ is chosen to satisfy $\sum_i \lambda_i = 1$. The plus notation means that the expression takes the value inside the parenthesis if this value is positive, otherwise it is zero. The ergodic capacity (3.2) then becomes $\mathcal{C} = \sum_{i=1}^{M} E_{\sigma_i}\left[\log\left(\mu\gamma\sigma_i^2\right)\right]$, where σ_i^2 has the distribution of the underlying Wishart matrix eigenvalues. For full-rank $\mathbf{H}_0$, as $\gamma \to \infty$, $\mu \to \frac{1}{M}$, and the capacity approaches

$$\mathcal{C} \overset{\gamma\to\infty}{\approx} M\log\left(\frac{1}{M}\right) + M\log(\gamma) + \sum_{i=1}^{M}\log(\sigma_i^2)\ . \tag{3.12}$$

Without CSIT, on the other hand, using an equi-power isotropic input with the covariance $\mathbf{Q} = \mathbf{I}/N$, the ergodic mutual information is given by $\mathcal{C}_0 = \sum_{i=1}^{M} E_{\sigma_i}\left[\log\left(1 + \frac{1}{N}\gamma\sigma_i^2\right)\right]$.

At high SNRs, this expression approaches

$$\mathcal{C}_0 \overset{\gamma\to\infty}{\approx} M\log\left(\frac{1}{N}\right) + M\log(\gamma) + \sum_{i=1}^{M}\log(\sigma_i^2)\ . \tag{3.13}$$

Subtracting (3.12) and (3.13) side-by-side yields the capacity gain in (3.11). □

Rank-deficient channels with non-full-rank $\mathbf{R}_t$

This section considers transmit covariance CSIT with rank-deficient $\mathbf{R}_t$, given zero channel mean and uncorrelated receive antennas. With rank-deficient $\mathbf{R}_t$, transmit covariance CSIT helps to increase the capacity additively at high SNRs, regardless of the number of receive antennas. Let K_t be the rank of $\mathbf{R}_t$ ($K_t < N$), this high-SNR capacity gain can be precisely quantified in the case $K_t \leq M$ as

$$\Delta\mathcal{C} = K_t\log\left(\frac{N}{K_t}\right)\ . \tag{3.14}$$

The derivation of this result is as follows. For transmit covariance CSIT, the optimal input beam directions are given by $\mathbf{R}_t$ eigenvectors (3.6). Let $\mathbf{\Lambda}_t$ be the eigenvalue matrix of $\mathbf{R}_t$, the average mutual information can then be written as

$$\begin{aligned}
\mathcal{I} &= E_{\mathbf{H}_w}\left[\log\det\left(\mathbf{I}_M + \gamma\mathbf{H}_w\mathbf{\Lambda}_t\mathbf{\Lambda}_Q\mathbf{H}_w^*\right)\right] \\
&= E_{\mathbf{H}_w}\left[\log\det\left(\mathbf{I}_M + \gamma\sum_{i=1}^{K_t}\lambda_{t,i}\lambda_{Q,i}\mathbf{h}_{w,i}\mathbf{h}_{w,i}^*\right)\right] \\
&= E_{\mathbf{H}_w}\left[\log\det\left(\mathbf{I}_{K_t} + \gamma\mathbf{H}_{w[K_t]}^*\mathbf{H}_{w[K_t]}\mathbf{\Lambda}_{t[K_t]}\mathbf{\Lambda}_{Q[K_t]}\right)\right]\ ,
\end{aligned}$$

where $\mathbf{\Lambda}_{t[K_t]}$ is the square, diagonal matrix of the non-zero eigenvalues of $\mathbf{\Lambda}_t$, $\mathbf{\Lambda}_{Q[K_t]}$ is the square, diagonal matrix containing the corresponding eigenvalues of $\mathbf{Q}$, and $\mathbf{H}_{w[K_t]}$ of size $M \times K_t$ contains the corresponding K_t columns of $\mathbf{H}_w$. With $K_t \leq M$, the matrix $\mathbf{H}_{w[K_t]}^*\mathbf{H}_{w[K_t]}\mathbf{\Lambda}_{t[K_t]}$ has rank K_t, hence at high SNRs, the optimal $\mathbf{\Lambda}_Q$ approaches equi-power on the K_t non-zero eigen-modes of $\mathbf{\Lambda}_t$. (This equi-power input is not always optimal at high SNRs if $K_t > M$, but a capacity gain still exists.) Without the CSIT, however, the optimal input distributes power equally on all N eigen-modes of $\mathbf{R}_t$. The

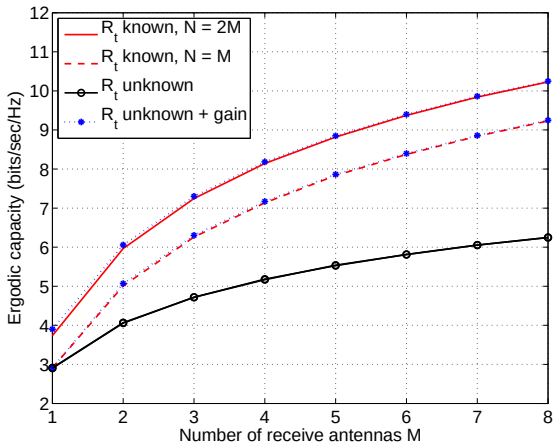

Figure 3.3: Capacity of channels with rank-one transmit correlation at SNR = 10dB, without and with transmit covariance CSIT.

difference in the corresponding mutual information then results in (3.14), similar to the proof of Theorem 4.

Figure 3.3 provides an example of the capacity with and without transmit covariance CSIT for rank-one correlated channels with various antenna configurations at 10dB SNR. The capacity without CSIT plus the gain (3.14) is also included. For rank-one correlation, having more transmit antennas helps to increase the capacity with transmit covariance CSIT, but does not without the CSIT.

3.3 Optimal input characterizations

The capacity-optimal input signal with dynamic CSIT can be analytically established in certain cases. At low SNRs, as specified in Theorem 1, it is typically single-mode beamforming with the direction as a function of CSIT. Hence, mode-dropping almost always occurs at low SNRs. At high SNRs, the optimal input depends not only on the CSIT, but also on the antenna configurations. For systems with equal or fewer transmit than receive antennas, the optimal input approaches isotropic equi-power. For systems with more transmit than receive antennas, however, it may not approach equi-power at high SNRs, depending on the CSIT. Specifically, for statistical CSIT with high-K mean

or highly-conditioned transmit covariance, signifying strong antenna correlation, mode-dropping may also occur at high SNRs. The intuition can be obtained by considering a 4×2 channel with different CSIT. With perfect CSIT, the optimal input has only 2 eigen-modes at high SNRs. Without CSIT, however, the optimal input at all SNRs is i.i.d. isotropic, which has 4 modes. Therefore there exists partial CSIT, with which the optimal input has 3 modes at high SNRs, implying mode-dropping.

This section considers impacts of antenna configurations and the CSIT on the optimal input covariance. It first briefly discusses the optimal input for systems with $N \leq M$. It then provides simplified analysis on the conditions for mode-dropping at high SNRs in systems with $N > M$. Two effects are considered: of the K factor and of the transmit antenna correlation. To isolate each effect, a simplified channel model is used in each case.

3.3.1 Systems with equal or fewer transmit than receive antennas

For $N \leq M$ systems with dynamic CSIT, the optimal input signal is known asymptotically at both low and high SNRs. At low SNRs, it is typically single-mode beamforming (Theorem 1), and at high SNRs, it approaches equi-power. Interestingly, the optimal input covariance here can be closely approximated by the closed-form Jensen input covariance, discussed in Section 3.5.1. This Jensen covariance becomes optimal at both low and high SNRs. At other SNRs, it produces a mutual information that is a tight lower-bound to the capacity. For the two special cases, transmit covariance CSIT and mean CSIT, the Jensen beam directions are optimal at all SNRs; only the power allocation is then approximated. More details can be found in Section 3.5.1.

3.3.2 Systems with more transmit than receive antennas

For $N > M$ systems with dynamic CSIT, the capacity-optimal input, especially its power allocation, depends heavily on the channel effective mean and covariance matrices. If the channel is uncorrelated with zero mean, as with i.i.d. Rayleigh fading, then the optimal input covariance is the identity matrix at all SNRs [6], implying equi-power allocation. However, if the mean is strong, characterized by a high K factor, or the transmit antennas

are highly correlated, characterized by a large condition number of $\mathbf{R}_t$, the optimal input may drop modes not only at low SNRs (Theorem 1) but also at high SNRs. A closed-form solution for the optimal input covariance, as a function of the channel mean and covariance, is still unknown. Furthermore, at high SNRs, the Jensen covariance, which approaches equi-power, is no longer a good approximation.

This section provides some simple characterizations on effects of the K factor and the transmit antenna correlation on the optimal input at high SNRs. The analysis focuses on two simple channel models, belonging to the special mean CSIT and covariance CSIT cases. Of these, the optimal beam directions are known (3.4), (3.6), thus only the power allocation needs to be specified. Each considered model results in the optimal allocation with only two distinct power levels. Conditions that lead to dropping the lower power level at high SNRs are analyzed.

Effects of the K factor

In an uncorrelated channel with $N > M$, given statistical CSIT, as K increases from 0 to infinity, the optimal number of input modes at high SNRs reduces from N to M. Thus, a sufficiently high K will result in less than N optimal modes, leading to mode-dropping at high SNRs. The mode-dropping effect, however, depends more broadly on the channel mean eigenvalues, of which K is a function. To isolate the impact of K alone, consider an uncorrelated channel, in which the channel mean has equal eigenvalues and hence is unitary. Thus, the power allocation here depends solely on K, but not the entire $\mathbf{H}_m$. The threshold for K, above which mode dropping occurs at high SNRs, can be obtained as stated in the following theorem.

Theorem 5. *Consider a channel (2.28) with $N > M$, uncorrelated antennas, and unitary channel mean. Specifically, the mean and transmit covariance are given as*

$$\begin{aligned} \mathbf{H}_m\mathbf{H}_m^* &= \frac{K}{K+1}\mathbf{I}_M \\ \mathbf{R}_t &= \frac{1}{K+1}\mathbf{I}_N \,, \end{aligned} \tag{3.15}$$

and the receive covariance is $\mathbf{R}_r = \mathbf{I}$. With statistical CSIT, the condition on K, with

which the optimal input activates only M out of the maximum N modes at all SNRs, is given as

$$tr\left(E_{\mathbf{h}_{w,j}}\left[\left(\sum_{j=1}^{M}\left(\sqrt{K}\mathbf{e}_j+\mathbf{h}_{w,j}\right)\left(\sqrt{K}\mathbf{e}_j+\mathbf{h}_{w,j}\right)^*\right)^{-1}\right]\right)\leq 1\ , \tag{3.16}$$

where $\mathbf{e}_i$ is the M-vector with the i^{th} element equal to 1 and the rest zero, and $\mathbf{h}_{w,j}\sim\mathcal{N}(\mathbf{0},\mathbf{I}_M)$ are i.i.d.

The matrix expression under expectation in (3.16) has the inverted non-central complex Wishart distribution. This expectation has no closed-form solution so far, but can be evaluated numerically.

Proof: Given mean and transmit covariance (3.15), let $\beta=\sqrt{K/(K+1)}$, and perform the SVD of the mean as

$$\mathbf{H}_m=\beta\mathbf{U}_m\mathbf{V}_m^*\ , \tag{3.17}$$

then the optimal beam directions are given by $\mathbf{V}_m$ (3.4). The optimal power allocation can be completely characterized by the K factor, or β, and the SNRs. Because of symmetry, this optimal solution contains only two different power levels: λ_1 for the first M eigen-modes, corresponding to the non-zero eigen-modes of $\mathbf{H}_m^*\mathbf{H}_m$, and λ_2 for the rest $N-M$ modes, where $\lambda_1\geq\lambda_2$ [51]. Thus the optimal solution $\mathbf{Q}$ for problem (3.1) has the form

$$\mathbf{Q}=\mathbf{V}_m\mathbf{\Lambda}_Q\mathbf{V}_m^*\ , \tag{3.18}$$

where $\mathbf{\Lambda}_Q$ is a diagonal matrix with M diagonal entries as λ_1 and $N-M$ as λ_2.

Let $\tilde{\mathbf{H}}$ be the zero-mean part of $\mathbf{U}_m^*\mathbf{H}\mathbf{V}_m$, then its N columns are i.i.d. with the distribution $\tilde{\mathbf{h}}_j\sim\mathcal{N}\left(\mathbf{0},(1-\beta^2)\mathbf{I}_M\right)$. The first M columns of $\mathbf{U}_m^*\mathbf{H}\mathbf{V}_m$ can then

be expressed as $\beta\mathbf{e}_i + \tilde{\mathbf{h}}_i$, $1 \le i \le M$. Problem (3.1) can now be written as

$$\begin{aligned} \max_{\lambda_1,\lambda_2} \quad & E_{\tilde{\mathbf{h}}_i}\left[\log\det\left(\mathbf{I}_M + \lambda_1\gamma\sum_{i=1}^{M}\left(\beta\mathbf{e}_i+\tilde{\mathbf{h}}_i\right)\left(\beta\mathbf{e}_i+\tilde{\mathbf{h}}_i\right)^* + \lambda_2\gamma\sum_{i=M+1}^{N}\tilde{\mathbf{h}}_i\tilde{\mathbf{h}}_i^*\right)\right] \\ \text{subject to} \quad & M\lambda_1 + (N-M)\lambda_2 = 1 \\ & \lambda_1 \ge 0,\ \lambda_2 \ge 0\ . \end{aligned} \tag{3.19}$$

Of interested is the condition on K (or β) that results in the optimal $\lambda_1^\star = 1/M$, and hence $\lambda_2^\star = 0$, implying mode-dropping. Based on the convexity of this problem, the sufficient and necessary condition for this optimality is

$$\mathrm{tr}\left(E_{\tilde{\mathbf{h}}_j}\left[\left(\mathbf{I} + \frac{\gamma}{M}\sum_{j=1}^{M}(\beta\mathbf{e}_j+\tilde{\mathbf{h}}_j)(\beta\mathbf{e}_j+\tilde{\mathbf{h}}_j)^*\right)^{-1}\right]\right) \le \frac{M}{1+\gamma\left(1-\beta^2\right)}\ , \tag{3.20}$$

where $\tilde{\mathbf{h}}_j \sim \mathcal{N}\left(\mathbf{0}, (1-\beta^2)\mathbf{I}_M\right)$. The derivation is given in Appendix A.1. This condition depends on M, β and γ and can be evaluated numerically. The condition, however, is independent of the number of transmit antennas N. From this condition, a threshold for K, above which mode-dropping occurs, can be established. As $\gamma \to \infty$, it becomes (3.16), which signifies mode-dropping at all SNRs. □

The threshold (3.20) is independent of the number of transmit antennas N. Thus if the channel mean is strong enough, the rank of this mean will dictate the number of active modes, regardless of the larger number of antennas. Figure 3.4 provides examples of this K factor threshold versus the SNR, derived from (3.20), for systems with 2 receive- and more than 2 transmit-antennas. When K is above this threshold, signifying a strong channel mean or a good channel estimate, the optimal power allocation activates only two modes and drops the rest at all SNRs.

Effects of the transmit antenna correlation

In a zero-mean channel, the condition number of the transmit covariance matrix $\mathbf{R}_t$ can influence the number of optimal input modes. When the condition number is 1, corresponding to an identity covariance matrix, all N transmit modes are active. When

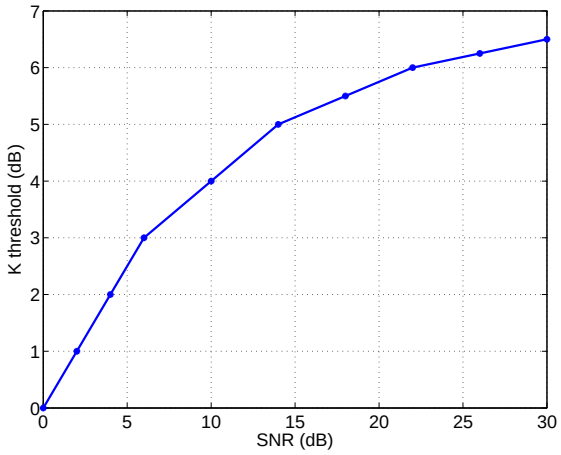

Figure 3.4: K factor thresholds for systems with 2 receive and more than 2 transmit antennas, above which using 2 modes is capacity-optimal for the mean CSIT (3.15) at all SNRs.

the condition number is infinite, implying a rank-deficient covariance $\mathbf{R}_t$, the number of active modes must be less than N at all SNRs, as no power should be allocated in $\mathbf{R}_t$ null-space. Thus there must be a finite threshold for $\mathbf{R}_t$ condition number, above which mode-dropping occurs at all SNRs. Similar to the K factor, however, $\mathbf{R}_t$ condition number is a function of the eigenvalues, on which the optimal input power allocation depends. To isolate the impact of $\mathbf{R}_t$ condition number, consider a zero-mean channel with a transmit covariance matrix having only two distinct eigenvalues. The threshold on the condition number of this matrix for mode-dropping at all SNRs is given as follows.

Theorem 6. *Consider a zero-mean channel ($\mathbf{H}_m = \mathbf{0}$) with correlated transmit antennas and uncorrelated receive antennas. Furthermore, the transmit covariance matrix has the eigen-value decomposition as*

$$\mathbf{R}_t = \mathbf{U}_t \; diag\left(\xi_1 \dots \xi_1 \; \xi_2 \dots \xi_2\right) \; \mathbf{U}_t^* \; , \tag{3.21}$$

in which L eigenvalues equal ξ_1 and $N - L$ equal ξ_2, provided $N > L > M$ and $\xi_1 > \xi_2$. With statistical CSIT, the threshold for $\mathbf{R}_t$ condition number, $\kappa = \xi_1/\xi_2$, above which

mode-dropping occurs at all SNRs, is given as

$$\kappa \geq \frac{L}{L-M} \ . \tag{3.22}$$

This condition requires $N \geq M+2$.

Proof: Given zero channel mean and transmit covariance (3.21), the optimal input covariance $\mathbf{Q}$ has the eigenvectors given by $\mathbf{U}_t$ (3.6). Again because of symmetry, the optimal power allocation has only two levels: λ_1 for the first L eigen-modes corresponding to the L larger eigenvalues of $\mathbf{R}_t$, and λ_2 for the rest $N-L$ modes. The optimal $\mathbf{Q}$ therefore has the EVD as

$$\mathbf{Q} = \mathbf{U}_t \mathbf{\Lambda}_Q \mathbf{U}_t^* \ , \tag{3.23}$$

where $\mathbf{\Lambda}_Q$ is a diagonal matrix with L diagonal entries as λ_1 and $N-L$ as λ_2.

From (2.18), the channel can be written as $\mathbf{H} = \mathbf{H}_w \mathbf{R}_t^{1/2}$. Let $\tilde{\mathbf{H}} = \mathbf{H}_w \mathbf{U}_t$, then the N columns of $\tilde{\mathbf{H}}$ are i.i.d. with distribution $\tilde{\mathbf{h}}_i \sim \mathcal{N}(\mathbf{0}, \mathbf{I}_M)$, $1 \leq i \leq N$. The mutual information optimization problem (3.1) is now equivalent to

$$\begin{aligned} \max_{\lambda_1,\lambda_2} \quad & E_{\mathbf{h}_i}\left[\log\det\left(\mathbf{I}_M + \gamma\lambda_1\xi_1 \sum_{j=1}^{L} \tilde{\mathbf{h}}_i\tilde{\mathbf{h}}_i^* + \gamma\lambda_2\xi_2 \sum_{j=L+1}^{N} \tilde{\mathbf{h}}_i\tilde{\mathbf{h}}_i^*\right)\right] \\ \text{subject to} \quad & L\lambda_1 + (N-L)\lambda_2 = 1 \\ & \lambda_1 \geq 0 \ , \ \ \lambda_2 \geq 0 \ . \end{aligned} \tag{3.24}$$

Of interest is the condition that results in the optimal $\lambda_2^\star = 0$ and $\lambda_1^\star = 1/L$.

Based on the convexity of this problem, the sufficient and necessary condition for the optimal $\lambda_2 = 0$ is

$$\mathrm{tr}\left(E_{\tilde{\mathbf{h}}_i}\left[\left(\mathbf{I}_M + \frac{\gamma\xi_1}{L}\sum_{j=1}^{L}\tilde{\mathbf{h}}_i\tilde{\mathbf{h}}_i^*\right)^{-1}(\gamma\xi_2+1)\right]\right) \leq M \ , \tag{3.25}$$

where $\tilde{\mathbf{h}}_j \sim \mathcal{N}(\mathbf{0}, \mathbf{I}_M)$. The derivation is given in Appendix A.2. At high SNRs

$(\gamma \to \infty)$, this condition becomes

$$\frac{L\xi_2}{\xi_1}\mathrm{tr}\left(E_{\tilde{\mathbf{h}}_i}\left[\left(\sum_{j=1}^{L}\tilde{\mathbf{h}}_i\tilde{\mathbf{h}}_i^*\right)^{-1}\right]\right) \leq M \ .$$

Noting that the matrix under expectation is an inverted complex central Wishart matrix with rank M and L degrees of freedom, which has the first moment as $\mathbf{I}_M/(L-M)$ [59, 47], the above condition results in (3.22). The finite expectation requires $L > M$, and since $N > L$, this relation implies $N \geq M+2$. Thus, mode dropping at all SNRs occurs only if $N \geq M+2$. Consequently, as the SNR increases to infinity, the optimal power allocation for this transmit covariance CSIT always activate at least $M+1$ modes. □

From (3.22), noting that $L/(L-M) \leq N-1$, a looser bound on $\mathbf{R}_t$ condition number for dropping the weaker eigen-modes at all SNRs can be obtained as

$$\kappa = \frac{\xi_1}{\xi_2} \geq N-1 \ . \tag{3.26}$$

This condition can be used as the first check for mode-dropping.

Figure 3.5 shows an example of the optimal power allocation for a 4×2 zero-mean channel with transmit covariance eigenvalues as [1.25 1.25 1.25 0.25]. This covariance matrix has the condition number $\kappa = 5 > 3$, satisfying (3.22). The optimal power allocation therefore only activates 3 modes, dropping 1 mode, at all SNRs.

Remarks

The two conditions (3.16) and (3.22), although specific to each respective channel and CSIT model, provide intuition on effects of the channel mean and the transmit antenna correlation on the optimal input power allocation. The conditions for channels with both non-zero mean and transmit antenna correlation are likely to be further relaxed, such that mode dropping occurs at all SNRs for even a lower K factor and a lower correlation condition number. Subsequently, for $N > M$, channels with high K or strong transmit antenna correlation tend to result in mode dropping with statistical CSIT at all SNRs.

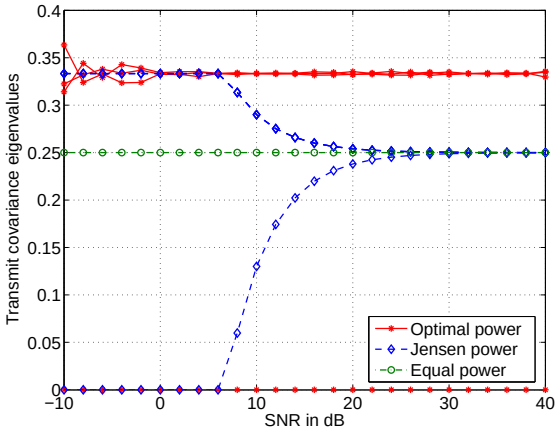

Figure 3.5: Input power allocations for a 4×2 zero-mean channel with transmit covariance eigenvalues [1.25 1.25 1.25 0.25]. Each allocation scheme contains 4 power levels, corresponding to the 4 eigen-modes of the transmit covariance. The optimal allocation has 3 equal modes, as does the Jensen power at low SNRs. The fourth mode of the optimal scheme always has zero power.

3.4 Capacity optimization

The previous sections have analytically established asymptotic capacity gains and the optimal input covariance at low and high SNRs. This section focuses on building an optimization program to solve for the capacity (3.1) non-asymptotically at any SNR. The program assumes channel model (2.28), in which the channel has a non-zero mean and correlated transmit antennas, but uncorrelated receive. The transmitter has statistical CSIT consisting of the mean and the transmit covariance.

Problem (3.1) is convex, hence solving for $\mathbf{Q}$ can be performed numerically up to a desired precision. Since $\mathbf{Q}$ is a Hermitian matrix of size $N\times N$, it contains N^2 real scalar variables. These include N real entries on the diagonal and $\frac{1}{2}N(N-1)$ complex entries in the upper triangle, each contributes two real variables. Thus, the optimization variable size is N^2.

For the special CSIT cases, in which the eigenvectors $\mathbf{U}_Q$ of the optimal $\mathbf{Q}$ are known analytically (3.4, 3.6), the optimization only needs to find the eigenvalues $\mathbf{\Lambda}_Q$. Let

$$\mathbf{S} = \gamma \mathbf{U}_Q^* \mathbf{H}^* \mathbf{H} \mathbf{U}_Q \ , \tag{3.27}$$

then $\mathbf{S}$ is known perfectly at the receiver and its distribution is known at the transmitter. Using $\det(\mathbf{I}+AB)=\det(\mathbf{I}+BA)$, problem (3.1) now becomes

$$\begin{aligned} \max \quad & E_{\mathbf{S}}[\log\det(\mathbf{I}+\mathbf{S}\mathbf{\Lambda_Q})] \\ \text{subject to} \quad & \begin{aligned} \operatorname{tr}(\mathbf{\Lambda}_Q) &= 1 \\ \mathbf{\Lambda}_Q &\succcurlyeq 0\,, \end{aligned} \end{aligned} \tag{3.28}$$

where $\mathbf{\Lambda}_Q$ is a diagonal matrix of size $N\times N$, and the expectation is performed over the known distribution of $\mathbf{S}$. The number of unknowns here is reduced to N real variables.

3.4.1 Convex optimization methods

The Newton method is used to solve both problems (3.1) and (3.28). In problem (3.1), when the positive semidefinite constraint $\mathbf{Q}\succcurlyeq 0$ is active, meaning some eigenvalues of the optimal $\mathbf{Q}$ are zero, the program employs a barrier interior-point method, using the Newton method for the inner iterations [54]. Such a barrier implementation is not necessary for problem (3.28) because of the simple diagonal structure of $\mathbf{\Lambda}_Q$. In both problems, since the expectation in the objective function has no closed-form, the underlying stochastic nature complicates the optimization by making it difficult to compute the exact function value, the gradient, and the Hessian needed at each optimization step. These values are approximated using sets of channel samples. As the number of transmit antennas N grows, the number of samples needs to be increased. The gap between the current function value and the optimal value, or the function gap-to-optimal value used in the stopping criterion, is also approximated by Monte-Carlo simulations. Therefore, the variance of these sample means dictates the numerical precision.

Solving for the eigenvalues $\mathbf{\Lambda}_Q$ in the special CSIT cases

Consider first the simpler problem (3.28) with N real variables. Denote $\lambda=\operatorname{diag}(\mathbf{\Lambda}_Q)$, a real column-vector consisting of the N unknown eigenvalues. The problem becomes an optimization in λ with the equality constraint $\mathbf{1}^T\lambda=1$ and inequality $\lambda\succcurlyeq 0$ (element-wise). The Newton method can be implemented very efficiently. The condition $\lambda\succcurlyeq 0$ is handled as follows: when ever a Newton step produces a negative λ_i value, this eigenvalue

is set to zero, and the optimization continues with the other variables, re-adjusted for the unit sum. This step is equivalent to dropping a mode in a water-filling process.

The Newton method requires calculating the gradient and the Hessian of the objective function. Noting that the objective function in (3.28) has no closed-form, the expectation operator is approximated by taking the sample mean over a set of channel samples. An independent set of samples is generated for each Newton step to ensure that the approximation, and therefore the optimization result, is independent of any particular sample set. For each channel sample, compute the following matrices

$$\mathbf{P} = \mathbf{I} + \mathbf{S}\boldsymbol{\Lambda} \;, \quad \mathbf{Y} = \mathbf{P}^{-1} \;, \quad \mathbf{Z} = \mathbf{Y}\mathbf{S} \;. \tag{3.29}$$

The largest computational cost is calculating $\mathbf{Y}$, due to the matrix inversion. The gradient of the log det function in (3.28) with respect to λ is then a $N \times 1$ row-vector with elements given by [60]

$$(\nabla g)_i = -E\left[\mathrm{tr}\left(\mathbf{P}^{-1}\frac{\partial \mathbf{P}}{\partial \lambda_i}\right)\right] = -E\left[\tilde{\mathbf{y}}_i^T \mathbf{s}_i\right] = -E\left[Z_{ii}\right] \;, \quad i = 1 \ldots N$$

where $\tilde{\mathbf{y}}_i^T$ is row i of $\mathbf{Y}$, $\mathbf{s}_i$ is column i of $\mathbf{S}$, and Z_{ii} is the i^{th} diagonal element of $\mathbf{Z}$. The Hessian can also be formed as a $N \times N$ matrix with elements given by

$$\left(\nabla^2 g\right)_{ij} = E\left[\mathrm{tr}\left(\mathbf{P}^{-1}\frac{\partial \mathbf{P}}{\partial \lambda_i}\mathbf{P}^{-1}\frac{\partial \mathbf{P}}{\partial \lambda_j}\right)\right] = E\left[\tilde{\mathbf{y}}_j^T \mathbf{s}_i \tilde{\mathbf{y}}_i^T \mathbf{s}_j\right] = E\left[Z_{ji} Z_{ij}\right] \;, \quad i,j = 1 \ldots N \;. \tag{3.30}$$

The gradient and the Hessian of the objective function are then obtained as the mean of these values over all channel samples.

For these special CSIT cases, transmit power optimization (3.28) can also be efficiently performed using an iterative algorithm involving the MMSE of the data streams transmitted on separate eigen-beams [61]. This algorithm requires predetermined beam directions and finds the optimal power allocation along those beams. For general statistical CSIT, however, the optimal beam directions are still unknown. The next section describes a method for solving for the optimal $\mathbf{Q}^\star$ in that case.

Solving for the covariance Q in the general case

The general problem (3.1) is similarly solved using the Newton method. Because of the matrix form of the unknown $\mathbf{Q}$, however, the PSD constraint $\mathbf{Q} \succcurlyeq 0$ needs special handling. Specifically, a barrier interior-point method is implemented if this constraint is active, meaning the optimal $\mathbf{Q}$ has at least one zero-eigenvalue. This condition is heuristically established when the initial Newton step without involving the PSD constraint produces a non-positive semidefinite $\mathbf{Q}$. Otherwise, the program proceeds, ignoring the PSD constraint. By using a good starting point (such as the Jensen covariance in Section 3.5.1), this heuristic check leads to the optimal solution, while reducing the run time.

For the Newton method, the objective function value and its gradient and Hessian are again approximated by sample means, using an independent set of channel samples at each step. The gradient and the Hessian in each Newton step are computed as follows. Since $\mathbf{Q}$ is a Hermitian matrix, form a vector of unknown variables from the real and imaginary parts of $\mathbf{Q}$ as

$$\mathbf{q} = \left[\frac{q_{11}}{2} \cdots \frac{q_{NN}}{2}\ q_{R21}\ q_{R32} \cdots q_{RN1}\ q_{I21}\ q_{I32} \cdots q_{IN1}\right]^T , \tag{3.31}$$

where $\mathbf{Q}_R = \mathcal{R}e(\mathbf{Q})$, $\mathbf{Q}_I = \mathcal{I}m(\mathbf{Q})$, and the lower-case letters refer to the entries in the corresponding upper-case matrix with the same subscript. The factor $\frac{1}{2}$ is introduced for uniformity in the gradient and the Hessian formula (with respect to $\mathbf{q}$). The length of $\mathbf{q}$ is N^2. For each channel sample, compute $\mathbf{G} = \gamma \mathbf{H}^* \mathbf{H}$ and

$$\mathbf{R} = \mathbf{I} + \mathbf{G}\mathbf{Q}\ , \quad \mathbf{W} = \mathbf{R}^{-1}\ , \quad \mathbf{X} = \mathbf{W}\mathbf{G}\ . \tag{3.32}$$

The most intensive step is to compute $\mathbf{W}$, involving matrix inversion. Once $\mathbf{X}$ is computed, the gradient and the Hessian follow directly. Noting that $\mathbf{X}$ is Hermitian, the gradient of the log det function in (3.1) has the elements given as

$$\begin{aligned} \frac{\partial f}{\partial q_{Rij}} &= -E\left[\mathrm{tr}\left(\mathbf{R}^{-1}\frac{\partial \mathbf{R}}{\partial q_{Rij}}\right)\right] = -E\left[\tilde{\mathbf{w}}_j^T \mathbf{g}_i + \tilde{\mathbf{w}}_i^T \mathbf{g}_j\right] = -2E\left[\mathcal{R}e(\mathbf{X})_{ij}\right] \\ \frac{\partial f}{\partial q_{Iij}} &= -E\left[\mathrm{tr}\left(\mathbf{R}^{-1}\frac{\partial \mathbf{R}}{\partial q_{Iij}}\right)\right] = -jE\left[\tilde{\mathbf{w}}_j^T \mathbf{g}_i - \tilde{\mathbf{w}}_i^T \mathbf{g}_j\right] = -2E\left[\mathcal{I}m(\mathbf{X})_{ij}\right]\ , \end{aligned} \tag{3.33}$$

where $\tilde{\mathbf{w}}_i^T$ is row i of $\mathbf{W}$, $\mathbf{g}_i$ is column i of $\mathbf{G}$, and $\mathcal{R}e(.)$ and $\mathcal{I}m(.)$ represent the real and imaginary parts. The Hessian has the elements calculated as

$$\begin{aligned}
\frac{\partial^2 f}{\partial q_{Rij}\partial q_{Rkl}} &= 2E\left[\mathcal{R}e(X_{lj}X_{ik} + X_{kj}X_{il})\right] \\
\frac{\partial^2 f}{\partial q_{Iij}\partial q_{Ikl}} &= 2E\left[\mathcal{R}e(X_{lj}X_{ik} - X_{kj}X_{il})\right] \\
\frac{\partial^2 f}{\partial q_{Rij}\partial q_{Ikl}} &= 2E\left[\mathcal{I}m(X_{lj}X_{ik} + X_{kj}X_{il})\right] \\
\frac{\partial^2 f}{\partial q_{Iij}\partial q_{Rkl}} &= 2E\left[\mathcal{I}m(-X_{lj}X_{ik} + X_{kj}X_{il})\right] \ .
\end{aligned} \tag{3.34}$$

The gradient and Hessian of the objective function are then obtained as the sample means of these values over all channel samples.

When the PSD constraint on $\mathbf{Q}$ is tight, equivalently the optimal input signal drops modes, the program uses the barrier method [54], which iteratively solves the following problem for different values of t:

$$\begin{aligned}
\max \quad & E_{\mathbf{G}}[\log\det(\mathbf{I} + \mathbf{G}\mathbf{Q})] + \log\det(\mathbf{Q})/t \\
\text{subject to} \quad & \mathrm{tr}(\mathbf{Q}) = 1 \ ,
\end{aligned} \tag{3.35}$$

where $\mathbf{G} = \gamma\mathbf{H}^*\mathbf{H}$ and $t > 0$. The second term in the objective function, $\log\det(\mathbf{Q})/t$, ensures that $\mathbf{Q}$ stays PSD, by choosing a large enough initial value for t. Then during the optimization, if any eigenvalue of $\mathbf{Q}$ approaches zero, $\log\det(\mathbf{Q})/t$ approaches minus infinity, preventing this eigenvalue from becoming negative.

Solving (3.35) involves two iterative loops. The inner loop uses the Newton method to find $\mathbf{Q}^\star$, given a value of t. The additional term $\log\det(\mathbf{Q})/t$ is independent of the channel, thus its gradient and Hessian, established similarly to (3.33) and (3.34) respectively, can be calculated exactly with little overhead. Then the outer loop increases the barrier value t by multiplying it with μ, a positive optimization parameter. This increase in t leads to diminishing impact of $\log\det(\mathbf{Q})/t$ on the optimal function value. The inner optimization is performed again for the new value of t, using the previous optimal $\mathbf{Q}^\star$ as the starting point. Since this starting point is PSD and close to optimal, the new $\mathbf{Q}^\star$ is also PSD,

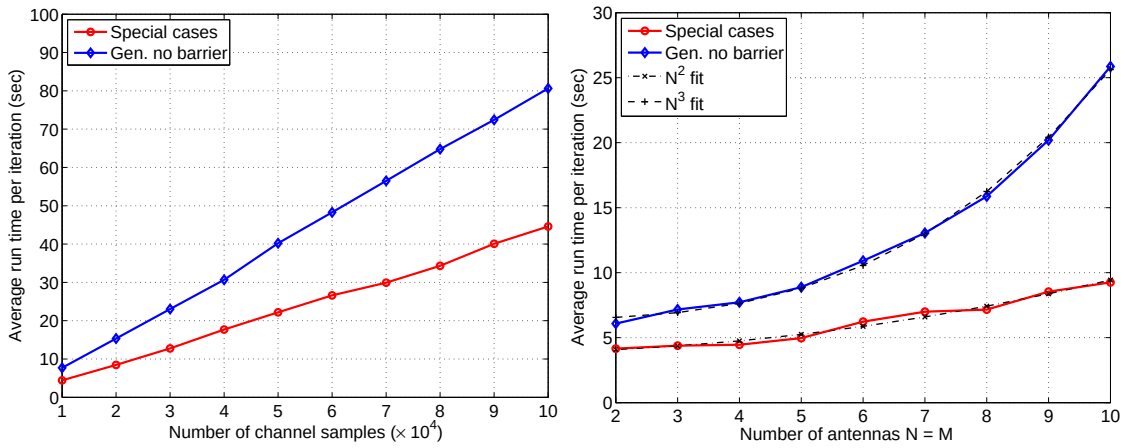

(a) (b)

Figure 3.6: Optimization runtime complexity versus (a) the number of channel samples (at $N = M = 4$) and (b) the number of antennas ($N = M$, at 10000 samples).

ensured by $\log\det(\mathbf{Q})/t$. The two steps are repeated until a desired tolerance is satisfied. Thus, the barrier implementation takes longer to execute because of this double loop.

3.4.2 Optimization complexity and examples

Complexity assessment

The optimization programs were written using Matlab. Figure 3.6 shows the computational complexity in terms of program runtime per Newton iteration versus both the number of channel samples and the number of antennas $N = M$. The runtime scales linearly with the number of channel samples, but at different rates for each problem (3.1) and (3.28). For the number of transmit antennas N in the range of interest ($N \leq 10$), the runtime for the special-case problem (3.28) scales as N^2, faster than the order of N^3 predicted by theory [54]. For the general-case problem (3.1) without the barrier implementation, the runtime scales as N^3, not N^6 as theoretically predicted.

Numerical examples

Figure 3.7 presents an example of the optimization process for the general problem (3.1), showing the mutual information value and its gap to the optimal value versus the number

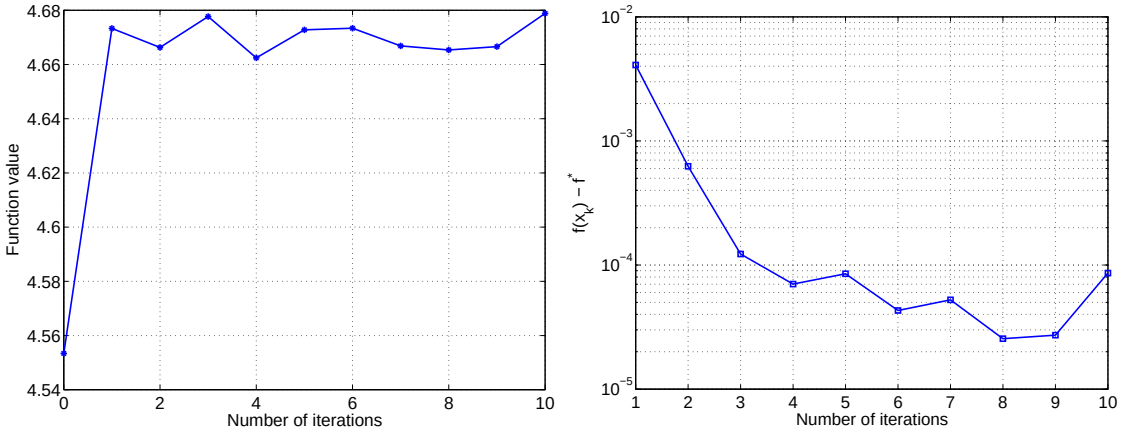

(a) (b)

Figure 3.7: An optimization example of finding the ergodic capacity of a 4×2 channel at SNR $= 10$dB, using 20000 independently generated channel samples in each iteration. The optimization and channel parameters are given in Appendix B.2. (a) Mutual information value (nats/sec/Hz); (b) Its gap-to-optimal.

of Newton iterations. This example does not invoke the barrier method. The optimization parameters and channel mean and covariance are given in the Appendix B.2. The optimization chooses the starting point as the Jensen covariance (see Section 3.5.1), resulting in a fast convergence. The fluctuation in the function value and its gap-to-optimal value over different iterations is caused by the approximation of expected values as sample means, using an independent sample set at each iteration. Thus, the function error-floor in Figure 3.7(b) is dictated by the number of channel samples, but not the number of iterations as in deterministic optimization.

3.5 Capacity analysis using the optimization program

The developed program provides a way of evaluating the capacity of a MIMO channel with statistical CSIT (channel mean and transmit covariance) accurately. The optimization also results in the optimal input covariance $\mathbf{Q}^\star$, or its eigenvalues $\mathbf{\Lambda}^\star$ in the special cases. The program thus provides a handy tool to study the capacity and the effects of various channel parameters on it.

The numerical optimization, however, costs time and computational resource. Hence,

it is also of interest to find a simple bound to the capacity and an approximation of the optimal input covariance, which can provide analytical insight. The numerical optimization can help assess the tightness of such a bound.

The next section discusses a simple, sub-optimal input-covariance, based on the Jensen inequality, and the associated lower-bound to the capacity. Then using this bound and the numerical optimization program, MIMO capacity is analyzed in terms of various parameters: relative transmit-receive antenna configurations, the CSIT quality ρ, and the channel K factor.

3.5.1 Channel capacity and the Jensen-optimal input covariance

Consider maximizing Jensen's upper-bound on the mutual information, and using its optimizer $\mathbf{Q}_J$ to approximate the optimal input covariance $\mathbf{Q}^\star$. A closed-form analytical solution for $\mathbf{Q}_J$ is available. The Jensen bound on the average mutual information is

$$E\left[\log\det(\mathbf{I}+\mathbf{HQH}^*)\right] \quad \leq \quad \log\det\left(\mathbf{I}+E[\mathbf{H}^*\mathbf{H}]\mathbf{Q}\right) \ .$$

Since with statistical CSIT, the transmitter knows the channel distribution, it can establish $E[\mathbf{H}^*\mathbf{H}]$. Perform the eigenvalue decomposition

$$E[\mathbf{H}^*\mathbf{H}] = \mathbf{U}_R\mathbf{D}_R{\mathbf{U}_R}^* \ , \tag{3.36}$$

then the covariance $\mathbf{Q}_J$ that maximizes the Jensen bound has the eigenvectors given by $\mathbf{U}_R$, and the eigenvalues obtained by standard water-filling on $\mathbf{D}_R$ as

$$\lambda_i(\mathbf{Q}_J^\star) = \left(\mu - \frac{1}{\gamma d_{R,i}}\right)_+ \ , \quad i = 1\ldots N \ , \tag{3.37}$$

where $d_{R,i}$ are the diagonal elements of $\mathbf{D}_R$, and μ is chosen to satisfy $\sum_{i=1}^{N}\lambda_i(\mathbf{Q}_J) = 1$. That is

$$\mathbf{Q}_J = \mathbf{U}_R\mathbf{\Lambda}_J\mathbf{U}_R^* \ , \tag{3.38}$$

with $\mathbf{\Lambda}_J = \mathrm{diag}(\lambda_i)$ as given in (3.37).

Using the Jensen covariance $\mathbf{Q}_J$ as the input covariance results in a *Jensen mutual*

information value

$$\mathcal{I}_J = \mathcal{I}(\mathbf{Q}_J) \tag{3.39}$$

satisfying $\mathcal{I}_J \leq \mathcal{I}_o$ in (3.1). For statistical CSIT, $\mathcal{I}_J$ can be used to lower-bound the capacity. For dynamic CSIT, averaging $\mathcal{I}_J$ over the initial channel measurement distribution as in (3.2), a lower-bound to the channel ergodic capacity is obtained as

$$\mathcal{C}_J = E_{\mathbf{H}_0}[\mathcal{I}_J] \; . \tag{3.40}$$

The tightness of this capacity lower-bound depends on the tightness of the Jensen mutual information in (3.39).

Tightness of the capacity lower-bound based on the Jensen covariance

Using statistical CSIT as a representative, this section discusses the tightness of the Jensen mutual information (3.39) as a lower-bound to the capacity. The tightness depends on the relative transmit-receive antenna configuration and the SNR. For systems with equal or fewer transmit than receive antennas ($N \leq M$), results show that the Jensen mutual information is a tight lower-bound to the capacity at all SNRs. Any minor difference between $\mathcal{I}_J$ and $\mathcal{I}_o$ occurs only at mid-range SNRs, because of a small difference in power allocation. Otherwise, at low SNRs, the optimal power allocation is typically single mode, while at high SNRs, it approaches equi-power, as does the Jensen covariance. Figure 3.8 shows an example of the channel capacity and the Jensen mutual information for a 4×4 system in (a), together with the eigenvalues of $\mathbf{Q}^\star$ and $\mathbf{Q}_J$ in (b). The channel has a non-zero mean and transmit antenna correlation, given in Appendix B.2. The mutual information with equal power allocation is also included for comparison.

For systems with more transmit than receive antenna ($N > M$), the Jensen mutual information is also a tight lower-bound to the capacity at low SNRs. At high SNRs, however, it exhibits a gap to the capacity. This gap occurs depending on the channel mean and the transmit antenna correlation. A higher K or more correlated channel (measured by, for example, a higher condition number of the correlation matrix) will result in a bigger gap. The main reason for this gap at high SNRs is the difference in the

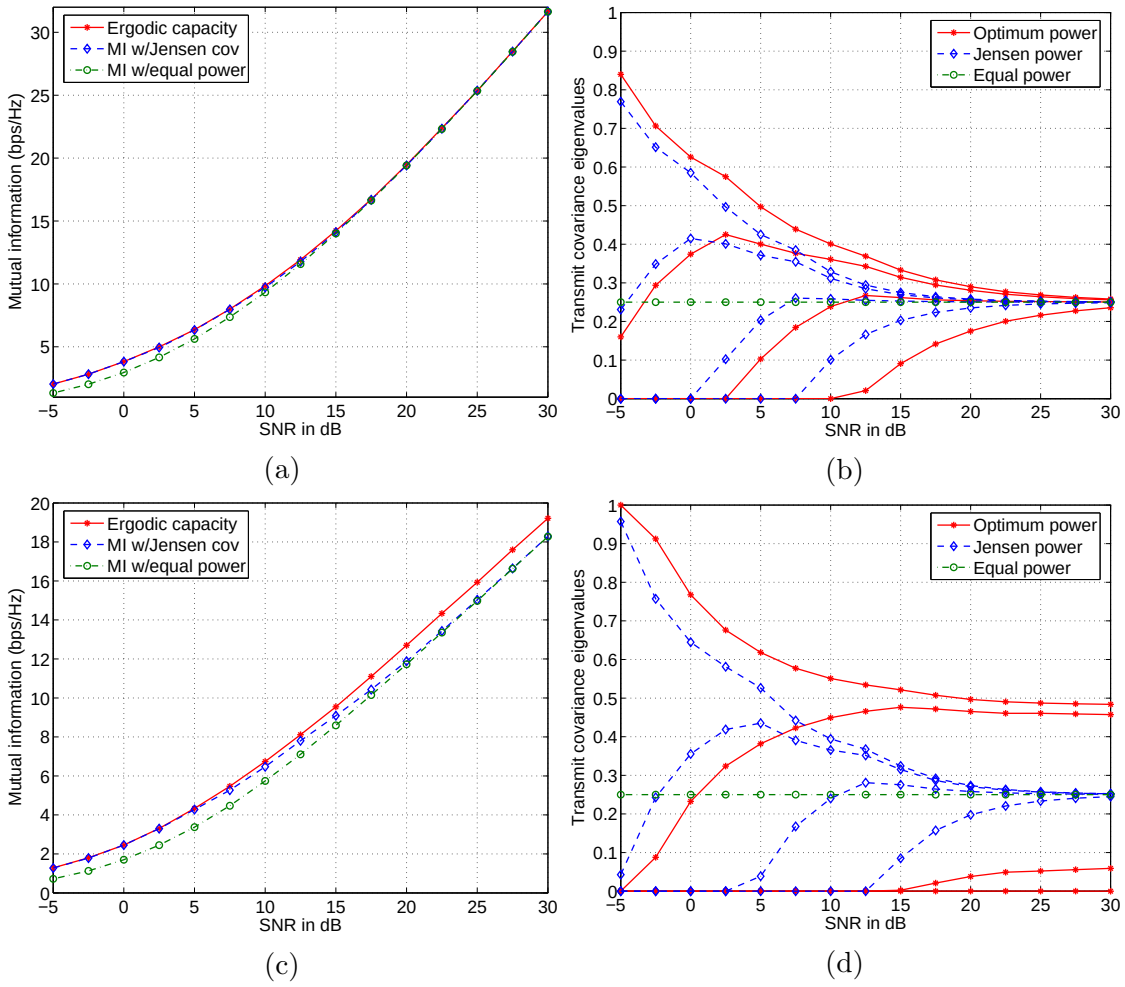

Figure 3.8: Capacity and mutual information of (a) a 4×4 system, (c) a 4×2 system; with the corresponding power allocations in (b) and (d). The channel mean and transmit covariance are specified in Appendix B.2.

power allocation. In contrast to equi-power in the Jensen solution, the capacity-optimal input can converge to non-equi-power. The optimal convergence values are still unknown analytically. Using simplified channel models, section 3.3 examines conditions for the optimal input to have at least one zero-power mode at high SNRs. Figures 3.8(c) and (d) illustrate the mutual information and the input power allocations for a 4×2 channel with the mean and correlation matrices given in Appendix B.2.

These comparisons also reveal that the value of CSIT depends on the antenna configuration and the SNR. For $N \leq M$, CSIT helps increase the capacity only at low SNRs. At high SNRs, the optimal input approaches equi-power and the capacity gain from CSIT

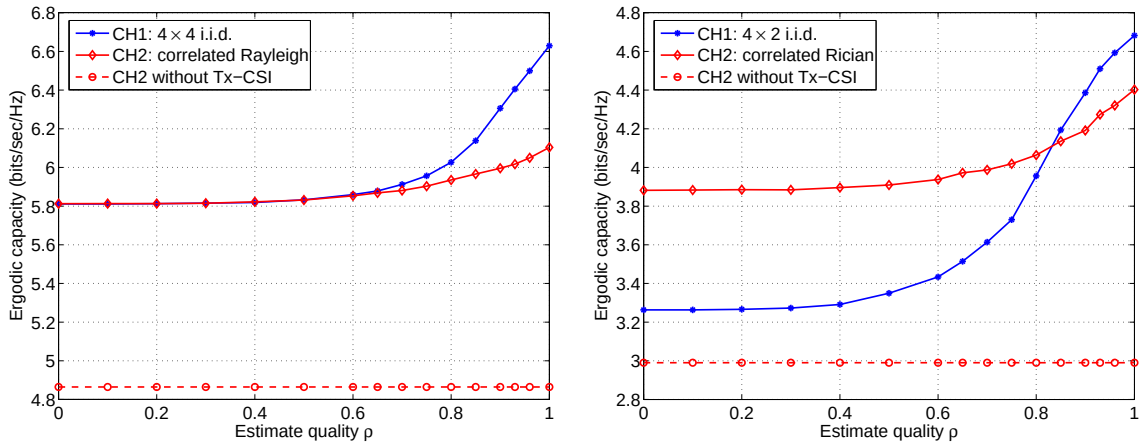

(a) 4×4 channels. (b) 4×2 channels.

Figure 3.9: Ergodic capacity versus the CSIT quality ρ at SNR = 4dB.

diminishes. For $N > M$, however, CSIT can help increase the capacity at all SNRs. The asymptotic capacity gains at low and high SNRs are quantified in Section 3.2.

3.5.2 The capacity versus dynamic CSIT quality

Since the Jensen mutual information is a tight lower-bound to the capacity at low SNRs, it is used to plot the capacity versus the CSIT quality ρ in Figure 3.9. The capacity increases with higher ρ. The increment, however, is sensitive to ρ only when ρ is larger than about 0.6, corresponding to a relatively good channel estimate. This observation implies that in dynamic CSIT, the initial channel measurement adds value only when its correlation with the current channel is relatively strong; otherwise, the channel statistics provide most information.

Two antenna configurations are examined in Figure 3.9: 4×4 in (a) and 4×2 in (b). In each configuration, an i.i.d. Rayleigh fading channel and a correlated Rician channel are studied. The mean and covariance matrices of the correlated Rician channels are given in Appendix B.2. Results show that the range of capacity gain from the CSIT for the i.i.d. channels is larger than for the correlated ones. Note that as the SNR increases, the capacity gains for the 4×4 channels decrease to 0, but increase for the 4×2 channels to up to 2 bps/Hz (3.11). For reference, the capacity of the correlated Rician channels without CSIT is also included. For correlated Rician channels, knowing the channel statistics

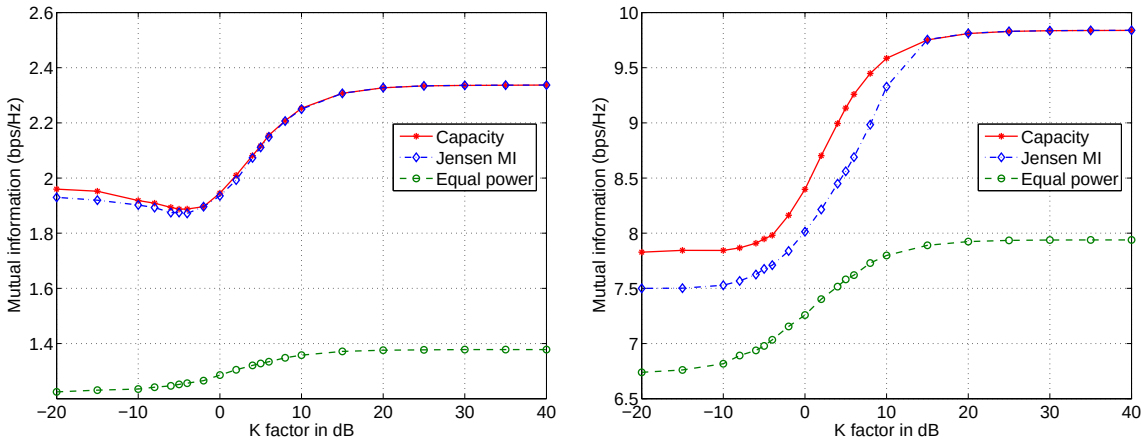

(a) SNR = -2dB. (b) SNR = 12dB.

Figure 3.10: Ergodic capacity and mutual information versus the K factor.

alone ($\rho = 0$) can enhance the capacity. Furthermore, at low SNRs, correlated Rician channels can have higher capacity than i.i.d. Rayleigh ones, as shown in (b).

3.5.3 Effects of the K factor

The channel Rician K factor affects the ergodic capacity differently depending on the SNR. Figure 3.10 shows the capacity versus K at two different SNRs for 4×2 channels with the mean and covariance given in Appendix B.2. Notice that at a low SNR (-2dB), the capacity is a non-monotonous function of the K factor, and a minimum exists. This effect is partly caused by the transmit antenna correlation impact: at low K, the correlation effect becomes more dominant, and at low SNRs, this correlation helps increase the capacity. At a higher SNR (12 dB), the correlation impact diminishes for full-rank correlation. Provided that the channel mean is also full-rank, the capacity then monotonically increases with the K factor. The increment, however, diminishes with higher K.

For systems with more transmit than receive antennas, a higher K factor also causes the SNR point, at which the Jensen mutual information starts diverging from the channel capacity, to increase. This effect implies that with higher K factor, the Jensen mutual information is a tight lower-bound to the capacity for a larger range of SNRs. Figure 3.11 presents this K factor threshold versus the SNR for the 4×2 channels. When K is above this threshold, the Jensen mutual information tightly lower-bounds the capacity.

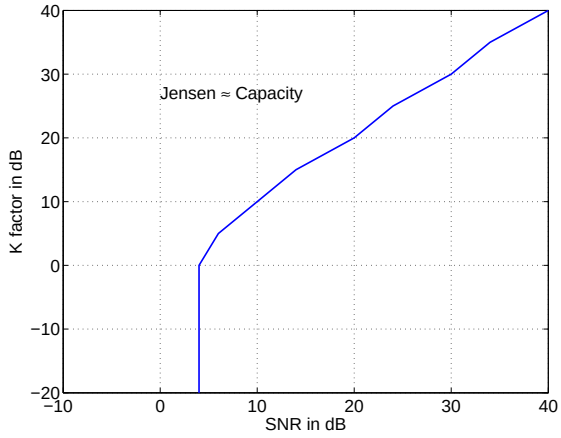

Figure 3.11: K factor threshold for the 4×2 channels for tight lower-bound of the ergodic capacity by the Jensen mutual information (difference < 0.03 bps/Hz).

The difference then is less than 0.03 bps/Hz, which is within the numerical precision for optimizing the capacity.

3.6 Chapter summary

This chapter has studied the MIMO capacity with dynamic CSIT. The study contains two parts: an analysis of the capacity gain and optimal input asymptotically at low and high SNRs, and a convex optimization program to find the capacity numerically. The analysis shows that, at low SNRs, dynamic CSIT helps increase the capacity multiplicatively, and the optimal input is typically simple single-mode beamforming. At high SNRs, the capacity gain depends on the relative number of antennas. For systems with equal or fewer transmit than receive antennas, the gain diminishes to zero, since the optimal input approaches equi-power with increasing SNR. For systems with more transmit than receive antennas, however, the gain may exist even at high SNRs and depends on the CSIT. Specifically, systems with strong transmit antenna correlation or strong mean can lead to an additive capacity gain with the CSIT, produced by an optimal input with mode-dropping at high SNRs. For systems with rank-deficient transmit correlation, knowing this correlation at the transmitter can also additively increase the capacity at high SNRs.

The second part focuses on a convex program to calculate the capacity with statistical CSIT, involving a non-zero mean and transmit antenna correlation. The program employs the Newton and barrier interior-point methods. Due to the underlying stochastic nature, the gradient, Hessian, and function values in each Newton step are evaluated using Monte-Carlo simulations. The computational cost grows linearly with the number of channel samples in Monte-Carlo, and quadratically-to-cubically with the number of transmit antennas. The program is then used to assess a capacity lower-bound based on the Jensen-optimal input. This simple lower-bound is often tight at all SNRs for systems with equal or fewer transmit than receive antennas. For others, the bound is tight at low SNRs but diverges at high SNRs. This divergence at high SNRs is caused by the difference in power allocation and depends on the CSIT – the channel mean and the transmit antenna correlation. A stronger mean or correlation causes a larger divergence. Furthermore, a higher channel K factor results in later divergence at a higher SNR.

Applied to dynamic CSIT, optimization results illustrate an increasing capacity with better CSIT quality ρ. The capacity gain from the CSIT, however, is sensitive to ρ for large ρ only, at roughly $\rho \geq 0.6$. Otherwise, the gain equals that with $\rho = 0$, corresponding to statistical CSIT. Furthermore, the capacity gain depends not only on ρ but also on the channel statistics. Compared to a correlated Rician channel, the gain is higher for an i.i.d. Rayleigh fading channel at high CSIT quality ρ, but becomes lower as ρ decreases.

Having analyzed the capacity gain from dynamic CSIT, the next chapter will discuss precoding designs to exploit the CSIT.

Chapter 4

PRECODING SCHEMES EXPLOITING DYNAMIC CSIT

Precoding is a transmitter processing technique that exploits CSIT. As discussed in Section 1.2, the separation between a precoder, dependent on the CSIT, and a channel code, independent of the CSIT, is capacity-optimal for many CSIT forms, including dynamic CSIT. For flat-fading MIMO channels, the optimal precoder is linear. It functions as a multimode beamformer. The beam directions and power allocation are the left singular vectors and the squared singular values of the precoding matrix, respectively. The right singular vectors function as an input shaping matrix.

This chapter focuses on designing linear precoders for dynamic CSIT. A precoder can be designed according to alternative criteria, roughly categorized as fundamental and practical. An example of a fundamental criterion is the system ergodic capacity. The precoder then shapes the covariance of the optimal zero-mean Gaussian input. A practical criterion, on the other hand, can be minimizing an error probability for a specific system. A common system configuration includes a space-time block code (STBC) exploiting channel diversity and a linear precoder exploiting the CSIT. STBCs are often designed for i.i.d. Rayleigh fading channels, assuming no CSIT. The STBC and precoder combination, therefore, is robust to channel fading and can exploit the available CSIT at the same time. Moreover, if the STBC is capacity-lossless without CSIT, then the combined configuration

is capacity-optimal with CSIT. Such a setup also provides flexibility in designing precoders to adapt to various CSIT conditions, without changing the STBC or the detection scheme in an existing system.

MIMO precoding design has been an active research area. Many of the earlier designs focused on the perfect CSIT case, often jointly optimizing both the precoder and decoder for various performance criteria based on the MSE or the SNR [62, 63, 64]. More recent work considered partial CSIT, but only the special cases of transmit covariance CSIT and mean CSIT. These include precoders optimal for the channel ergodic capacity, given transmit covariance CSIT [48, 49, 55], or mean CSIT [48, 50, 65]. Others are based on an error rate criterion with mean CSIT [42, 66, 67], or transmit covariance CSIT [68, 69]. The precoding solutions for these partial-CSIT cases then reduce to fixed beam directions at all SNRs, given by the singular- or eigen-vectors of the mean or transmit covariance matrix, with per-beam power allocation, obtained by a numerical water-filling solution dependent on the SNR.

This chapter first considers a precoder that simultaneously exploits both the channel mean and the transmit covariance to minimize the pair-wise error probability (PEP) in MIMO systems. Because of the interaction of the mean and the covariance, the precoder solution does not have predetermined beam directions. Instead, both the direction and power loading of each beam depend on both the mean and covariance matrices, and are functions of the SNR. The optimal precoder is established using a *dynamic* water-filling process, in which the beams direction and power evolve with each iteration. Asymptotic analyses reveal that the precoder depends primarily on the channel mean at high K factors and primarily on the transmit covariance at high SNRs.

The precoder can be directly applied to dynamic CSIT, exploiting the effective mean and effective transmit covariance. It achieves a coding gain in the form of an SNR advantage, attributed to the optimal beam directions and the water-filling-type power allocation among these beams. When the CSIT is partial, no diversity gain can be extracted from the channel information. The transmit diversity is then controlled by the STBC. When the CSIT is perfect, the precoder achieves the maximum diversity order, together with the coding gain.

In addition to the PEP-based precoder, this chapter also briefly examines precoders based on the capacity of a system using a predetermined code, posed as a stochastic optimization problems. Only special CSIT cases are considered here. The precoder optimal input shaping matrix and beam directions are discussed. The chapter then provides a comparative analysis of these different precoders in terms of structure and performance.

The chapter is organized as follows. Section 4.1 outlines the system configuration. Section 4.2 discusses the precoding design criteria based on the PEP and the system capacity. The optimal precoder based on the PEP is discussed in Section 4.3. Section 4.4 analyzes the gain, asymptotic behavior, and special cases of this precoder design. Other precoding designs based on the system capacity, generalized to stochastic criteria, for special CSIT cases are discussed in Section 4.5. Section 4.6 compares these precoders structure and performance. Finally, Section 4.7 provides a summary.

4.1 System configuration

For precoding design, consider a Rician channel with transmit antenna correlation alone. The channel model is given in (2.18), but with $\mathbf{R}_r = \mathbf{I}$. Furthermore, the transmit covariance matrix $\mathbf{R}_t$ is assumed to be full-rank and, hence, is invertible. The rank of the channel mean $\mathbf{H}_m$, on the other hand, can be arbitrary. Dynamic CSIT for this channel is obtained accordingly from (2.25) and (2.27). Since dynamic CSIT consists of an effective channel mean and an effective covariance, a precoding design for dynamic CSIT can also be applied to any CSIT model with known channel mean and covariance at the transmitter. Thus, in the sequel, design algorithms are developed for the representative case of statistical CSIT, consisting of the mean $\mathbf{H}_m$ and the transmit covariance $\mathbf{R}_t$. The algorithms can then be applied to dynamic CSIT by replacing $\mathbf{H}_m$ with the effective mean and $\mathbf{R}_t$ with the effective transmit covariance.

Consider a system in which the transmitter contains an encoder and a linear precoder, depicted in Figure 4.1. The encoder assumes no channel knowledge, and the precoder exploits the CSIT. The encoder can include either a channel code, a space-time code, or

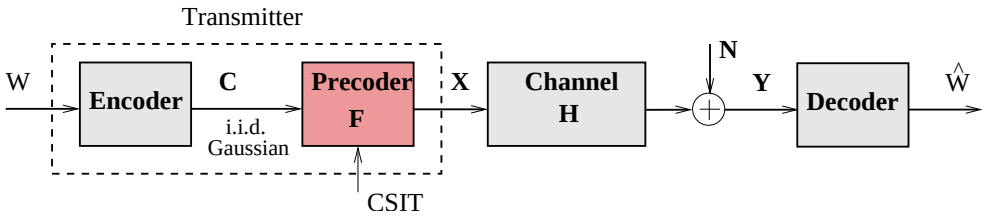

Figure 4.1: Configuration of a system with linear precoder.

both. In such a system, the precoder can be viewed as a processing block to enhance performance in addition to existing codes, based on the available CSIT. This scenario covers many practical wireless systems, such as those in wireless local-area-networks (802.11) and metropolitan-area-networks (802.16). Furthermore, if the encoder is capacity-optimal for a channel without CSIT, then combining it with a linear precoder is optimal with CSIT [13]. The capacity-optimal signal for an i.i.d. Rayleigh fading MIMO channel without CSIT is zero-mean complex Gaussian with an identity covariance matrix [6]. Therefore, the linear precoder has the effect of shaping the transmit signal, such that it has a covariance matrix optimal for the channel with CSIT.

At each time instant, the linear precoder functions as a beamformer with either one or multiple beams, as analyzed in Section 1.3. The beam directions are the left singular vectors of the precoder matrix; the beam power loadings are the squared singular values. The precoder right singular vectors form an input shaping matrix, which combines the output symbols of the encoder to feed into each beam. A separate precoder provides the flexibility of adapting to various CSIT conditions, without changing the encoder or the detection algorithm already implemented. Detection in a system with precoding is performed over the effective channel created by the precoder and the actual channel. The receiver can construct the precoder using the same algorithm and parameters as the transmitter, which implicitly implies that the receiver must know all the parameters that the transmitter knows. This assumption is reasonable since the receiver can usually obtain channel measurements more readily than the transmitter through the use of pilots, and both can agree on using the same precoding design algorithm.

To maintain a constant average sum transmit power, the precoding matrix must satisfy

the power constraint

$$\mathrm{tr}(\mathbf{F}\mathbf{F}^*) = 1. \tag{4.1}$$

Consider a block encoder with $\mathbf{C}$ as a codeword of size $N \times T$, the receive signal block, of size $M \times T$, can be written as

$$\mathbf{Y} = \mathbf{HFC} + \mathbf{N}\,,$$

where $\mathbf{N} \sim \mathcal{N}(0, \mathbf{I}\sigma^2)$ is the additive complex white Gaussian noise, with σ^2 being the noise power per spatial dimension. The codeword $\mathbf{C}$ here has been scaled according to the transmit power.

To focus on exploiting CSIT, the ideal maximum-likelihood (ML) receiver is used. The decoded codeword therefore is obtained as

$$\hat{\mathbf{C}} = \arg\min_{\mathbf{C}\in\mathbb{C}} ||\mathbf{Y} - \mathbf{HFC}||_F^2\,, \tag{4.2}$$

where $\mathbb{C}$ is the codebook, and the subscript F here denotes the Frobenius norm.

4.2 Precoding design criteria

A linear precoder can be designed based on alternate criteria, using either a fundamental or practical measure. The fundamental measures include the capacity and the error exponent, while the practical measures contain, for example, the pair-wise error probability (PEP), detection mean square-error (MSE), and the received SNR [19]. Fundamental measures usually assume ideal channel coding. The ergodic capacity assumes that the channel evolves through all possible realizations over arbitrarily long codewords, while the error exponent applies for finite codeword lengths. Analyses using practical measures, on the other hand, usually apply to uncoded systems and assume a quasi-static block-fading channel. The choice of the design criterion depends on the system setup, operating parameters, and the channel (fast or slow fading). For examples, systems with strong channel coding, such as turbo or low-density parity check codes with long codewords, may operate at close to the capacity limit and thus are qualified to use a coded fundamental criterion.

Those with weaker channel codes, such as convolutional codes with small free distances, are more suitable using a practical measure with uncoded analysis. The operating SNR is also important in deciding the criterion. A lower SNR usually favors uncoded analysis, while at high SNR, precoders designed according to coded criteria can yield better performance.

Two criteria are considered in this thesis: the pair-wise error probability (PEP) and the system capacity. The PEP criterion represents a group of optimization problems with closed-form, deterministic objective function. Based on the PEP, an optimal precoder with dynamic CSIT is obtained in Section 4.3. The system capacity criterion, on the other hand, represents a group of optimization problem with non-closed-form, stochastic objective function. For this group, only precoders for the special cases, mean CSIT and covariance CSIT, are analyzed in Section 4.5. These two criteria are established next.

4.2.1 The pair-wise error probability measure

The pair-wise error probability is the probability that a codeword $\hat{\mathbf{C}}$ has a better detection metric than the transmitted codeword $\mathbf{C}$. With ML detection (4.2), applying the Chernoff bound, similar to [70], the PEP can be tightly upper-bounded by

$$P(\mathbf{C} \to \hat{\mathbf{C}}) \leq \exp\left(-\frac{||\mathbf{HF}(\mathbf{C}-\hat{\mathbf{C}})||_F^2}{4\sigma^2}\right). \tag{4.3}$$

The PEP depends on the codeword pair $(\mathbf{C}, \hat{\mathbf{C}})$, in particular, the codeword distance product matrix defined as

$$\mathbf{A} = \frac{1}{P}(\mathbf{C}-\hat{\mathbf{C}})(\mathbf{C}-\hat{\mathbf{C}})^*, \tag{4.4}$$

where P is the average sum transmit power. Since $\mathbf{C}$ is scaled according to the transmit power, this normalization ensures that $\mathbf{A}$ is power-independent. The Chernoff bound (4.3) can then be written as

$$f(\mathbf{H}, \mathbf{A}, \mathbf{F}) = \exp\left(-\frac{\gamma}{4}\mathrm{tr}\left(\mathbf{HFAF}^*\mathbf{H}^*\right)\right), \tag{4.5}$$

where $\gamma = P/\sigma^2$ is the SNR.

While the PEP is not the system codeword-error rate, it is a measure strongly related to the system performance. The system average codeword-error probability can be written as

$$\bar{P}_e = E_{\mathbf{H}}\left[\sum_i p_i \Pr\Big(\bigcup_{j\neq i}(\mathbf{C}_i \to \mathbf{C}_j)\Big)\right],$$

where p_i is the probability of the codeword $\mathbf{C}_i$, and $(\mathbf{C}_i \to \mathbf{C}_j)$ is the event that $\mathbf{C}_i$ is mis-detected as $\mathbf{C}_j$. The above error expression is usually not tractable and, therefore, does not lend itself to the analysis of the precoder design problem. The PEP, averaged over the channel fading, is chosen instead as the performance criterion. The exact PEP expression, however, is still complex to analyze. Therefore, the precoder is designed to minimize the Chernoff upper-bound on the PEP. The Chernoff bound tracks the performance well and provides an analytical framework for establishing closed-form precoder solutions. The PEP with the Chernoff bound is a framework commonly used in the literature [70, 42, 68].

Minimum-distance and average-distance designs

The Chernoff bound on the PEP can be minimized either for a chosen codeword distance $\mathbf{A}$ or for the average distance over the codeword distribution. The corresponding criterion is referred to as the PEP per-distance and the average PEP, respectively. In both cases, the performance averaged over channel fading is of interest.

For the PEP per-distance criterion, since the PEP is codeword-pair dependent, a design rule is needed for picking the codeword distance product matrix $\mathbf{A}$ (4.4), over which the PEP is optimized. Noting that the Chernoff bound expression (4.5) is monotonic in $\mathbf{A}$ (specifically, $\mathbf{A}_1 \succcurlyeq \mathbf{A}_2$ implies $f(\mathbf{H}, \mathbf{A}_1, \mathbf{F}) \leq f(\mathbf{H}, \mathbf{A}_2, \mathbf{F})$), two options are considered. The first is the minimum distance, corresponding to the largest PEP. Of interest is the average performance over channel fading; therefore, this criterion can be expressed as

$$\mathbf{F} = \arg\min_{\mathbf{F}}\left\{\max_{\mathbf{A}} E_{\mathbf{H}}\big[f(\mathbf{H}, \mathbf{A}, \mathbf{F})\big]\right\}. \tag{4.6}$$

If the occurrence probability of the minimum-distance codeword pairs is not small, these pairs will dominate the error performance; thus, the minimum-distance design will lead to a reasonable overall performance gain. This distance criterion guarantees a minimum

precoding gain, based on the gain obtained from optimizing the error bound, and has often been used in the literature [42].

Another option is the average distance over all codeword pairs. Since the precoder only acts on one column of the codeword $\mathbf{C}$ at a time, and detection is performed jointly over the whole code-block of T symbol periods, an average-distance measure is chosen as

$$\bar{\mathbf{A}} = \frac{1}{PT} E\left[(\mathbf{C}-\hat{\mathbf{C}})(\mathbf{C}-\hat{\mathbf{C}})^*\right] = \frac{1}{PT}\sum_{i\neq j} p_{ij}\Delta_{ij}\Delta_{ij}^*, \tag{4.7}$$

where $\Delta_{ij} = \mathbf{C}_i - \mathbf{C}_j$, and p_{ij} is the probability of the pair $(\mathbf{C}_i, \mathbf{C}_j)$ among all pairs of distinct codewords. In effect, $\bar{\mathbf{A}}$ is the covariance of the codeword-error statistics. The design criterion in this case becomes

$$\mathbf{F} = \arg\min_{\mathbf{F}} \left\{ E_{\mathbf{H}}\big[f(\mathbf{H}, E[\mathbf{A}], \mathbf{F})\big] \right\}. \tag{4.8}$$

The average distance leads to a smaller value of the Chernoff bound (4.5) compared to the minimum distance. Therefore, the gain obtained from optimizing this bound may not be guaranteed to be the minimum precoding gain of the system. However, the average distance has an advantage over the minimum distance for non-orthogonal STBCs, in that $\bar{\mathbf{A}}$ is more likely to be a scaled-identity matrix. The implication of a scaled-identity $\mathbf{A}$ will be discussed in Section 4.3.2.

PEP per-distance criterion

Assume that a codeword distance product matrix $\mathbf{A}$ has been chosen, based on the appropriate design choice. The objective is to find a precoder $\mathbf{F}$ to minimize the expression $E_{\mathbf{H}}[f(\mathbf{H}, \mathbf{A}, \mathbf{F})]$, where f is the Chernoff bound in (4.5). Given the probability density distribution of the channel

$$g(\mathbf{H}) = \frac{1}{\pi^{MN}\det(\mathbf{R}_t)^M} \exp\Big(-\mathrm{tr}\big[(\mathbf{H}-\mathbf{H_m})^*\mathbf{R}_t^{-1}(\mathbf{H}-\mathbf{H_m})\big]\Big),$$

averaging (4.5) over the channel statistics results in the following bound on the average PEP

$$E_{\mathbf{H}}\left[\text{PEP}\right] \leq \frac{\exp\left[\text{tr}(\mathbf{H}_m\mathbf{W}^{-1}\mathbf{H}_m^*)\right]}{\det(\mathbf{W})^M}\det(\mathbf{R}_t)^M\exp\left[-\text{tr}(\mathbf{H}_m\mathbf{R}_t^{-1}\mathbf{H}_m^*)\right], \tag{4.9}$$

where

$$\mathbf{W} = \frac{\gamma}{4}\mathbf{R}_t\mathbf{F}\mathbf{A}\mathbf{F}^*\mathbf{R}_t + \mathbf{R}_t\,. \tag{4.10}$$

Expression (4.9) is a special case of a general problem setup in [42], in which the upper bound is given for a more general statistical CSIT model, including a non-zero mean $\mathbf{H}_m$ (2.19) and a full covariance $\mathbf{R}_0$ (2.16). The same reference provides the precoder solution for mean CSIT ($\mathbf{H}_m \neq \mathbf{0}$ but $\mathbf{R}_0 = \mathbf{I}$, equivalent to uncorrelated antennas) in systems using orthogonal STBCs. The formulation and solution in this thesis apply to the statistical CSIT in the form of an arbitrary mean and Kronecker antenna correlation (2.17), assuming uncorrelated receive antennas. The precoder design problem for a non-Kronecker covariance, or antenna correlation, still remains unsolved.

Minimizing the bound in (4.9) is equivalent to minimizing the logarithm of this bound, and ignoring the constant terms leads to the following objective function

$$J = \text{tr}(\mathbf{H}_m\mathbf{W}^{-1}\mathbf{H}_m^*) - M\log\det(\mathbf{W})\,, \tag{4.11}$$

which is convex in the matrix variable $\mathbf{W}$. Combining this objective function with the power constraint (4.1), an optimization problem for designing $\mathbf{F}$ can be posed as

$$\begin{aligned} \min_{\mathbf{F}} \quad J &= \text{tr}(\mathbf{H}_m\mathbf{W}^{-1}\mathbf{H}_m^*) - M\log\det(\mathbf{W}) \\ \text{subject to} \quad \mathbf{W} &= \frac{\gamma}{4}\mathbf{R}_t\mathbf{F}\mathbf{A}\mathbf{F}^*\mathbf{R}_t + \mathbf{R}_t \\ \text{tr}(\mathbf{F}\mathbf{F}^*) &= 1\,. \end{aligned} \tag{4.12}$$

In this problem, the objective function is deterministic and depends on the known channel parameters, mean $\mathbf{H}_m$ and transmit covariance $\mathbf{R}_t$. Because of the non-linear equality constraint on $\mathbf{F}$, the problem is non-convex in $\mathbf{F}$, but can be transformed into a convex problem in certain cases, as discussed in more detail in Section 4.3.

Average PEP criterion

Another formulation is obtained by averaging the PEP over both the codeword distribution and the fading statistics. This average PEP criterion is independent of the specific codeword distance $\mathbf{A}$.

For the system in Figure 4.1, assuming the input code is Gaussian distributed with zero mean, it has a normalized-covariance as

$$\mathbf{Q} = \frac{1}{TP} E[\mathbf{C}\mathbf{C}^*] \,, \tag{4.13}$$

where T is the code length in number of symbols. The average codeword distance (4.7), assuming that $\mathbf{C}$ and $\hat{\mathbf{C}}$ are independent, then becomes

$$\bar{\mathbf{A}} = \frac{1}{TP} \left(E[\mathbf{C}\mathbf{C}^*] + E[\hat{\mathbf{C}}\hat{\mathbf{C}}^*] \right) = 2\mathbf{Q} \,. \tag{4.14}$$

After averaging over the codeword distribution, the Chernoff bound on the PEP (4.3) depends only on the codeword covariance matrix $\mathbf{Q}$ as [71]

$$E_{\mathbf{C}} \left[\text{PEP} \right] \leq \det \left(\frac{\gamma}{2} \mathbf{H}\mathbf{F}\mathbf{Q}\mathbf{F}^*\mathbf{H}^* + \mathbf{I} \right)^{-M} \,.$$

The precoder optimization problem in this case becomes

$$\begin{aligned} \min_{\mathbf{F}} \quad & E_{\mathbf{H}} \left[\det \left(\frac{\gamma}{2} \mathbf{H}\mathbf{F}\mathbf{Q}\mathbf{F}^*\mathbf{H}^* + \mathbf{I} \right)^{-M} \right] \\ \text{subject to} \quad & \text{tr}(\mathbf{F}\mathbf{F}^*) = 1 \,. \end{aligned} \tag{4.15}$$

This formulation aims at finding the precoder $\mathbf{F}$ to minimize the Chernoff bound on the PEP, averaged over all codeword distances and the channel statistics, subject to the transmit power constraint.

4.2.2 The system capacity measure

The ergodic capacity criterion aims at maximizing the transmission rate with vanishing error, assuming asymptotically long codewords. Given dynamic CSIT, the capacity-optimal

signal is zero-mean Gaussian-distributed with an optimal covariance. For the system in Figure 4.1, assuming the predetermined input code is Gaussian distributed with covariance $\mathbf{Q}$ (4.13), the transmit signal covariance is then $\mathbf{FQF}^*$. With Gaussian additive noise, the mutual information between the channel input and output can be obtained explicitly as [46]

$$\mathcal{I}(X,Y) = \log\det(\mathbf{I} + \gamma\mathbf{HFQF}^*\mathbf{H}^*)\,,$$

where γ is the SNR. The system ergodic-capacity and optimal signal are established by maximizing this mutual information, subject to the transmit power constraint as

$$\begin{aligned} \max \quad & E_{\mathbf{H}}\big[\text{logdet}(\mathbf{I} + \gamma\mathbf{HFQF}^*\mathbf{H}^*)\big] \\ \text{subject to} \quad & \text{tr}(\mathbf{FF}^*) = 1\,. \end{aligned} \tag{4.16}$$

If the encoder in Figure 4.1 produces i.i.d. codewords so that $\mathbf{Q} = \mathbf{I}$, the above formulation coincides with the channel information capacity discussed in Chapter 3. Otherwise, it provides the system capacity. Subsequently, this formulation is referred to as the capacity criterion.

For both the capacity (4.16) and the average-PEP (4.15) criteria, the objective function involves an expectation that has no closed-form. The function under expectation is concave (or convex) in the Hermitian PSD matrix variable $\mathbf{HFQF}^*\mathbf{H}^*$. Depending on $\mathbf{Q}$, the problems can be transformed to be convex. These formulations belong to a class of stochastic optimization problems, which also includes the error-exponent and the MMSE criteria [19]. Problems in this class have similar solvability and are discussed in Section 4.5.

4.3 Optimal precoders based on the PEP per-distance

This section discusses precoder solutions based on the PEP per-distance criterion (4.12). Because of the non-linear power constraint, this problem is not convex in $\mathbf{F}$ and, hence, is not directly tractable in the original variable $\mathbf{F}$. The tractability of this problem is dependent on the structure of the matrix $\mathbf{A}$, which in turn depends on the STBC.

STBCs can be divided into two categories: orthogonal and non-orthogonal. Section 4.3.1 considers precoder design with orthogonal STBC, which lends an attractive property to $\mathbf{A}$. Section 4.3.2 then extends the analysis to general STBCs.

4.3.1 Precoder design with orthogonal STBC

Consider precoding with orthogonal STBC (OSTBC) [17]. Because of orthogonality, the distance product matrix (4.4) of an OSTBC has a special form

$$\mathbf{A} = \frac{1}{P}(\mathbf{C} - \hat{\mathbf{C}})(\mathbf{C} - \hat{\mathbf{C}})^* = \mu\mathbf{I},$$

where μ represents the codeword distance, dependent on the specific codeword pair.

Let μ_0 be the value corresponding to the matrix $\mathbf{A}$ chosen for the precoder optimization problem. Based on the design choice (Section 4.2.1), μ_0 can be either the minimum or the average distance over all distinct-codeword pairs. The numerical simulation section (Section 4.3.3) provides examples of how μ_0 is calculated in each case.

A scaled-identity matrix $\mathbf{A}$ helps to significantly simplify the optimization problem (4.12). The variable $\mathbf{W}$ is now a linear function of $\mathbf{F}\mathbf{F}^*$, and (4.12) becomes

$$\begin{aligned} \min_{\mathbf{F}} \quad & J &=& \operatorname{tr}(\mathbf{H}_m\mathbf{W}^{-1}\mathbf{H}_m^*) - M\log\det(\mathbf{W}) \\ \text{subject to} \quad & \mathbf{W} &=& \frac{\mu_0\gamma}{4}\mathbf{R}_t\mathbf{F}\mathbf{F}^*\mathbf{R}_t + \mathbf{R}_t \\ & \operatorname{tr}(\mathbf{F}\mathbf{F}^*) &=& 1\,. \end{aligned} \tag{4.17}$$

Denote $\eta_0 = \frac{1}{4}\mu_0\gamma$. This problem can be cast in terms of $\mathbf{W}$ as follows:

$$\begin{aligned} \min_{\mathbf{W}} \quad & \operatorname{tr}(\mathbf{H}_m\mathbf{W}^{-1}\mathbf{H}_m^*) - M\log\det(\mathbf{W}) \\ \text{subject to} \quad & \operatorname{tr}(\mathbf{R}_t^{-1}\mathbf{W}\mathbf{R}_t^{-1} - \mathbf{R}_t^{-1}) = \eta_0 \\ & \mathbf{R}_t^{-1}\mathbf{W}\mathbf{R}_t^{-1} - \mathbf{R}_t^{-1} \succcurlyeq 0\,, \end{aligned} \tag{4.18}$$

where the inequality results from the positive semi-definite (PSD) property that $\mathbf{F}\mathbf{F}^* \succcurlyeq 0$. Formulation (4.18) is convex in the matrix variable $\mathbf{W}$ and can be solved analytically.

Problem analysis

Problem (4.18) is now analyzed using the Lagrangian dual method [54]. Let $\mathbf{\Phi}$ be the following function of $\mathbf{W}$:

$$\mathbf{\Phi}(\mathbf{W}) = \mathbf{R}_t^{-1}\mathbf{W}\mathbf{R}_t^{-1} - \mathbf{R}_t^{-1} \,, \tag{4.19}$$

then the two constraints in (4.18) can be rewritten in terms of $\mathbf{\Phi}$ as

$$\begin{aligned} \mathrm{tr}(\mathbf{\Phi}) &= \eta_0 & (4.20)\\ \mathbf{\Phi} &\succcurlyeq 0 \,. & (4.21) \end{aligned}$$

Form the Lagrangian of (4.18) as

$$\mathcal{L}(\mathbf{W}, \nu, \mathbf{Z}) = \mathrm{tr}(\mathbf{H}_m\mathbf{W}^{-1}\mathbf{H}_m^*) - M\log\det(\mathbf{W}) + \nu\left[\mathrm{tr}(\mathbf{\Phi}) - \eta_0\right] - \mathrm{tr}(\mathbf{Z}\mathbf{\Phi}) \,, \tag{4.22}$$

where ν is the Lagrange multiplier associated with the equality constraint (4.20), and $\mathbf{Z} \succcurlyeq 0$ is the Lagrange multiplier in the matrix form associated with the inequality constraint (4.21). Strong duality holds for problem (4.18), easily verifiable using Slater's condition [54]. This condition requires the existence of a strictly feasible point: a positive definite matrix $\mathbf{\Phi}_0 \succ 0$ satisfying the equality constraint (4.20). An example is $\mathbf{\Phi}_0 = \eta_0\mathbf{I}/N$. Therefore, the primal and dual optimal-points of (4.18) satisfy the Karush-Kuhn-Tucker (KKT) conditions [54]

$$\begin{aligned} \mathrm{tr}(\mathbf{\Phi}^\star) &= \eta_0\\ \mathbf{\Phi}^\star &\succcurlyeq 0\\ \mathbf{Z}^\star &\succcurlyeq 0\\ \mathrm{tr}(\mathbf{Z}^\star\mathbf{\Phi}^\star) &= 0\\ \left.\frac{\partial\mathcal{L}(\mathbf{W},\nu,\mathbf{Z})}{\partial\mathbf{W}}\right|_{\mathbf{W}^\star,\nu^\star,\mathbf{Z}^\star} &= 0 \,, \end{aligned}$$

where $(.)^\star$ denotes the optimal value, and $\mathbf{\Phi}^\star$ is the value of $\mathbf{\Phi}$ evaluated at the optimal $\mathbf{W}^\star$.

In particular, the three conditions $\mathbf{\Phi}^\star \succcurlyeq 0$, $\mathbf{Z}^\star \succcurlyeq 0$, and $\mathrm{tr}(\mathbf{Z}^\star\mathbf{\Phi}^\star) = 0$ imply that all

eigenvalues of the positive semi-definite product $\mathbf{Z}^\star\mathbf{\Phi}^\star$ are zero. Thus, $\mathbf{\Phi}^\star$ and $\mathbf{Z}^\star$ must have the same eigenvectors, and their eigenvalue patterns are complementary; that is, if $\lambda_i(\mathbf{\Phi}^\star) > 0$, then $\lambda_i(\mathbf{Z}^\star) = 0$ and vice-versa. $\mathbf{Z}$ effectively ensures that $\mathbf{\Phi}$ is positive semi-definite: $\mathbf{Z}$ represents the eigen-modes that are dropped in a water-filling solution, whereas $\mathbf{\Phi}$ represents the modes that are active (with non-zero power). Therefore, if power is distributed over the correct number of positive eigenvalues of $\mathbf{\Phi}$, while the rest are set to zero, then in the Lagrangian (4.22), the term $\mathrm{tr}(\mathbf{Z\Phi})$ is automatically zero at the optimal values and, hence, can be ignored. From this observation, a two-step algorithm for solving problem (4.18) is outlined below.

Precoding design algorithm

In the first step, assume that the optimal $\mathbf{\Phi}^\star$ is full-rank, effectively ignoring the PSD inequality constraint (4.21), and solve for $\mathbf{W}$. If the solution of this step produces $\mathbf{\Phi} \succcurlyeq 0$, then it is also the solution for the original problem (4.18). The matrix $\mathbf{\Phi}$ becomes the scaled precoder-product $\eta_0\mathbf{F}\mathbf{F}^*$, which is full-mode in this case. However, if the solution of the first step does not produce a PSD $\mathbf{\Phi}$, then the algorithm proceeds to the second step. In this step, the weakest eigenvalue of $\mathbf{\Phi}$ is set to zero, effectively reducing the rank of $\mathbf{\Phi}$ by 1, and the problem is re-solved. This step is iterated until $\mathbf{\Phi}$ is PSD. The second step is equivalent to dropping a mode in a water-filling process. In both steps, finding the solution for $\mathbf{\Phi}$ essentially reduces to solving for the Lagrange multiplier ν, as detailed next.

By ignoring $\mathrm{tr}(\mathbf{Z\Phi})$ in the Lagrangian (4.22), the optimality condition is obtained by differentiating this Lagrangian with respect to $\mathbf{W}$ [60] to arrive at

$$-\mathbf{W}^{-1}\mathbf{H}_m^*\mathbf{H}_m\mathbf{W}^{-1} - M\mathbf{W}^{-1} + \nu\mathbf{R}_t^{-2} = 0\,. \tag{4.23}$$

This is a quadratic matrix equation. Solving this equation leads to the solution for $\mathbf{W}$ as

$$\mathbf{W} = \frac{1}{2\nu}\mathbf{R}_t\Big(M\mathbf{I}_N + \mathbf{\Psi}^{\frac{1}{2}}\Big)\mathbf{R}_t\,, \tag{4.24}$$

where

$$\mathbf{\Psi} = M^2\mathbf{I}_N + 4\nu\mathbf{R}_t^{-1}\mathbf{H}_m^*\mathbf{H}_m\mathbf{R}_t^{-1}\,. \tag{4.25}$$

The derivation is given in Appendix A.3. From the above solution for $\mathbf{W}$, the solution for $\mathbf{\Phi}$ can be established according to (4.19).

It is left to find the Lagrange multiplier ν, based on the transmit-power equality constraint (4.20). The algorithm for solving for ν in each of the two steps is given below.

Step 1. Full-mode solution

The full-mode solution is obtained by solving for ν, assuming $\mathbf{\Phi}$ is full-rank. Equation (4.20) can then be written as

$$\mathrm{tr}\Big(\frac{1}{2\nu}\left(M\mathbf{I}_N + \mathbf{\Psi}^{\frac{1}{2}}\right) - \mathbf{R}_t^{-1}\Big) = \eta_0\,. \tag{4.26}$$

Let λ_i $(i = 1 \ldots N)$ be the eigenvalues of $\mathbf{R}_t^{-1}\mathbf{H}_m^*\mathbf{H}_m\mathbf{R}_t^{-1}$, sorted in increasing order, $\beta_0 = 2\left[\mathrm{tr}\left(\mathbf{R}_t^{-1}\right) + \eta_0\right]$, and noting that $\lambda\left(a\mathbf{I} + A\right) = a + \lambda(A)$, the above equation becomes

$$MN + \sum_{i=1}^{N}\sqrt{M^2 + 4\nu\lambda_i} - \beta_0\nu = 0\,. \tag{4.27}$$

In the general case $(N > 1)$, this equation does not appear to have a closed-form solution. Nevertheless, solving for ν can be done efficiently using a binary search, called the "inner algorithm", as outlined below.

Inner algorithm.

Since the left-hand-side expression in (4.26) is monotonous in ν, the following lower and upper bounds on the solution for ν can be established:

$$\nu_{\text{lower}} = \frac{4N^2\lambda_1}{\beta_0^2} + \frac{2MN}{\beta_0}\,, \qquad \nu_{\text{upper}} = \frac{4N\alpha_0}{\beta_0^2} + \frac{2MN}{\beta_0}\,, \tag{4.28}$$

where λ_1 is the minimum eigenvalue and α_0 is the trace of $\mathbf{R}_t^{-1}\mathbf{H}_m^*\mathbf{H}_m\mathbf{R}_t^{-1}$. The lower bound is obtained from (4.27) by replacing all λ_i with λ_1, while the upper bound by applying the Cauchy-Schwartz inequality [72] to the summation term. A numerical binary search can then be performed between these bounds to find the

solution for (4.27) up to a desired precision. The number of iterations depends on the problem parameters, but convergence usually occurs rapidly since this is one-dimensional binary search.

Step 2. Mode-dropping solution

If the full-mode solution does not produce $\mathbf{\Phi} \succcurlyeq 0$, then the weakest eigen-mode of $\mathbf{\Phi}$ is dropped and (4.26) is re-solved for ν. This step is equivalent to a water-filling iteration. The total power will now be distributed over the $N-1$ largest eigenvalues of $\mathbf{\Phi}$, and the power constraint (4.26) changes to

$$\sum_{i=k+1}^{N} \lambda_i\Big(\frac{1}{2\nu}\left(M\mathbf{I}_N + \mathbf{\Psi}^{1/2}\right) - \mathbf{R}_t^{-1}\Big) = \eta_0 \,, \tag{4.29}$$

where $k = 1$, the number of modes dropped, and $\lambda_i(\cdot)$ is the ith eigenvalue of the matrix in the parenthesis, sorted in increasing order ($\lambda_1 \leq \cdots \leq \lambda_N$). The solution for $\mathbf{\Phi}$ is obtained after solving this equation for ν, forming the right-hand-side expression in (4.19), and forcing its smallest eigenvalue to be zero, after which, it satisfies (4.20). If this solution does not satisfy (4.21), then the number of dropped modes k is increased by 1, and (4.29) is re-solved. Again, the above equation does not have a closed-form solution, but can be solved using an efficient binary search, called the "outer algorithm", as described below.

Outer algorithm.

There is no explicit function relating the eigenvalues of a general matrix sum to the individual eigenvalues; therefore, each eigenvalue in (4.29) cannot be written as an explicit function of ν (except in the special cases discussed in Section 4.4.3). Fortunately, the sum of eigenvalues in (4.29) is monotonous in ν, allowing the derivation of upper and lower bounds on ν. A binary search can then be performed to efficiently find the solution between these two bounds up to any desired numerical precision. The bounds in the general case with k modes dropped ($1 \leq k \leq N-1$) are

$$\nu_{\text{upper}} = \frac{\lambda_N}{\beta_k^2} + \frac{M}{\beta_k} \,, \qquad \nu_{\text{lower}} = \frac{\lambda_1}{\beta_k^2} + \frac{M}{\beta_k} \,, \tag{4.30}$$

where λ_N and λ_1 are the maximum and the minimum eigenvalues of $\mathbf{R}_t^{-1}\mathbf{H}_m^*\mathbf{H}_m\mathbf{R}_t^{-1}$, respectively, and

$$\beta_k = \frac{1}{N-k}\left(\eta_0 + \sum_{i=k+1}^{N}\frac{1}{\lambda_i(\mathbf{R}_t)}\right).$$

The derivation of these bounds is given in Appendix A.4.

Dynamic water-filling

The mode-dropping process above is similar to the water-filling process, in that at each outer iteration, an eigen-mode (the weakest among the active modes) is dropped, and the total transmit power is re-allocated over the rest of the modes. There is, however, a significant difference between this process and the conventional water-filling process. In conventional water-filling, only the power allocation, or the water level, changes after each iteration, but the mode directions remain the same. In our problem, the mode directions also evolve at each iteration, because of the interaction of the channel mean and the transmit covariance matrices. To see this effect more clearly, rewrite the expression for $\mathbf{\Phi}$ in the following form:

$$\mathbf{\Phi} \;=\; \frac{M}{2\nu}\mathbf{I}_N + \left(\frac{1}{2\nu}\mathbf{\Psi}(\nu)^{\frac{1}{2}} - \mathbf{R}_t^{-1}\right),$$

where the notation $\mathbf{\Psi}(\nu)$ emphasizes the dependence of $\mathbf{\Psi}$ on ν. The "water-level" here is $M/2\nu$, and the mode directions are determined by the eigenvectors of the matrix expression inside the large parenthesis, in which Ψ and $\mathbf{R}_t$ have different eigen-directions. When ν changes at each outer iteration, both the water-level (hence, the power allocation) and the mode directions change. Moreover, since the ν solution depends on the SNR, both the precoder power allocation and mode (beam) directions are functions of the SNR. For this reason, this process is called *dynamic* water-filling.

The optimal precoder solution with scaled-identity A

When ν is found satisfying the PSD constraint (4.21), then the matrix $\mathbf{\Phi}$ provides the solution for $\mathbf{F}\mathbf{F}^*$ as

$$\mathbf{\Phi} = \frac{1}{2\nu}\left(M\mathbf{I}_N + \mathbf{\Psi}^{\frac{1}{2}}\right) - \mathbf{R}_t^{-1} = \eta_0 \mathbf{F}\mathbf{F}^* \,. \tag{4.31}$$

From this product expression, an optimal precoder can be derived. The optimal precoder is not unique. Let the eigenvalue decomposition of $\mathbf{\Phi}$ be

$$\mathbf{\Phi} = \mathbf{U}_{\mathbf{\Phi}} \mathbf{\Lambda}_{\mathbf{\Phi}} \mathbf{U}_{\mathbf{\Phi}}^* \,,$$

then, in terms of the singular value decomposition, the optimal precoder matrix is

$$\mathbf{F} = \frac{1}{\sqrt{\eta_0}} \mathbf{U}_{\mathbf{\Phi}} \mathbf{\Lambda}_{\mathbf{\Phi}}{}^{1/2} \mathbf{V}^* \,. \tag{4.32}$$

The left singular vectors and the singular values of an optimal precoder are the eigenvectors and the scaled square-roots of the eigenvalues of $\mathbf{\Phi}$, respectively. The right singular vectors $\mathbf{V}$, however, can be any unitary matrix, attributed to the codeword distance product matrix $\mathbf{A}$ being scaled-identity. For simplicity, set $\mathbf{V} = \mathbf{I}$ for a precoder with scaled-identity $\mathbf{A}$.

Summary on precoding with OSTBC

By solving a convex optimization problem with matrix variables, this section has established an analytical design algorithm for a precoder used with an orthogonal STBC. The algorithm resembles the water-filling process. At first, it is assumed that all precoder eigen-modes are active, and power allocation is performed on all modes. If any mode has negative power, that mode is dropped, and the power is re-allocated accordingly. During this process, the precoder eigen-beam directions also evolve with the water-filling iterations. Each iteration essentially aims at finding a Lagrange multiplier solution, using an efficient binary search. The algorithm produces the optimal beam directions, or the precoder left singular vectors, and the optimal beam power allocation. The precoder right singular vectors, however, can be arbitrary, due to the isotropic property of the

orthogonal STBC, and are usually omitted.

4.3.2 Precoder design with general STBC

This section examines (4.12) when the codeword distance product matrix $\mathbf{A}$ (4.4) results from any STBC. For a non-orthogonal STBC, $\mathbf{A}$ is not always a scaled-identity matrix. Since the scaled-identity $\mathbf{A}$ case was solved in Section 4.3.1, this section focuses on solving for the non-identity $\mathbf{A}$ next, then discusses the precoder solution with general STBC in Section 4.3.2.

Problem analysis for a non-identity codeword distance product

When $\mathbf{A}$ is not a scaled-identity matrix, the optimization problem (4.12) is non-convex and more difficult. In particular, due to the non-convexity, it is not obvious if the problem can be solved exactly. This section analyzes and reformulates the problem, then applies different relaxations to obtain a precoder analytically.

To analyze (4.12) for a non-identity $\mathbf{A}$, consider the following more constrained problem:

$$\begin{aligned} \min_{\mathbf{F}} \quad & J &&= \operatorname{tr}\left(\mathbf{H}_m \mathbf{W}^{-1} \mathbf{H}_m^*\right) - M \log\det(\mathbf{W}) \\ \text{subject to} \quad & \mathbf{W} &&= \frac{\gamma}{4}\mathbf{R}_t \mathbf{F}\mathbf{A}\mathbf{F}^* \mathbf{R}_t + \mathbf{R}_t \\ & \operatorname{tr}(\mathbf{F}\mathbf{F}^*) &&= 1 \\ & \operatorname{tr}(\mathbf{F}\mathbf{A}\mathbf{F}^*) &&= p\,, \end{aligned} \tag{4.33}$$

where p is a positive constant. Since this problem is more constrained than the original problem (4.12), its optimal J value will be larger than, or equal to, the optimal J value in (4.12). The smallest optimal J value in (4.33) across different p values, however, will equal the optimal J value in (4.12), at which point, the two problems become equivalent.

Now consider problem (4.33) with different p values. In this problem, the condition $\operatorname{tr}(\mathbf{F}\mathbf{A}\mathbf{F}^*) = p$ acts as an additional transmit power constraint. Obviously, with more transmit power, the error probability, or the objective function J equivalently, will be smaller. Of interest is the problem with the largest feasible p; that is, the largest p

value such that there exists an $\mathbf{F}$ satisfying both equality constraints, $\mathrm{tr}(\mathbf{F}\mathbf{F}^*) = 1$ and $\mathrm{tr}(\mathbf{F}\mathbf{A}\mathbf{F}^*) = p$.

Applying the matrix inequality $\mathrm{tr}(AB) \leq \sum_i \lambda_i(A)\lambda_i(B)$ for PSD matrices [73] to obtain

$$p = \mathrm{tr}(\mathbf{F}\mathbf{A}\mathbf{F}^*) = \mathrm{tr}(\mathbf{F}^*\mathbf{F}\mathbf{A}) \leq \sum_i \lambda_i(\mathbf{F}^*\mathbf{F})\lambda_i(\mathbf{A}). \tag{4.34}$$

The equality occurs when the eigenvectors of $\mathbf{F}^*\mathbf{F}$ are the same as those of $\mathbf{A}$. Consider the SVD of the precoder $\mathbf{F} = \mathbf{U}_F\mathbf{D}\mathbf{V}_F^*$ as in (1.4), this equality condition means

$$\mathbf{V}_F = \mathbf{U}_\mathbf{A}\,, \tag{4.35}$$

where $\mathbf{A} = \mathbf{U}_\mathbf{A}\mathbf{\Lambda}_\mathbf{A}\mathbf{U}_\mathbf{A}^*$ is the eigenvalue decomposition of $\mathbf{A}$. Since the eigenvalues of $\mathbf{F}^*\mathbf{F}$ are the same as those of $\mathbf{F}\mathbf{F}^*$, the equality condition translates to $\lambda_i(\mathbf{F}\mathbf{A}\mathbf{F}^*) = \lambda_i(\mathbf{F}\mathbf{F}^*)\lambda_i(\mathbf{A})$.

Condition (4.35) ensures the largest value for p, without imposing any constraint on the eigenvalues of $\mathbf{F}\mathbf{A}\mathbf{F}^*$ or $\mathbf{F}\mathbf{F}^*$, except their orders relative to $\lambda_i(\mathbf{A})$. With this condition, problem (4.33) and the original problem (4.12) become equivalent when p is chosen to be the same as that resulted from the optimal solution of (4.12): $p = \sum_i \lambda_i(\mathbf{A})\lambda_i^\star(\mathbf{F}\mathbf{F}^*)$.

Based on these arguments, condition (4.35) is optimal for the original problem (4.12). Let $\mathbf{B} = \mathbf{F}\mathbf{A}\mathbf{F}^*$, this problem is then equivalent to

$$\begin{aligned} \min_{\mathbf{B}} \quad & J &&= \mathrm{tr}\left(\mathbf{H}_m\mathbf{W}^{-1}\mathbf{H}_m^*\right) - M\log\det(\mathbf{W}) \\ \text{subject to} \quad & \mathbf{W} &&= \frac{\gamma}{4}\mathbf{R}_t\mathbf{B}\mathbf{R}_t + \mathbf{R}_t \\ & \textstyle\sum_i \xi_i\lambda_i(\mathbf{B}) &&= 1 \\ & \mathbf{B} &&\succcurlyeq 0\,, \end{aligned} \tag{4.36}$$

where $\xi_i = [\lambda_i(\mathbf{A})]^{-1}$ are the inverses of the non-zero eigenvalues of $\mathbf{A}$.

By finding the optimal right singular vectors of $\mathbf{F}$ in (4.35), the original problem (4.12) has been reformulated into a new problem (4.36) in terms of the variable $\mathbf{B}$. This new formulation, however, is not convex in $\mathbf{B}$, because of the non-linear equality constraint involving the eigenvalues of $\mathbf{B}$. Next, this constraint is relaxed to obtain an analytical

precoder solution. Because of relaxation, the solution in this case may not be optimal for the original problem. Two different relaxations follow.

Minimum eigenvalue relaxation method

Employing the inequality $\sum_i \xi_i \lambda_i(\mathbf{B}) \leq \xi_{\max} \mathrm{tr}(\mathbf{B})$, the problem can be relaxed by replacing all ξ_i with $\xi_{\max}$, which is equivalent to approximating $\mathbf{A}$ in (4.12) with an identity matrix, scaled by the minimum non-zero eigenvalue of $\mathbf{A}$. This approximation effectively produces a smaller $\mathbf{W}$ (in the positive semi-definite sense), hence loosening the upper-bound on the PEP in (4.9). This relaxation results in the same problem formulation as in the orthogonal STBC case (4.17), where the value μ_0 for the minimum-distance design is

$$\mu_0 = \min_{\Delta_{ij}} \lambda_{\min}(\Delta_{ij}\Delta_{ij}^*) \,,$$

and for the average-distance design is $\mu_0 = \lambda_{\min}(\bar{\mathbf{A}})$ (with $\lambda_{\min} \neq 0$). This relaxation method works well if the condition number of $\mathbf{A}$ is reasonably small.

Trace relaxation method

Another relaxation method is to replace the equality constraint on the eigenvalues of $\mathbf{B}$ with the linear constraint $\mathrm{tr}(\mathbf{\Lambda}_{\mathbf{A}}^{-1}\mathbf{B}) = 1$, making the relaxed problem convex. Based on the inequality $\mathrm{tr}(AB) \geq \sum_i \lambda_{N-i+1}(A)\lambda_i(B)$ for ordered eigenvalues of Hermitian PSD matrices [72], this relaxation method results in a precoder with $\mathrm{tr}(\mathbf{F}\mathbf{F}^*) \leq 1$, meaning that the total transmit power may be less than the original constraint (4.1). A scaling factor can then be applied to the precoder solution of the relaxed problem to increase the power to meet the original constraint.

Noting that $\mathbf{B} = \frac{4}{\gamma}\left(\mathbf{R}_t^{-1}\mathbf{W}\mathbf{R}_t^{-1} - \mathbf{R}_t^{-1}\right)$, reformulate the problem in terms of $\mathbf{W}$ as

$$\begin{aligned} \min_{\mathbf{W}} \quad & \mathrm{tr}\left(\mathbf{H}_m\mathbf{W}^{-1}\mathbf{H}_m^*\right) - M\log\det(\mathbf{W}) \\ \text{subject to} \quad & \mathrm{tr}\left(\mathbf{\Lambda}_{\mathbf{A}}^{-1}\left(\mathbf{R}_t^{-1}\mathbf{W}\mathbf{R}_t^{-1} - \mathbf{R}_t^{-1}\right)\right) = \frac{\gamma}{4} \\ & \mathbf{R}_t^{-1}\mathbf{W}\mathbf{R}_t^{-1} - \mathbf{R}_t^{-1} \succcurlyeq 0 \,. \end{aligned} \tag{4.37}$$

This problem is similar to (4.18), but with a more general trace constraint; it can be

solved using a similar approach. The steps for solving this problem and the solutions for $\mathbf{W}$ and $\mathbf{B}$ are given in Appendix A.5.

The precoder solution with general STBC

Returning to the general STBC case, if the codeword distance product matrix $\mathbf{A}$ is a scaled-identity matrix, then the precoder solution is similar to that of the orthogonal STBC case (4.32). For a non-identity $\mathbf{A}$, employ one of the relaxation methods outlined above and solve for $\mathbf{B}$. Perform the eigenvalue decomposition of this matrix as $\mathbf{B} = \mathbf{U_B}\mathbf{\Lambda_B}\mathbf{U_B^*}$, then the precoder solution is

$$\mathbf{F} = \mathbf{U_B}\mathbf{\Lambda_B^{\frac{1}{2}}}\mathbf{\Lambda_A^{-\frac{1}{2}}}\mathbf{U_A^*} \,. \tag{4.38}$$

For an orthogonal STBC, since $\mathbf{A}$ is always a scaled-identity matrix, $\mathbf{U_A}$ is an arbitrary unitary matrix and, hence, can be omitted. For a non-orthogonal STBC, $\mathbf{U_A}$ depends on the STBC structure. Specifically, when $\mathbf{A}$ is not a scaled-identity matrix, the input signal produced by the STBC has a certain codeword-error shape with directions $\mathbf{U_A}$ and power loadings $\lambda_i(\mathbf{A})$. The precoder then matches both its input signal structure and the channel. It effectively re-maps the input signal directions from $\mathbf{U_A}$ into $\mathbf{U_B}$ and re-distributes the transmit power according to the CSIT to optimally match the channel. Note that the precoder beam directions (the left singular vectors $\mathbf{U_B}$) depend only on the CSIT; the input shaping matrix (the right singular vectors $\mathbf{U_A}$) depends only on the precoder input signal – the STBC structure; and the power allocation now depends on both sides.

Recall that the matrix $\mathbf{A}$ can be chosen based on the minimum- or the average-distance criterion. Between these two criteria, the average-distance criterion usually produces a scaled-identity matrix $\bar{\mathbf{A}}$, assuming equi-probability and independence between all input symbols. The reason is that STBCs commonly assume no CSIT and distribute power equally among all antennas and all symbols, leading to a white error-covariance. The minimum-distance criterion, on the other hand, can often produce a non-identity $\mathbf{A}$.

Summary on precoding with general STBC

This section has extended the precoder design algorithm in Section 4.3.1 to cover precoding with non-orthogonal STBC. In contrast to the isotropic property of an orthogonal STBC, a non-orthogonal STBC may pre-shape the input signal with a non-identity codeword distance product matrix $\mathbf{A}$. In that case, the precoder optimal right singular vectors are given by the eigenvectors of $\mathbf{A}$. For a non-identity $\mathbf{A}$, relaxations are used to find the precoder left singular vectors and the singular values. In general, the precoder solution contains matching singular vectors on each side to the STBC structure and to the channel respectively, while the singular values depend on both the STBC and the CSIT. The precoder essentially re-maps the spatial directions of the input signal to match those of the channel, based on the CSIT, and allocates transmit power accordingly in a water-filling fashion.

4.3.3 Design examples and performance results

This section shows design examples and simulation results for several system configurations, using two antenna setups: 2×1 and 4×1. The channel mean and transmit covariance matrices are generated arbitrarily and normalized according to Appendix B.1, in which the covariance matrix is Hermitian and positive definite. These matrices are given in Appendix B.3. The covariance matrix for the 2×1 channel has the eigenvalues as $[1.96,\ 0.04]$ and the condition number of 47.93, representing a strong antenna correlation. The covariance matrix for the 4×1 channel has the eigenvalues as $[2.05,\ 1.48,\ 0.41,\ 0.06]$ and the condition number of 34.2. In all systems, the K factor is chosen to be 0.1, except when studying the effect of K on the precoder.

Precoders with orthogonal STBC

This section first discusses a design example for precoding with the Alamouti STBC [74], which is capacity-optimal for a 2×1 system, then presents error-rate simulation results.

The Alamouti STBC is given as

$$\mathbf{C} = \begin{pmatrix} c_1 & -c_2^* \\ c_2 & c_1^* \end{pmatrix},$$

where c_i are symbols from a chosen constellation.

Codeword distance of the Alamouti STBC

The value for μ_0 in (4.17) is established as follows. For the minimum-distance design, $\mathbf{A} = \frac{d^2}{P}\mathbf{I}$, where d is the minimum distance in the signal constellation. Consider a square QAM constellation with M_c points for example, the average symbol power is $P = d^2(M_c - 1)/6$, thus $\mu_0 = 6/(M_c - 1)$.

For the average-distance design, assuming that each codeword contains n distinct symbols that are independent and equally likely, the codeword distance product matrix (4.7) can be rewritten as

$$\bar{\mathbf{A}} = \frac{1}{TP} E_{\mathbf{C}\neq\hat{\mathbf{C}}}\left[(\mathbf{C}-\hat{\mathbf{C}})(\mathbf{C}-\hat{\mathbf{C}})^*\right] = \frac{1}{TP}\frac{M_c^{2n}}{M_c^{2n}-M_c^n} 2\left(E[\mathbf{C}\mathbf{C}^*] - E[\mathbf{C}\hat{\mathbf{C}}^*]\right), \quad (4.39)$$

where the ratio factor results from averaging over only pairs of distinct codewords. This expression applies to any signal constellation of size M_c. Since $\mathbf{C}$ and $\hat{\mathbf{C}}$ are chosen independently, $E[\mathbf{C}\hat{\mathbf{C}}^*] = 0$. For a STBC that gives equal weight to all symbols, it is plausible that $E[\mathbf{C}\mathbf{C}^*] = \mu P\mathbf{I}$ for some μ. Hence, the average-distance criterion usually produces a scaled-identity matrix $\bar{\mathbf{A}}$. For the Alamouti code with QPSK, for example, $\bar{\mathbf{A}} = \frac{64}{15}\mathbf{I}$, or $\mu_0 = 4.26$.

Numerical results

Figure 4.2(a) shows the performance of a 2×1 system using the Alamouti code and QPSK modulation. For this system, the minimum-distance and the average-distance precoders perform exactly the same. The precoding gain is around 2.2dB at low and medium SNRs and diminishes at higher SNRs. When the SNR increases, as discussed in Section 4.4.2, the precoder becomes increasingly dependent on the transmit covariance and approaches

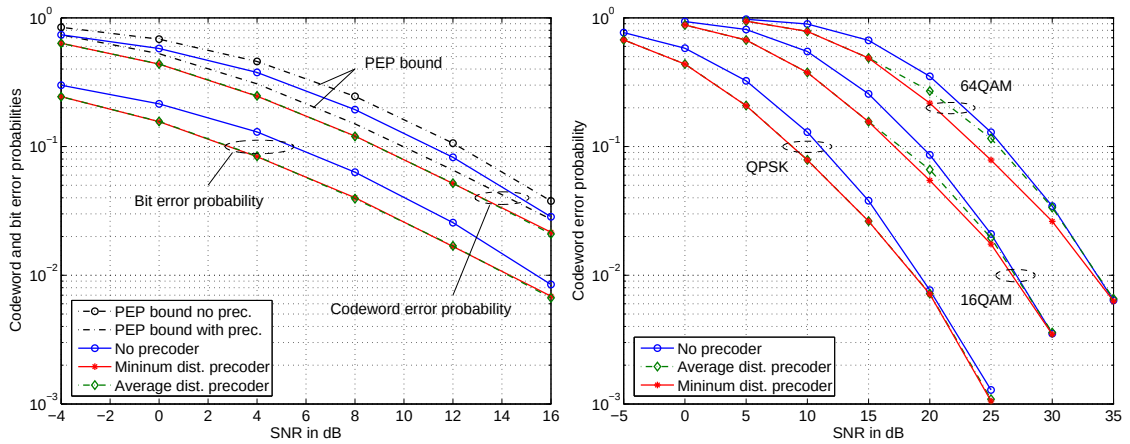

Figure 4.2: Performance of a 2×1 system with and without precoding, using the Alamouti code and (a) QPSK modulation, (b) various QAMs.

equi-power on the non-zero eigen-modes of $\mathbf{A}$. With OSTBC, the matrix $\mathbf{A}$ is always full-rank; thus, the value of water-filling power allocation decreases at a high SNR, leading to the diminishing precoding gain.

Figure 4.2(b) shows the performance for the same 2×1 system with different QAM orders. The precoding gain of the minimum-distance design is consistent over different constellation sizes, whereas the average-distance precoding gain is reduced with larger constellation at high SNRs. With a larger constellation, the number of minimum-distance codeword pairs becomes larger, while at a higher SNR, the minimum-distance pairs become more dominant in affecting the error probability. Therefore, the minimum-distance precoder design results in more gain than the average-distance design in this domain.

Precoders with non-orthogonal STBC

This section continues with an example of a linear precoder design with non-orthogonal STBC. This example uses the quasi-orthogonal STBC (QSTBC) [75, 76] specifically. The name quasi-orthogonal results from the groups of columns of this code being orthogonal to each other, allowing simple ML decoding over pairs of symbols. The code itself is non-orthogonal and provides partial diversity; however, it achieves a higher rate than an OSTBC for more than two transmit antennas. Consider the following form of the

QSTBC:

$$\mathbf{C} = \begin{pmatrix} c_1 & c_2 & c_3 & c_4 \\ -c_2^* & c_1^* & -c_4^* & c_3^* \\ c_3 & c_4 & c_1 & c_2 \\ -c_4^* & c_3^* & -c_2^* & c_1^* \end{pmatrix}, \tag{4.40}$$

where c_i are symbols from a chosen constellation $\mathcal{C}$. In [66], a precoder exploiting mean CSIT in a system with the QSTBC is derived, using an asymptotic analysis.

The codeword distance product matrix for the QSTBC

For this code, the codeword distance product matrix $\mathbf{A}$ (4.4) has the form

$$\mathbf{A} = \frac{1}{P} \begin{pmatrix} a & 0 & b & 0 \\ 0 & a & 0 & b \\ b & 0 & a & 0 \\ 0 & b & 0 & a \end{pmatrix},$$

where $a = \sum_{i=1}^{4} |\Delta c_i|^2$ and $b = \Delta c_1 \Delta c_3^* + \Delta c_1^* \Delta c_3 + \Delta c_2 \Delta c_4^* + \Delta c_2^* \Delta c_4$, with $\Delta c_i = c_i - \hat{c}_i$, where $\hat{c}_i$ are symbols in $\hat{\mathbf{C}}$.

For the minimum-distance design, $\mathbf{A}$ is given by the case in which there is only one symbol difference between the two codewords, thus $\mathbf{A}_{\min} = \min_{\mathcal{C}}(|\Delta c|^2)\mathbf{I}/P$. For the average-distance design, assuming that all symbols c_i are independent and equally likely, and that $E[c_i] = 0$, $\bar{\mathbf{A}}$ (4.39) is also a scaled-identity matrix with $\mu_0 = 2M_c^8/(M_c^8 - M_c^4)$. In this QSTBC example, $\mathbf{A}$ is a scaled-identity matrix in both designs; hence, no relaxation is needed to solve for the precoder, and the precoder right singular vectors can be omitted.

Although the STBC diversity order, or the minimum rank of $\mathbf{A}$, is 2 in this case, the precoder is not limited to rank 2. At each time instance, the precoder acts as a beamformer on a separate column of the space-time code. Since there are 4 different symbols in each column, the precoder can form a maximum of four orthogonal beams, one per symbol, matching the statistically preferred directions in the channel. This beamforming effect causes the precoder rank to be independent of the STBC diversity order. Rather, it depends on the number of different symbols in each column of the code. Only when the

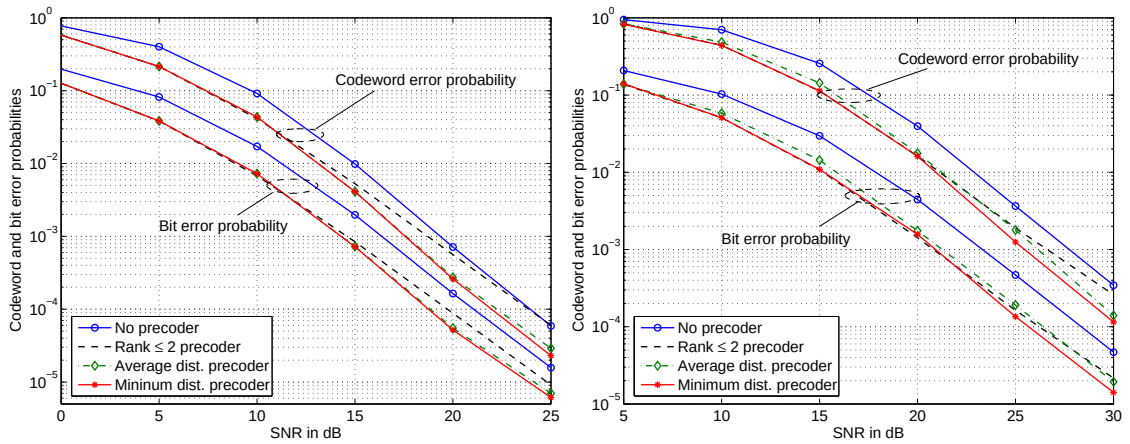

Figure 4.3: Performance of a 4×1 system with and without precoding, using the QSTBC and (a) QPSK modulation, (b) 16 QAM.

SNR is not high enough, the precoder reduces its rank by dropping modes.

Numerical results

Figure 4.3(a) shows the performance curves for a 4×1 system using the QSTBC and QPSK modulation. The result reveals that both the minimum-distance and the average-distance precoder designs perform similarly for the QPSK modulation, with a precoding gain of around 1.7dB – 2dB. Also shown is the performance of a precoder that has its rank limited to 2. This precoder gain reduces rapidly as the SNR increases; it eventually performs even worse than without precoding at very high SNRs. This example illustrates that the precoder rank should not depend on the STBC diversity order.

Figure 4.3(b) shows similar performance curves for the 16QAM constellation with Gray bit-mapping. In this case, the minimum-distance precoder design performs slightly better than the average-distance design, due to the larger constellation at high SNRs effect, which is also observed in Figure 4.2(b). The difference is small, however, at around 0.5dB. With this larger constellation, the precoding gain is higher; the minimum-distance precoding gains are around 1.8 – 2.5dB.

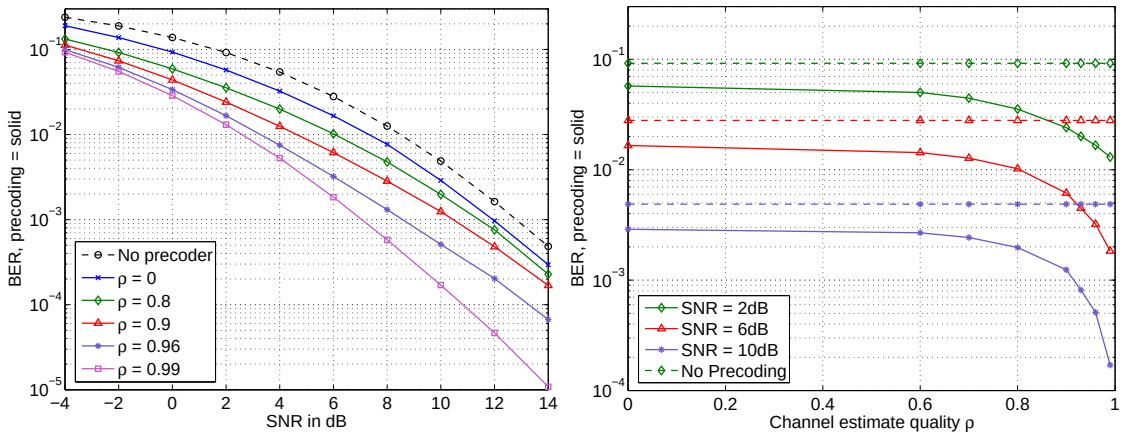

(a) (b)

Figure 4.4: Performance of the minimum-distance PEP precoder in a 4×1 system with OSTBC, given dynamic CSIT.

Precoding with dynamic CSIT

The precoding designs (4.32) and (4.38) can be applied directly to dynamic CSIT, using the effective channel mean $\hat{\mathbf{H}}$ (2.25) and the effective transmit covariance $\mathbf{R}_{t,e}$ (2.27) in the place of the channel statistics. This section considers the performance of a 4×1 system, given dynamic CSIT. The channel parameters, mean and transmit covariance, are the same as in the simulation for Figure 4.3, as given in Appendix B.3. This system, however, employs a rate 3/4 orthogonal STBC for 4 transmit antennas [17]. The error performance is averaged over multiple initial channel measurements, independently generated from the channel distribution, and multiple channel estimates given each initial measurement.

Figure 4.4(a) shows the system bit-error-rate (BER) given different CSIT qualities ρ. The performance improves with higher ρ. When $\rho = 0$, the precoding gain is that of statistical CSIT alone. As $\rho \to 1$, the gain increases to a maximum of 6dB, which is the maximum coding gain possible from perfect CSIT for a 4×1 channel.

Figure 4.4(b) presents the BER as a function of the CSIT quality ρ at different SNRs. This result shows that the gain is sensitive to ρ only when $\rho \geq 0.6$, at which dynamic CSIT has an advantage over statistical CSIT. This observation implies that the initial channel measurement helps to increase the precoding gain only when its correlation with the current channel is reasonably strong, $\rho \geq 0.6$ in this case; otherwise, precoding on the

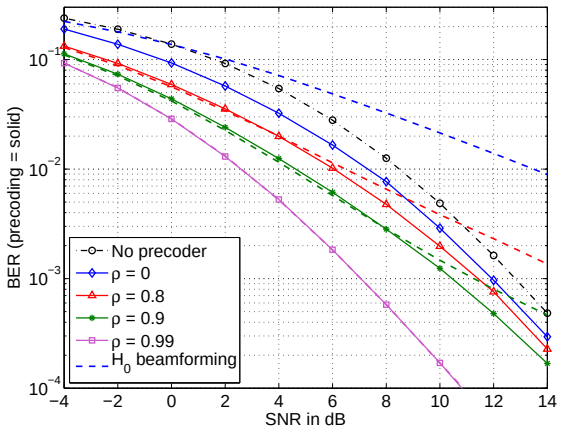

Figure 4.5: Performance comparison between the minimum-distance PEP precoder and the beamforming scheme relying only on outdated channel measurements.

channel statistics alone ($\rho = 0$) can extract most of the gain.

The precoder is compared with a beamforming scheme that uses only the initial channel measurement $\mathbf{H}_0$ as shown in Figure 4.5. With perfect CSIT (numerically represented by $\rho = 0.99$), these two schemes coincide and are optimal for a 4×1 MISO channel. However, as ρ decreases, the $\mathbf{H}_0$ beamforming scheme starts loosing diversity at high SNRs and eventually performs even worse than without precoding. The precoder exploiting dynamic CSIT, on the other hand, provides gains over no precoding for all ρ values. This result illustrates the robustness of the dynamic CSIT model.

4.4 Analyses of PEP-based precoders

This section analyzes the precoding design based on the PEP per-distance criterion, derived in the previous section. The analyses include the precoding gain, asymptotic precoders with increasing K factor and SNR, and precoders for special scenarios: transmit covariance CSIT and mean CSIT.

4.4.1 The precoding gain

The precoding gain can include two components: diversity and coding. The diversity gain refers to an increase in the asymptotic slope of the error rate curve vs the SNR as

the SNR increases to infinity. The coding gain, on the other hand, refers to an SNR advantage, corresponding to a parallel shift of the error rate curve to lower SNRs with the same asymptotic slope. Coding gains can be measured at a finite SNR.

Diversity gain

Diversity is a high-SNR measure, obtained as the dominant exponent of the error probability expressed in terms of the SNR. Specifically, the system diversity order is defined as

$$d = \lim_{\mathrm{SNR}\to\infty} \frac{\log_{10}\left(\bar{P}_e\right)}{\log_{10}(\mathrm{SNR})} ,$$

where $\bar{P}_e$ is the average system error probability. The system diversity can also be obtained from the exponent of the maximum PEP [70, 71]. Since the Chernoff bound on the PEP is asymptotically tight at high SNR, this diversity order can be derived by examining the Chernoff bound (4.3) while taking $\gamma \to \infty$.

For partial CSIT ($\rho < 1$), the effective transmit covariance is non-zero. The Chernoff bound (4.3) can be averaged over the effective channel statistics to obtain (4.9). Noting that only $\mathbf{W}$ depends on γ, the system diversity order can be derived from this averaged bound as

$$d = \lim_{\gamma\to\infty} -\frac{\mathrm{tr}\left(\hat{\mathbf{H}}\mathbf{W}^{-1}\hat{\mathbf{H}}^{*}\right) - M\log\det(\mathbf{W})}{\log\gamma} .$$

From (4.10), as $\gamma \to \infty$ then $\mathbf{W}^{-1} \to \mathbf{0}$; thus, the trace term in the above expression vanishes, and the diversity order becomes

$$d = \lim_{\gamma\to\infty} \frac{M\log\det(\mathbf{W})}{\log\gamma} . \tag{4.41}$$

As $\gamma \to \infty$, the precoding solution (4.38) approaches a precoder with equi-power allocation on the non-zero eigen-modes of $\mathbf{A}$, and the left and right singular vectors given by the eigenvectors of $\mathbf{R}_t$ and $\mathbf{A}$, respectively (see Section 4.4.2, equ.(4.48)). Thus at high SNR, $\mathbf{W}$ (4.10) approaches

$$\mathbf{W}_{\gamma\ \mathrm{limit}} = \frac{\gamma}{4L}\mathbf{U}_t\mathbf{\Lambda}_t^2\mathbf{\Lambda}_A\mathbf{U}_t , \tag{4.42}$$

where L is the minimum number of non-zero eigenvalues of $\mathbf{A}$, determined by the diversity

order of the STBC. The rank of $\mathbf{W}_{\gamma\,\text{limit}}$ is L. Thus, the system diversity order in (4.41) is ML. Therefore, with partial CSIT, the precoder and the CSIT quality ρ have no impact on the system diversity. With optimal ML detection, the system diversity is solely determined by the STBC.

For perfect CSIT ($\rho = 1$), the Chernoff bound (4.3) can be used directly to derive the optimal precoder and the diversity order. The optimal precoder is single-mode beamforming on the dominant eigen-mode of $\mathbf{H}^*\mathbf{H}$ (see Section 4.4.2, equ.(4.44)). This precoder achieves the maximum diversity order of MN (see [7], Section 5.4.4). The proof is based on loosening the bound (4.3), by replacing $\mathbf{A}$ with $\mathbf{I}\lambda_{\max}(\mathbf{A})$ and using no precoder ($\mathbf{F} = 1/\sqrt{N}\,\mathbf{I}$); this relaxed bound has the diversity order MN. Thus, the precoder for perfect CSIT achieves the full diversity, regardless of the STBC.

The above analysis shows that the diversity obtained by the precoder depends on the CSIT. When the CSIT is partial, no diversity can be extracted by the precoder; the STBC then plays an essential role in obtaining transmit diversity in the system. Only when the CSIT is perfect that the precoder delivers the full transmit diversity. In all cases, however, the precoder achieves a coding gain, as discussed next.

Coding gain

The coding gain is the essential value of precoding and comes in the form of an SNR advantage. The simulation results in Section 4.3.3 illustrate that this gain depends on the SNR, the CSIT, and the number of antennas. The gain is usually significant at low and medium SNRs. It may diminish at high SNRs, depending on the system configuration, such as in systems with OSTBC. The coding gain increases with higher CSIT quality ρ, likewise with higher channel K factor. It also depends on the specific channel mean and transmit covariance matrices. Some channels favor precoding with larger gains, while for others, the gain is less significant. A variety of factors can contribute to this effect: for example, the condition numbers of the mean and covariance matrices, how closely the eigenvectors of these matrices align. This effect is not studied here and can be a subject for further research. Furthermore, the number of antennas also affects the coding gain. The gain tends to increase with increasing number of transmit antennas. Precoding on

a channel with the same transmit antenna correlation but with more receive antennas also tends to produce a higher gain. Note that precoding with the focus on extracting an array gain is fundamentally different from, and complementary to, achieving the diversity-multiplexing frontier at high SNRs [71, 77, 78].

Summary on the precoding gain

The precoding gain is attributed to two factors: the optimal beam directions, which achieve a coding gain from array beamforming, and the water-filling-type power allocation among these beams, which also results in an SNR advantage. With partial CSIT ($\rho < 1$), precoding on effective channel statistics obtains only coding gain, but not diversity gain. This lack of diversity gain is a property of statistical channel information, in which the precise directions of each channel realization are unknown to the transmitter. The STBC, therefore, plays an important role in capturing the channel diversity here. When the CSIT is perfect ($\rho = 1$), however, the precoder can also deliver the maximum diversity gain.

4.4.2 Asymptotic precoder results

This section analyzes several asymptotic behaviors of the optimal precoder based on the PEP per-distance criterion. Two effects are studied: of the K factor and of the SNR increasing to infinity. In each case, the precoder solution asymptotically depends only on one of the two channel statistical parameters, either the mean or the transmit covariance. These asymptotic precoder solutions are obtained in closed-form for all STBC cases without relaxation.

The effect of a high K factor on the precoder

This section investigates the effect on the optimal precoder as the channel K factor increases to infinity. An infinite K can correspond to a non-fading channel, or to perfect instantaneous CSIT. In either case, it is useful to study this limit, so that applicable scenarios can be identified.

When K approaches infinity, the objective function (4.11) is invalid since it also approaches infinity; hence, the full upper-bound (4.9) is used. With the K factor, the

channel model (2.18) can be written as

$$\mathbf{H} = \sqrt{\frac{K}{K+1}}\dot{\mathbf{H}}_m + \mathbf{H}_w\sqrt{\frac{1}{K+1}}\dot{\mathbf{R}}_t^{1/2}\,,$$

where $\dot{\mathbf{H}}_m$ and $\dot{\mathbf{R}}_t$ are normalized channel mean and transmit covariance as discussed in Appendix B.1. The upper-bound (4.9) can then be re-written as

$$E_{\mathbf{H}}\left[\text{PEP}\right] \leq \frac{\exp\left[\text{tr}\left(K\dot{\mathbf{H}}_m\mathbf{W}_0^{-1}\dot{\mathbf{H}}_m^*\right)\right]}{\det\left(\mathbf{W}_0\right)^M}\det\left(\dot{\mathbf{R}}_t\right)^M\exp\left[-\text{tr}\left(K\dot{\mathbf{H}}_m\dot{\mathbf{R}}_t^{-1}\dot{\mathbf{H}}_m^*\right)\right], \quad (4.43)$$

where

$$\mathbf{W}_0 = \frac{\gamma}{4(K+1)}\dot{\mathbf{R}}_t\mathbf{F}\mathbf{A}\mathbf{F}^*\dot{\mathbf{R}}_t + \dot{\mathbf{R}}_t\,.$$

Express $\mathbf{W}_0$ in the form $\mathbf{W}_0 = \dot{\mathbf{R}}_t^{1/2}\left(\mathbf{Q}+\mathbf{I}\right)\dot{\mathbf{R}}_t^{1/2}$, where

$$\mathbf{Q} = \frac{\gamma}{4(K+1)}\dot{\mathbf{R}}_t^{\frac{1}{2}}\mathbf{F}\mathbf{A}\mathbf{F}^*\dot{\mathbf{R}}_t^{\frac{1}{2}}.$$

With sufficiently large K, the largest eigenvalue of the PSD Hermitian matrix $\mathbf{Q}$ will be less than 1, and the following expansion [60] can be applied:

$$\mathbf{W}_0^{-1} = \dot{\mathbf{R}}_t^{-\frac{1}{2}}\left(\mathbf{I}-\mathbf{Q}+\mathbf{Q}^2-\mathbf{Q}^3+\ldots\right)\dot{\mathbf{R}}_t^{-\frac{1}{2}}.$$

Replacing this expression into the upper bound (4.43), and noting that

$$K\mathbf{W}_0^{-1} - K\mathbf{R}_0^{-1} \to -\frac{\gamma}{4}\mathbf{F}\mathbf{A}\mathbf{F}^* \quad \text{as} \quad K\to\infty,$$

the limiting upper bound on the average PEP is

$$P_{\text{K limit}} = \exp\left[-\text{tr}\left(\frac{\gamma}{4}\dot{\mathbf{H}}_m\mathbf{F}\mathbf{A}\mathbf{F}^*\dot{\mathbf{H}}_m^*\right)\right].$$

Minimizing $P_{\text{K limit}}$ is equivalent to maximizing the trace expression. Apply the inequality $\text{tr}(ABC) \leq \sum_i \sigma_i(A)\sigma_i(B)\sigma_i(C)$ [73] with $\sigma_i(.)$ as sorted singular values, where the equality is achieved when the right singular vectors of A (and B) align with the

left singular vectors of B (and C, respectively). Taking the power constraint (4.1) into account, the optimal precoder $\mathbf{F}$ has the form

$$\mathbf{F} = \mathbf{u}\mathbf{v}^* \,, \tag{4.44}$$

where $\mathbf{u}$ is the dominant eigenvector of $\dot{\mathbf{H}}_m^* \dot{\mathbf{H}}_m$ and $\mathbf{v}$ is the dominant eigenvector of $\mathbf{A}$. In other words, the optimal precoder, in the limit of an infinite K factor, is a single-mode beamformer, matching the dominant right singular vector of the channel mean. This result applies regardless of the STBC or the choice of the minimum- or the average-distance design, as the left singular vectors of $\mathbf{F}$ are independent of $\mathbf{A}$.

For a multiple-input single-output (MISO) system at infinite K (or perfect channel knowledge), single-mode beamforming is also optimal for achieving the channel capacity [41]. Therefore, the proposed precoding solution is optimal for a MISO system in the PEP criterion and asymptotically optimal in capacity. For a MIMO system, however, the optimal solution in the limit of infinite K differs between the two criteria: PEP per-distance and capacity. Whereas the capacity solution calls for water-filling over the eigen-modes of the channel, the PEP solution places all transmit power on the dominant mode. Thus, for a MIMO channel with high K factor, a precoder based on the PEP per-distance criterion is suitable for use along with a STBC with a rate of one or less. However, as K increases, the role of the STBC becomes less important in obtaining diversity. Moreover, the power loading on the precoder dominant mode increases as K increases; therefore, precoding can be combined with adaptive modulation and coding to take the full advantage of high K. At a low K factor, due to the multi-mode beamforming effect, a higher rate STBC can also be used with the PEP per-distance precoder in a MIMO system.

High SNR precoder analysis

To analyze the effect of the SNR γ on the precoder, examine the objective function (4.11), noting that γ affects $\mathbf{W}$ as given in (4.10). When $\gamma \to \infty$ then $\mathbf{W}^{-1} \to \mathbf{0}$; thus in the

limit, the objective function becomes

$$J_{\text{SNR limit}} = -M \log\det\left(\frac{\gamma}{4}\mathbf{R}_t\mathbf{F}\mathbf{A}\mathbf{F}^*\mathbf{R}_t + \mathbf{R}_t\right). \tag{4.45}$$

At high SNR, the precoder asymptotically depends only on the covariance $\mathbf{R}_t$. The precoder design problem is now equivalent to maximizing $\log\det\left(\frac{\gamma}{4}\mathbf{F}\mathbf{A}\mathbf{F}^* + \mathbf{R}_t^{-1}\right)$, subject to the power constraint (4.1). If $\mathbf{A}$ is a scaled-identity matrix, this is the standard water-filling problem [46]. For the non-identity $\mathbf{A}$, using the same analysis as in Section 4.3.2 for the non-asymptotic case, the optimal precoder right singular vectors are given by the eigenvectors of $\mathbf{A}$; that is, $\mathbf{V} = \mathbf{U}_{\mathbf{A}}$. Again, denoting $\mathbf{B} = \mathbf{F}\mathbf{A}\mathbf{F}^*$, the problem can be re-cast as follows:

$$\begin{aligned} \max_{\mathbf{B}} \quad & J_2 = \log\det\left(\frac{\gamma}{4}\mathbf{B} + \mathbf{R}_t^{-1}\right) \\ \text{subject to} \quad & \sum_i \xi_i\lambda_i(\mathbf{B}) \;=\; 1\,, \end{aligned} \tag{4.46}$$

where $\xi_i = 1/\lambda_i(\mathbf{A})$ for non-zero eigenvalues. Let $\mathbf{R}_t = \mathbf{U}_t\mathbf{\Lambda}_t\mathbf{U}_t^*$ be the eigenvalue decomposition of $\mathbf{R}_t$, then $J_2 = \log\det\left(\frac{\gamma}{4}\mathbf{U}_t^*\mathbf{B}\mathbf{U}_t + \mathbf{\Lambda}_t^{-1}\right)$. Noting that the eigenvalues of $\mathbf{U}_t^*\mathbf{B}\mathbf{U}_t$ are the same as those of $\mathbf{B}$, the transformation does not affect the constraint in (4.46). Thus, by the Hadamard inequality [72], J_2 is maximum when $\mathbf{U}_t^*\mathbf{B}\mathbf{U}_t$ is diagonal. This maximum implies that the optimal left singular vectors of $\mathbf{F}$ are the eigenvectors of $\mathbf{R}_t$. The optimization problem now becomes

$$\begin{aligned} \max_{\lambda_i(\mathbf{B})} \quad & \sum_i \log\left(\frac{\gamma}{4}\lambda_i(\mathbf{B}) + \lambda_i(\mathbf{R}_t^{-1})\right) \\ \text{subject to} \quad & \sum_i \xi_i\lambda_i(\mathbf{B}) \;=\; 1\,. \end{aligned}$$

This problem is convex and can be solved exactly, using the standard Lagrange multiplier technique [54], to obtain the solution

$$\lambda_i(\mathbf{B}) = \left(\frac{\lambda_i(\mathbf{A})}{\kappa} - \frac{4\lambda_i(\mathbf{R}_t^{-1})}{\gamma}\right)_+ \tag{4.47}$$

where κ is chosen to satisfy the equality constraint $\sum_i \xi_i\lambda_i(\mathbf{B}) = 1$.

Thus for the high SNR limit, the optimal precoder has the SVD as

$$\mathbf{F} = \mathbf{U}_t \mathbf{D} \mathbf{U}_{\mathbf{A}}^{*} \,, \tag{4.48}$$

where the singular-value matrix $\mathbf{D}$ has the diagonal entries obtained from (4.47) as $d_i = (\lambda_{ii}(\mathbf{B})/\lambda_i(\mathbf{A}))^{1/2}$. As SNR $\rightarrow \infty$, this solution approaches equi-power distribution on all the eigen-modes of $\mathbf{R}_t$ that correspond to the non-zero eigen-modes of $\mathbf{A}$.

K-factor vs SNR threshold for single-mode beamforming

Comparing the two limiting cases of the infinite K (4.44) and the infinite SNR (4.48), the precoder $\mathbf{F}$ converges in each case to a solution that depends on only one of the two statistical channel parameters: either the channel mean $\mathbf{H}_m$ or the transmit covariance $\mathbf{R}_t$. When the channel becomes more static, indicated by a high K factor, the channel mean dominates the precoder solution. At a high SNR, however, the fluctuation in the channel becomes more pronounced; hence, the transmit antenna correlation, equivalent to the channel covariance, tends to dominate the precoder solution. A parallel observation is that, as K increases, the precoder tends to drop modes until it becomes a single-mode beamformer, with an asymptotic direction as the dominant right singular vector of the channel mean. On the other hand, as the SNR increases, the precoder tends toward full-mode beamforming on all eigenvectors of the transmit covariance matrix with equal power allocation. These effects are observed, provided that all other parameters are kept constant when the variable of interest, the K factor or the SNR, varies. If both the K factor and the SNR increase, then there exists a K factor threshold for single-mode beamforming that increases with the SNR.

Figure 4.6 shows an example of the single- and multi-mode beamforming regions, as a function of the K factor and the SNR, for the 2×1 system using the Alamouti code and QPSK modulation. There are two noticeably different effects in this figure. In the high SNR high K-factor domain, single-mode beamforming is due to high K alone. At lower SNR, however, single-mode beamforming is also the result of the low SNR, when the precoder drops a mode due to insufficient power. The switching point between these

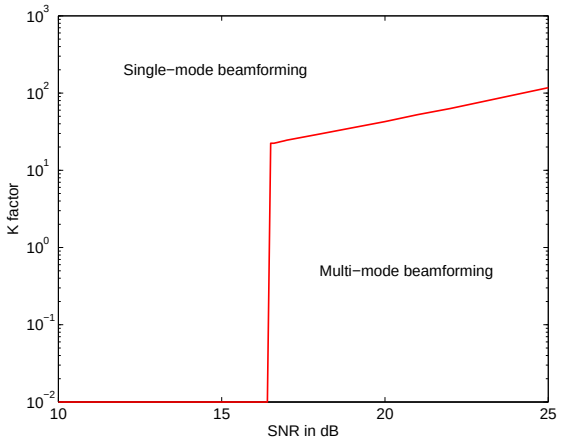

Figure 4.6: Single-mode and multi-mode beamforming regions of the precoder for a 2×1 system.

two effects depends on the specific channel parameters (mean and covariance). Therefore, the precoder is a multi-mode beamformer only at a sufficiently high SNR with sufficiently low K factor.

4.4.3 Special scenarios of the precoder design

This section analyzes the precoder design for two special scenarios: transmit covariance CSIT, when the channel has zero mean but is correlated, and mean CSIT, when the channel is uncorrelated with non-zero mean. Precoding for transmit covariance CSIT with general STBC was previously studied in [68], and for mean CSIT with OSTBC in [42]. The analysis here shows that the result in this thesis covers both these special cases. Furthermore, the latter case of precoding for mean CSIT is extended to the general STBC and an optimal precoder solution is obtained without relaxation.

Precoding with transmit covariance CSIT

Consider a channel with zero mean ($\mathbf{H}_m = 0$) and correlated transmit antennas, corresponding to a correlated Rayleigh fading channel. When the codeword distance product matrix $\mathbf{A}$ is a scaled-identity matrix, from (4.25), then $\mathbf{\Psi} = M^2\mathbf{I}$. Thus, the power

constraint equation (4.26) becomes a standard water-filling problem

$$\mathrm{tr}\left(\frac{M}{\nu}\mathbf{I}_N - \mathbf{R}_t^{-1}\right) = \eta_0 \,. \tag{4.49}$$

The optimal precoder $\mathbf{F}$ then has its beam directions given by the eigenvectors of $\mathbf{R}_t$ and the power allocation obtained via standard water-filling [46] on the eigenvalues of $\mathbf{R}_t$. No numerical binary search is required for ν in this case, and solving for the optimal precoder is simple.

With non-identity $\mathbf{A}$, the original problem (4.12) simplifies to a formulation similar to the asymptotically high SNR case (4.45). The result also reduces to $\mathbf{F}$ with the left singular vector given by the eigenvectors of $\mathbf{R}_t$, the right singular vectors by the eigenvectors of $\mathbf{A}$, and the power allocation by closed-form water-filling (4.47), without the necessity of a binary search. This result agrees with the solution established in [68], which was proved using Hadamard and geometric-arithmetic mean inequalities.

Precoding with mean CSIT

Now consider an uncorrelated channel ($\mathbf{R}_t = \mathbf{I}$) with non-zero mean, which can correspond to an uncorrelated Rician channel, or to a channel estimate with uncorrelated error at the transmitter. Again the precoder solution is simplified in this case. Specifically, a closed-form analytical solution can be obtained with all STBC, for both cases of scaled-identity and non-scaled-identity $\mathbf{A}$.

Scaled-identity $\mathbf{A}$

When $\mathbf{A}$ is a scaled-identity matrix, then $\mathbf{\Psi} = M^2\mathbf{I} + 4\nu\mathbf{H}_m^*\mathbf{H}_m$, and the power constraint equation (4.26) becomes a simpler water-filling problem

$$\mathrm{tr}\left(\frac{1}{2\nu}\left(M^2\mathbf{I} + 4\nu\mathbf{H}_m^*\mathbf{H}_m\right)^{\frac{1}{2}} - \left(1 - \frac{M}{2\nu}\right)\mathbf{I}\right) = \eta_0 \,. \tag{4.50}$$

The precoder solution has its left singular vectors given by the eigenvectors of $\mathbf{H}_m^*\mathbf{H}_m$, or the right singular vectors of the channel mean. The power loadings can be found using the inner and outer algorithms, in which the computation is simpler in this case as the

eigenvalues in the outer equation (4.29) can now be expressed explicitly in terms of ν. This result is similar to the solution established in [42] for precoding with OSTBC.

Non-identity $\mathbf{A}$

For a non-identity $\mathbf{A}$, re-visit the original problem formulation (4.12) to obtain

$$\begin{aligned} \min_{\mathbf{F}} \quad & J &=& \operatorname{tr}(\mathbf{H}_m \mathbf{W}^{-1} \mathbf{H}_m^*) - M \log\det(\mathbf{W}) \\ \text{subject to} \quad & \mathbf{W} &=& \frac{\gamma}{4} \mathbf{F}\mathbf{A}\mathbf{F}^* + \mathbf{I} \\ & \operatorname{tr}(\mathbf{F}\mathbf{F}^*) &=& 1\,. \end{aligned}$$

Note that the log det term in the objective function J depends only on $\mathbf{F}$ and $\mathbf{A}$, but not $\mathbf{H}_m$. Apply the inequality $\det(A+B) \leq \prod_i \lambda_i(A)\lambda_i(B)$ [73], then without modifying the eigenvalues of $\mathbf{F}$ or $\mathbf{A}$, the expression $\log\det(\mathbf{W}) = \log\det(\mathbf{A}) + \log\det(\frac{\gamma}{4}\mathbf{F}^*\mathbf{F} + \mathbf{A}^{-1})$ is maximized when the right singular vectors of $\mathbf{F}$ are the same as the eigenvectors of $\mathbf{A}$. Now, examine the trace term in J. Applying the inequality $\operatorname{tr}(AB) \geq \sum \lambda_i(A)\lambda_{n-i+1}(B)$ [72], then $\operatorname{tr}(\mathbf{H}_m \mathbf{W}^{-1} \mathbf{H}_m^*)$ is minimized when $\mathbf{W}$ has the same eigenvectors as those of $\mathbf{H}_m^*\mathbf{H}_m$. Noting that both inequalities place no constraints on the eigenvalues, except for their relative order, both the equality conditions can be simultaneously achieved by forcing the SVD of $\mathbf{F}$ to be

$$\mathbf{F} = \mathbf{U}_m \mathbf{D} \mathbf{U}_{\mathbf{A}}^*\,, \tag{4.51}$$

where $\mathbf{H}_m^*\mathbf{H}_m = \mathbf{U}_m \mathbf{\Lambda}_m \mathbf{U}_m^*$ is the eigenvalue decomposition of $\mathbf{H}_m^*\mathbf{H}_m$. This solution simultaneously determines the left and right singular vectors of $\mathbf{F}$ as $\mathbf{U}_m$ and $\mathbf{U}_A$, respectively.

It is now left to merely find the singular values of $\mathbf{F}$. Let $\mathbf{B} = \mathbf{F}\mathbf{A}\mathbf{F}^*$, and the problem can be reformulated in terms of $\lambda_i(\mathbf{B})$ as

$$\begin{aligned} \min_{\lambda_i(\mathbf{B})} \quad & \sum_i \left(1 + \frac{\gamma}{4}\lambda_i(\mathbf{B})\right)^{-1} \lambda_{m,i} - M \sum_i \log\left(1 + \frac{\gamma}{4}\lambda_i(\mathbf{B})\right) \\ \text{subject to} \quad & \sum_i \xi_i \lambda_i(\mathbf{B}) \;=\; 1 \\ & \lambda_i(\mathbf{B}) \;\geq\; 0\,, \end{aligned} \tag{4.52}$$

where $\xi_i = 1/\lambda_i(\mathbf{A})$, and $\lambda_{m,i}$ are the eigenvalues of $\mathbf{H}_m^*\mathbf{H}_m$. This problem is convex and can be solved using the standard Lagrange multiplier technique to obtain

$$\lambda_i(\mathbf{B}) = \left[\frac{\lambda_i(\mathbf{A})}{2\nu}\left(M + \sqrt{M^2 + 16\nu\frac{\lambda_{m,i}}{\gamma\lambda_i(\mathbf{A})}}\right) - \frac{4}{\gamma}\right]_+ \tag{4.53}$$

where ν is the Lagrange multiplier satisfying the constraint $\sum_i \xi_i\lambda_i(\mathbf{B}) = 1$. Depending on the number of dropped modes k (where $0 \le k \le N-1$), this ν value can be found using an one-dimensional binary search between the following two bounds:

$$\nu_{\text{upper}} = \frac{4\tilde{\lambda}_N}{\gamma\zeta_k^2} + \frac{M}{\zeta_k}\,, \qquad \nu_{\text{lower}} = \frac{4\tilde{\lambda}_1}{\gamma\zeta_k^2} + \frac{M}{\zeta_k}\,, \tag{4.54}$$

where $\tilde{\lambda}_N$ and $\tilde{\lambda}_1$ are the largest and smallest values of the set $\{\lambda_{m,i}/\lambda_i(\mathbf{A})|\ \lambda_i(\mathbf{A}) \neq 0,\ i = 1\ldots N\}$, respectively, and

$$\zeta_k = \frac{1}{N-k}\left(1 + \frac{4}{\gamma}\sum_{i=k+1}^{N}\frac{1}{\lambda_i(\mathbf{A})}\right)\,. \tag{4.55}$$

The derivation of (4.53) and (4.54) is given in Appendix A.6. The singular values of $\mathbf{F}$ are then $d_i = (\lambda_i(\mathbf{B})/\lambda_i(\mathbf{A}))^{1/2}$. Thus, mean CSIT also allows a closed-form optimal precoder solution with all STBCs.

Discussion on special scenario precoding

In both special cases when the channel mean or the transmit antenna correlation alone is present, the precoder solution is significantly simplified. The precoder beamforming directions are fixed and are given by the singular- or the eigen-vectors of the present channel parameter, and the power loadings are obtained by some form of water-filling over its eigenvalues. In these cases, closed-form optimal precoder solutions are available for all STBCs, and no relaxation is necessary.

4.5 Precoders based on the system capacity

This sections briefly examines other precoding designs based on stochastic optimization, including the system capacity (4.16) and the average PEP (4.15). For this group of criteria, the objective function involves an expectation that has no closed-form, the precoding optimization problems can be expressed in a general form as

$$\begin{aligned} \max \quad & E\big[f(\mathbf{I}+a\gamma\mathbf{HFQF}^*\mathbf{H}^*)\big] \\ \text{subject to} \quad & \mathrm{tr}(\mathbf{FF}^*)=1\ , \end{aligned} \tag{4.56}$$

where $f(.)$ is a concave function of the PSD matrix $\mathbf{HFQF}^*\mathbf{H}^*$, and a is a criterion dependent constant. For the capacity criterion, for example, f is $\log\det(.)$ and $a=1$, and for the average PEP, f is $-\det(.)^{-M}$ and $a=1/2$. Several other criteria, including the MMSE and the SNR [19], also belong to this group.

The optimal precoder in (4.56) has a closed-form solution for perfect CSIT (see [19] and references therein). For partial CSIT, usually only parts of the optimal precoders (1.4) can be obtained analytically. The optimal input shaping matrix, consisting of the precoder right singular vectors, can be established for all CSIT. For the special cases of mean CSIT and transmit covariance CSIT, the optimal beam directions, which are the precoder left singular vectors, can also be obtained analytically. The optimal beam power allocation, however, usually requires numerical techniques. These components of a precoder are discussed in more details below.

4.5.1 The optimal input-shaping matrix

For all CSIT, the input shaping matrix optimal for (4.56) is given by the eigenvectors of $\mathbf{Q}$. Let the eigenvalue decomposition of this matrix be $\mathbf{Q}=\mathbf{U}_Q\mathbf{\Lambda}_Q\mathbf{U}_Q^*$, then the precoder (1.4) has

$$\mathbf{V}_F=\mathbf{U}_Q\ . \tag{4.57}$$

The proof of this result is similar to the analysis leading to (4.35) in Section 4.3.2. This result implies that the precoder matches to the input-code covariance, so that it can

optimally collect the power from these codes.

This optimal input-shaping matrix results directly from the predetermined precoder-input covariance $\mathbf{Q}$, which is not an optimization variable nor involved in the power constraint (1.5). This covariance $\mathbf{Q}$ characterizes the code chosen for the system. When $\mathbf{Q}$ is an identity matrix, the optimal input-shaping matrix for (4.56) is an arbitrary unitary-matrix and can be omitted. For some other criteria, such as minimizing the maximum MSE among the received streams or the average BER, however, the optimal input-shaping matrix with $\mathbf{Q} = \mathbf{I}$ may be a specific rotational matrix [64, 79]. When channel coding such as a turbo-code is considered with practical constellation, a rotational matrix can also improve performance [80].

With the optimal input shaping matrix (4.57), let $\mathbf{\Theta} = \mathbf{FQF}^*$, then the constraint in (4.56) can be re-written in terms of the eigenvalues of $\mathbf{\Theta}$ as

$$\sum_i \lambda_i^{-1}(\mathbf{Q})\lambda_i(\mathbf{\Theta}) = 1 \ ,$$

provided the eigenvalues are sorted in the same order for both matrices, and the sum is over non-zero eigenvalues of $\mathbf{Q}$.

4.5.2 The optimal beam directions

The optimal beam directions can be obtained analytically only for mean CSIT and transmit covariance CSIT. The section generalizes existing results for $\mathbf{Q} = \mathbf{I}$ to arbitrary PSD $\mathbf{Q}$. For statistical CSIT that includes both a non-zero mean and a non-trivial covariance, the optimal beam directions for (4.56) are still unknown analytically.

With mean CSIT

Given the CSIT as a non-zero mean $\mathbf{H}_m$ and an identity covariance $\mathbf{R}_0 = \mathbf{I}$, problem (4.56) can be written as

$$\begin{aligned} \max \quad & E_{\mathbf{H}_w}\left[f\left(\mathbf{I} + a\gamma\left(\mathbf{H}_m + \mathbf{H}_w\right)\mathbf{\Theta}\left(\mathbf{H}_m + \mathbf{H}_w\right)^*\right)\right] \\ \text{subject to} \quad & \sum_i \lambda_i^{-1}(\mathbf{Q})\lambda_i(\mathbf{\Theta}) = 1 \ , \end{aligned} \tag{4.58}$$

where $\mathbf{H}_w$ contains i.i.d. Gaussian elements with zero-mean and unit variance. The optimal beam directions for this problem are given by the right singular vectors of $\mathbf{H}_m$

$$\mathbf{U}_F = \mathbf{U}_m \ , \tag{4.59}$$

where $\mathbf{H}_m = \mathbf{V}_m \mathbf{\Sigma}_m \mathbf{U}_m^*$ is the SVD of $\mathbf{H}_m$. The proof essentially follows from [65].

The directions (4.59) are the same as in the per-distance PEP-based precoder (4.51). Thus for mean CSIT, these beam directions are optimal for all studied criteria.

With transmit covariance CSIT

Given the CSIT as zero mean $\mathbf{H}_m = \mathbf{0}$ and a non-trivial transmit covariance $\mathbf{R}_t$, assuming receive covariance $\mathbf{R}_r = \mathbf{I}$, problem (4.56) can be transformed to

$$\begin{aligned} \max \quad & E_{\mathbf{H}_w}\left[f\left(\mathbf{I} + a\gamma \mathbf{H}_w \mathbf{R}_t^{1/2} \mathbf{\Theta} \mathbf{R}_t^{1/2} \mathbf{H}_w^* \right) \right] \\ \text{subject to} \quad & \sum_i \lambda_i^{-1}(\mathbf{Q}) \lambda_i(\mathbf{\Theta}) = 1 \ . \end{aligned} \tag{4.60}$$

The optimal beam directions for this problem are given by the eigenvectors of $\mathbf{R}_t$

$$\mathbf{U}_F = \mathbf{U}_t \ . \tag{4.61}$$

The proof can be found in Appendix A.7.

These directions are the same as in the PEP per-distance precoder (4.48). Thus for transmit covariance CSIT, these beam directions are also optimal for all studied criteria.

4.5.3 Power allocation

Unfortunately, little can be said about the optimal power allocation for (4.56). No closed-form solutions are available because of the stochastic nature of the problem. With mean CSIT and transmit covariance CSIT, the power optimization problem can be obtained by replacing the optimal beam directions into (4.58) and (4.60), respectively. These problems then become convex in terms of the variables $\lambda_i(\mathbf{\Theta})$ and can be solved numerically to arrive at the optimal solution. The optimal power allocation depends on the specific function

f, representing the criterion. In general, the optimal allocation follows the water-filling principle. Higher power is allocated to the mode corresponding to the stronger $\lambda_i(\mathbf{Q})$ and stronger $\sigma_i(\mathbf{H}_m)$ or $\lambda_i(\mathbf{R}_t)$, and reduced or no power to the weaker. In effect, the input-code modes are connected to the channel modes, based on CSIT, in the same sorting-order, and higher power is allocated to the stronger mode.

4.6 Precoding design comparison

Having established precoder designs under alternative criteria, this section compares these precoders both structurally and numerically. Their structural similarities and differences are discussed. Their performance is then evaluated in terms of the error rate, using a common simulation system.

4.6.1 Structural similarities and differences

The presented optimal precoding solutions under alternative criteria – PEP per-distance, average PEP, and system capacity – lead to several observations. For the similarities, all optimal precoders have the same right eigenvectors. These vectors form the input-shaping matrix, matched to the covariance of the precoder input signal, independent of the CSIT and the SNR. For the special CSIT cases (mean alone or transmit covariance alone), these precoders also have the same left eigenvectors. These vectors provide the beam directions, matched to the channel according to the CSIT, and are independent of the SNR. Only when both a non-zero channel mean and a non-trivial channel covariance are present that these beam directions may change with the SNR.

The main difference among the optimal precoding solutions under different criteria is the power allocation. This power allocation tends to follow the water-filling principle, in which higher power is allocated to stronger modes, and weak modes are dropped, depending on the SNR. The selectivity in the power allocation, however, varies according to the criterion; more selective schemes tend to drop more modes at low SNRs. In particular, the PEP criterion is more selective than the capacity. As the SNR increases, all the power allocation schemes, except for the PEP per-distance with perfect CSIT,

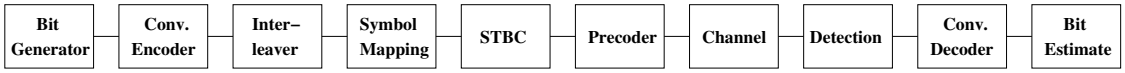

Figure 4.7: Simulation system configuration.

approach equi-power, but at different rates. A more selective scheme approaches equi-power more slowly. The precoder, in essence, optimally collects the input signal power and spatially redistributes this power into the channel according to the performance criterion and the CSIT.

4.6.2 Performance comparison

Using the simulation structure in Figure 4.7, the precoder designs are evaluated in terms of the system error performance for different CSIT scenarios. The simulation generates i.i.d. random bit streams, encodes this data with a convolutional code, interleaves and maps the coded bits into symbols, before encoding with a STBC and precoding for transmission. The signal is then sent through a randomly-generated channel and added white Gaussian noise. The receiver detects and decodes the signal, and measures both the uncoded and coded error rates, which refer to the system performance without and with the channel coding, respectively.

Simulation setup

The simulation system has 4 transmit and 2 receive antennas and employs the quasi-orthogonal STBC (4.40). Although a 4×2 system can support up to a spatial rate of 2, this STBC has only the spatial rate 1. With this STBC, the precoder input shaping matrix is the identity matrix and is omitted. The system implements the [133, 171] convolutional code with rate 1/2, used in the IEEE 802.11a wireless LAN standard [81], a block interleaver, and QPSK modulation. The receiver uses maximum-likelihood (ML) detection and a soft-input soft-output Viterbi decoder.

System performance is measured for several CSIT scenarios: perfect CSIT, transmit covariance CSIT, and dynamic CSIT (2.25) involving both channel mean and transmit covariance information. Assume quasi-static block-fading channels, the block-length for the perfect and covariance CSIT is 96 bits, and for dynamic CSIT is 48 bits. Performance

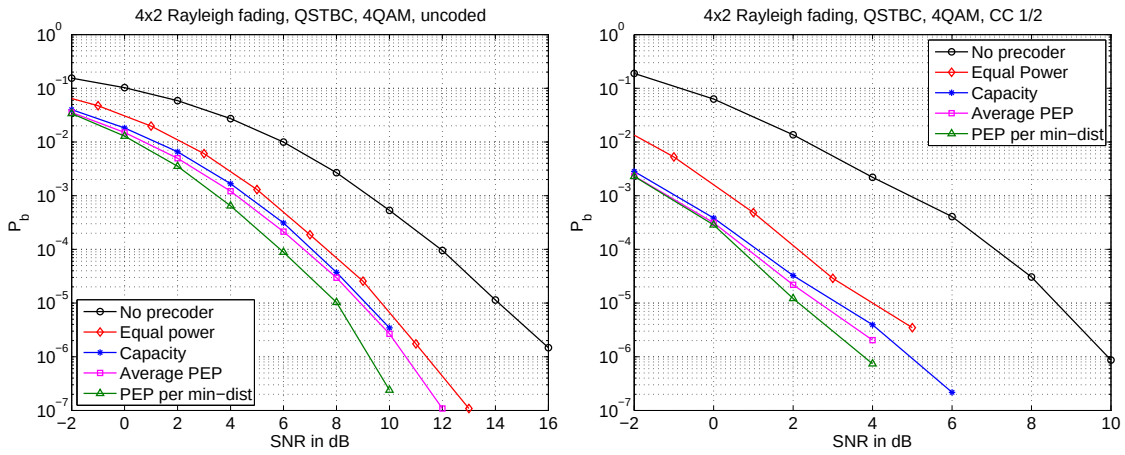

(a) (b)

Figure 4.8: Comparative precoding performance with perfect CSIT: (a) uncoded; (b) coded.

without and with different precoders, based on the PEP per minimum-distance (4.12), average PEP (4.15), and system capacity (4.16) criteria, are studied.

Precoding with perfect CSIT

Precoding solutions with perfect CSIT are available in closed-form. The optimal beam directions are given by the channel right singular vectors. For the average-PEP and the capacity criteria, the power allocation is obtained by standard water-filling on the appropriate eigenvalues [46]. For the minimum-distance PEP criterion, the optimal power concentrates only on the dominant channel singular vector and the precoder becomes single-mode beamforming (see Section 4.4.2).

For perfect CSIT, the channel is assumed to be i.i.d. Rayleigh fading ($\mathbf{H}_m = 0$ and $\mathbf{R}_0 = \mathbf{I}$). Figure 4.8 shows the error performance. All three precoder designs achieve substantial gains, measured in both uncoded and coded performance, with larger gain in the latter (up to 6dB SNR gain at 10^{-4} coded bit-error-rate). Such a gain is consistent with the analytical capacity gain (3.11). Since the QSTBC provides only partial diversity, some additional diversity gain is obtained by the precoder, evident through the higher slopes of the precoded error curves in the uncoded systems. In both uncoded and coded systems, however, most of the precoding gain appears in the form of a coding gain. This

coding gain is attributed to the optimal beam directions and the water-filling-type power allocation. To differentiate the gain from each effect, a 2-beam precoder with the optimal directions, given by the channel right singular vectors, but equal beam-power allocation is also studied. Results show that with perfect CSIT, optimal beam directions alone achieve a significant portion of the precoding gain. A water-filling-type power allocation further improves the gain, especially at low SNRs. Thus, both the precoder beam directions and the power allocation contribute to the performance gain.

These results also reveal only minor performance differences among precoder designs according to the three criteria. The minimum-distance PEP precoder, which also maximizes the received SNR, achieves the best gain here, attributed to the small number of receive antennas. The other two precoders, based on the capacity and the average PEP criteria, perform similarly. This relative performance order is dependent on the CSIT and the system configurations, including the number of antennas, channel coding, and the STBC; it may change for a different system.

Precoding with transmit covariance CSIT

With transmit covariance CSIT, the optimal beam directions are given by the covariance eigenvectors for all criteria. For the average-PEP and the capacity criteria, no closed-form solution is available for the optimal power allocation. The corresponding Jensen power approximation (see Section 3.5.1), which is accurate at low SNRs, is used instead. For the minimum-distance PEP criterion, water-filling over the transmit covariance eigenvalues provides the optimal power allocation (see Section 4.4.3).

The channel mean in this case is zero and the transmit covariance matrix for simulation is given in Appendix B.4. This matrix has the eigenvalues as $[2.717,\ 0.997,\ 0.237,\ 0.049]$ and a condition number of 55.5. Thus, the transmit antennas here are quite strongly correlated, chosen to emphasize the gain from covariance CSIT.

Figure 4.9 shows the performance results. All the three precoders again achieve significant gains in both uncoded and coded domains (approximately 3dB SNR gain at 10^{-4} coded bit-error-rate). The minimum-distance PEP precoder has now moved away from the single-beam solution. A single-beam precoder matched to the dominant eigenvector

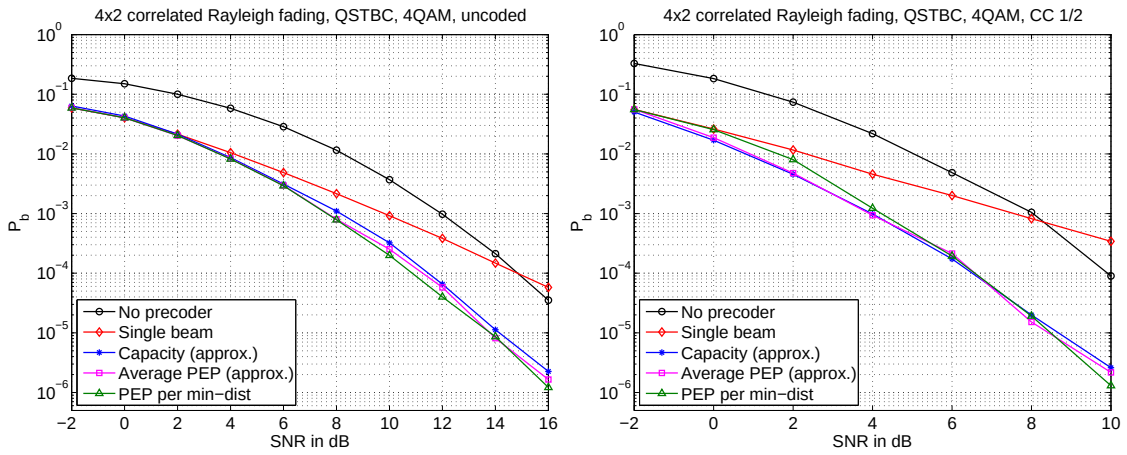

Figure 4.9: Comparative precoding performance with transmit covariance CSIT: (a) uncoded; (b) coded.

of the transmit covariance matrix is also included for comparison. In contrast to the perfect CSIT case, this single-beam scheme performs poorly; it has a diversity order of 1 and performs worse than no precoding at high SNRs.

Results from Figures 4.8 and 4.9 illustrate that the precoding gains depend strongly on the CSIT. Higher quality CSIT will improve the precoding gain – the perfect CSIT provides the best gain. Furthermore, for partial CSIT, no precoding diversity gain is present. All precoded error-rate curves in the uncoded domain in Figure 4.9 have the same diversity order of 2 as that of the QSTBC. Again, this figure shows similar performance among all precoders under the three criteria. The precoding gain also depends on the transmit antenna correlation. A more correlated channel will result in a higher precoding gain from transmit covariance CSIT.

Precoding with dynamic CSIT

This section examines precoding performance with dynamic CSIT. For the system capacity and average-PEP criteria, unfortunately, no analytical solutions exist for the optimal precoders. The optimal precoder based on the minimum-distance PEP (4.32) is used. Simulation results in the last two sections, however, suggest that precoders based on the capacity and the average-PEP criteria have similar performance for this system. The

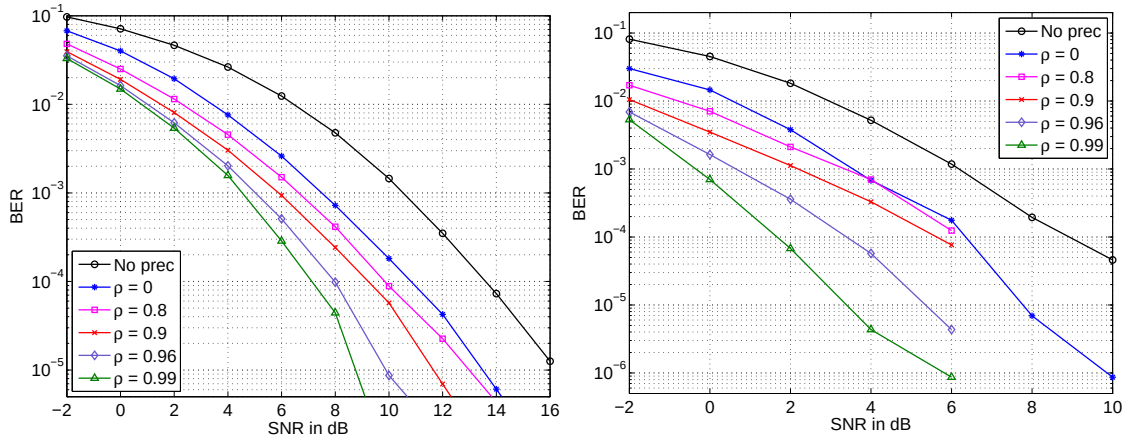

Figure 4.10: System performance with dynamic CSIT using the minimum-distance PEP precoder: (a) uncoded; (b) coded.

channel mean and transmit covariance matrices are given in Appendix B.4.

Figure 4.10 provides the uncoded and coded performance results for various CSIT quality ρ. Similarly to Figure 4.4, the precoding gain increases with higher CSIT quality. Figure 4.11 shows the regions of different number of precoding beams, as a function of the channel K factor and the SNR. A higher K factor leads to fewer beams, whereas a higher SNR leads to more beams. Other design criteria may lead to different precoding beam regions.

4.6.3 Discussion on the precoding gain

The presented simulation results show that precoding gains are significant in both uncoded and coded domains, usually with higher gains in the latter. The gain depends on the CSIT, the number of antennas, the system configuration, and the SNR. Better CSIT quality leads to higher precoding gain, although the gain is sensitive to high quality only (roughly $\rho \geq 0.6$). With dynamic CSIT, the precoding gain is robust and ranges from statistical to perfect CSIT gain. The gain usually increases with more antennas. For the simulated system configuration, similar performance is observed among precoders based on the alternative criteria: system capacity, average PEP, and minimum-distance PEP. The precoding gain is comprised of two parts: an array gain obtained by the optimal

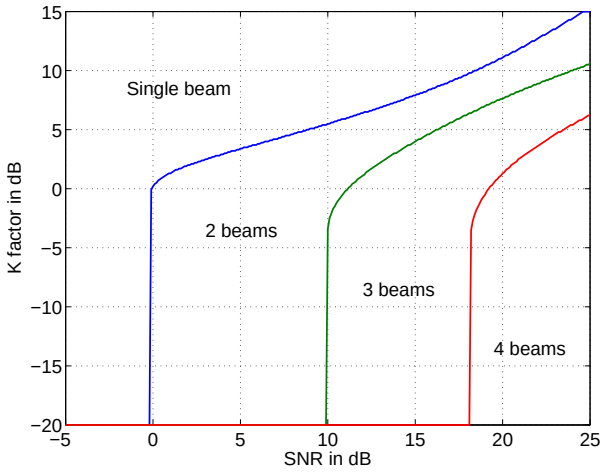

Figure 4.11: Regions of different numbers of beams of the minimum-distance PEP precoder for a 4×2 system.

beam directions, and a water-filling gain obtained by the power allocation; both result in an SNR advantage. When the CSIT is perfect, the precoders also deliver an additional diversity gain.

4.7 Chapter summary

This chapter has focused on precoding techniques that exploits dynamic CSIT, involving an effective channel mean and transmit covariance. It proposes linear precoder designs. A precoder design depends on the performance metric, which sets the design criterion. This criterion can be to maximize the system ergodic-capacity, assuming ideal coding for vanishing error, or to minimize an error probability at a fixed transmission rate. The choice of criterion usually depends on the specific system.

The chapter first considers a system employing a precoder in conjunction with a space-time block code (STBC) at the transmitter. Using convex optimization, the precoder is designed to minimize the Chernoff bound on the pair-wise error probability of the minimum- or the average-distance codeword pairs. Analytical precoder solutions are established for both systems with orthogonal and with non-orthogonal STBCs. The precoder right singular vectors act as the input shaping matrix, matched to the eigenvectors of the input ST codeword distance product matrix. The left singular vectors are the

beam directions matched to the channel, based on the CSIT. The singular values represent the beam power allocation, which depends on both the STBC and the CSIT. A dynamic water-filling algorithm establishes the optimal beam directions and power allocation, both of which evolve with the water-filling iterations and depend on the SNR. The algorithm involves simple and efficient binary searches to find the Lagrange multiplier. Asymptotic analyses of the precoder results reveal that the precoder depends primarily on the channel mean at high K factors, and on the transmit covariance at high SNRs.

The precoding gain is attributed to the optimal beam directions and water-filling-type beam power allocation. Simulations confirm significant gains, which depend on the channel mean and covariance matrices, the number of antennas, the choice of the codeword-pair distance, and the SNR. The gain with partial CSIT ($\rho < 1$) is a pure coding gain. With perfect CSIT ($\rho = 1$), the precoder also delivers the maximum diversity gain. With dynamic CSIT, the precoding gain ranges from statistical to perfect CSIT gain, depending on the CSIT quality ρ. The gain, however, is sensitive to ρ for high CSIT quality only, at approximately $\rho \geq 0.6$. Otherwise, the gain is similar to that obtained from statistical CSIT at $\rho = 0$.

The chapter also briefly considers precoding based on the system capacity and the average-PEP criteria, representing a group of stochastic optimization problems involving non-reducible expectation in the objective function. Analyses for the special cases, mean CSIT and transmit covariance CSIT, show that the optimal precoding beam directions are independent of the SNR and the design criterion, including the average-PEP and the capacity. The beam power allocation, on the other hand, depends heavily on both the SNR and the criterion. Simulations, however, suggest that system performance is more sensitive to the beam directions than to the power allocation, leading to only slight differences in the performance of these different precoding schemes.

In short, a precoder exploits the CSIT by spatially matching the transmit signal to the channel in the form of multi-mode beamforming. While this chapter focuses on dynamic CSIT, the next chapter will examine precoding for the high-K variable-phase CSIT.

Chapter 5

TRANSMISSION WITH HIGH-K VARIABLE-PHASE CSIT

The previous two chapters have focused on dynamic CSIT. This chapter considers a different CSIT scenario, in which the whole channel is not estimated but instead only some parameters are known. Consider a forward link at a base station, for example, which has dominant direct-path propagation and large antenna spacing, in the order of 10 carrier wavelengths. The amplitudes of the channel elements are stable over time because of direct-path propagation. Their phases, however, are highly sensitive to the direction of propagation because of the large antenna spacing. Such a scenario potentially leads to known channel amplitude but unknown phase at the transmitter. The distribution of the phase, nevertheless, can be obtained over time. This CSIT is captured in the high-K variable-phase model in Section 2.5.

Given high-K variable-phase CSIT, this chapter analyzes the optimal transmission scheme that achieves the ergodic capacity of a 2×1 channel. The channel consists of two complex elements. The CSIT includes their amplitudes (antenna gains) and the probability density function (pdf) of the phase shift between these two elements. The phase shift, but not the absolute phase at each antenna, is crucial in determining the

direction to transmit signals. The absolute phase of the reference antenna is canceled during receiver processing to recover the signal. For subsequent analysis, the phase-shift pdf is assumed to be symmetric around its mean. The specific pdf affects the optimal antenna power allocation. Analytical results are established for a general phase-shift pdf, and simulations are performed using the Rician phase distribution [28, 45]. The Rician phase pdf can be parameterized to cover the range from uniform distribution (unknown phase-shift) to the delta function (exact phase-shift knowledge).

The transmission-scheme goal is to maximize the channel ergodic capacity. To achieve the capacity, the input signal must be Gaussian distributed with zero mean. The main problem then is to find the optimal covariance matrix of this Gaussian input. With two transmit antennas, the input covariance can be parameterized in terms of three variables: the phase shift and the correlation between, and the normalized magnitude (or power) of the two transmitted signals.

The optimal scheme contains two categories, depending on the antenna gain ratio. If the two antenna gains are unequal, corresponding to a gain ratio different from 1, the optimal scheme is always beamforming on the mean of the channel phase-shift. The two antennas then transmit the same symbol but with different power, adjusted according to the gain ratio and the phase-shift pdf. When the two antennas have equal gains, the optimal scheme includes, but is not limited to, beamforming. The optimal signals from two equal-gain antennas can be different but correlated according to a given full-rank covariance matrix. In both cases, however, when there is no phase knowledge, corresponding to a uniform phase-shift pdf, the optimal scheme reduces to single antenna transmission.

This chapter organization is as follows. Section 5.1 poses the problem as maximizing the channel ergodic capacity and summarizes the main results. The optimal signal phase-shift is established in Section 5.2, followed by the optimal power allocation and signal correlation in Section 5.3. Section 5.4 provides simulation examples using the Rician pdf for the channel phase-shift. Section 5.5 discusses the benefits of the high-K variable-phase CSIT. Section 5.6 then summarizes the chapter.

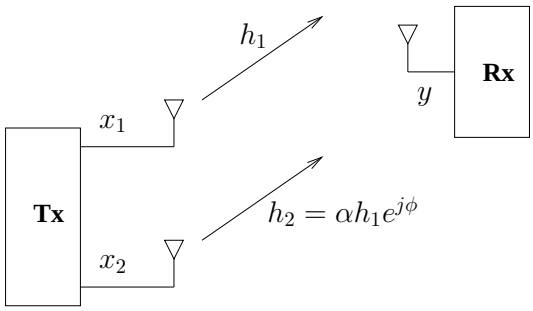

Figure 5.1: A 2×1 system with high-K variable-phase CSIT.

5.1 Capacity maximization and result summary

Consider a 2×1 system as depicted in Figure 5.1. Let $\mathbf{x} = [x_1 \ x_2]^T$ be the vector of transmit signals, and y be the receive signal, the input-output equation can then be written as

$$y = \mathbf{hx} + n \ , \tag{5.1}$$

where $\mathbf{h}$ is the channel and n is the additive white Gaussian noise. The channel $\mathbf{h}$ here is a row-vector of two elements $[h_1 \ h_2]$ with the relationship (2.13), repeated here for convenience

$$h_2 = \alpha e^{j\phi} h_1 \ , \tag{5.2}$$

where α is the antenna gain ratio ($0 \leq \alpha \leq 1$), and ϕ is the antenna phase shift ($-\pi \leq \phi \leq \pi$). The CSIT includes perfectly-known amplitudes of the two channel elements, and thus α, and their phase-shift pdf as $f(\phi)$. Let ϕ_0 be the mean value of ϕ, the pdf $f(\phi)$ is assumed to be symmetric around ϕ_0. The receiver, on the other hand, knows the whole channel $\mathbf{h}$ perfectly.

5.1.1 Ergodic capacity maximization

The goal of this chapter is to design a transmission scheme to achieve the channel ergodic capacity under the sum power constraint on the transmit antennas. Since the receiver has perfect channel knowledge, the channel ergodic capacity is achieved by Gaussian input signal with zero mean [46]. Consider a zero-mean Gaussian signal with covariance

$\mathbf{Q} = E[\mathbf{x}\mathbf{x}^*]$, the average mutual information conveyed by this input is

$$\mathcal{I} = E\log(1 + \gamma_0 \mathbf{h}\mathbf{Q}\mathbf{h}^*) \,, \tag{5.3}$$

where γ_0 is the ratio between the transmit signal power and the noise power, and the expectation is performed over the random channel phase-shift ϕ with pdf $f(\phi)$. The capacity-optimal signal has the covariance that maximizes this mutual information within the transmit power limit. Since the amplitudes of the channel coefficients are known to the transmitter, let the reference amplitude be absorbed into a signal-to-noise ratio defined as

$$\gamma = \gamma_0 |h_1|^2 \,,$$

and write the effective channel as

$$\tilde{\mathbf{h}} = [1 \;\; \alpha e^{j\phi}] \,.$$

Then the capacity-optimal input covariance is the solution to the following problem

$$\begin{aligned} \max_{\mathbf{Q}} \quad & E\log(1 + \gamma \tilde{\mathbf{h}}\mathbf{Q}\tilde{\mathbf{h}}^*) \\ \text{subject to} \quad & \mathrm{tr}(\mathbf{Q}) = 1 \\ & \mathbf{Q} \succcurlyeq \mathbf{0} \,, \end{aligned} \tag{5.4}$$

in which the trace constraint results from the sum transmit power limit, and the positive semi-definite constraint results from the property of a covariance matrix.

For a two-transmit-antenna system, the input covariance $\mathbf{Q}$ is a Hermitian matrix of size 2×2. Taking into account the sum power constraint $\mathrm{tr}(\mathbf{Q}) = 1$, this matrix $\mathbf{Q}$ can be expressed as

$$\mathbf{Q} = \begin{bmatrix} \eta & \frac{1}{2}\varrho e^{-j\psi} \\ \frac{1}{2}\varrho e^{j\psi} & 1-\eta \end{bmatrix} \,. \tag{5.5}$$

In this representation, η is the fraction of total power allocated to the first antenna, ψ is the signal phase-shift and ϱ is twice the magnitude of the covariance between the signals

transmitted from the two antennas. Specifically, ϱ is defined as

$$\varrho = 2\big|E[x_1 x_2^*] - E[x_1]E[x_2^*]\big| = 2\big|E[x_1 x_2^*]\big| \,,$$

where the last equality results from the signals having zero mean. Subsequently, ϱ is referred to simply as the signal correlation.

The three variables η, ψ, and ϱ define the transmission scheme. The constraints on these variables become

$$\begin{aligned} 0 &\leq \eta \leq 1 \\ -\pi &\leq \psi \leq \pi \\ 0 &\leq \varrho \leq 2\sqrt{\eta(1-\eta)} \,. \end{aligned} \tag{5.6}$$

The bounds on η follow immediately from its definition, whereas the bounds on ψ result from a predefined domain of the signal phase-shift. The lower bound on ϱ results from it being a magnitude, and the upper bound comes from the covariance relation

$$\big|E[x_1 x_2^*]\big| \leq \sqrt{E|x_1|^2 E|x_2|^2} \tag{5.7}$$

for zero-mean random variables. This upper-bound can also be obtained from the positive semi-definite property of the covariance matrix, $\mathbf{Q} \succcurlyeq \mathbf{0}$.

The average mutual information (5.3) can now be expressed in terms of these signal parameters. Noting that the phase-shift pdf $f(\phi)$ is symmetric around its mean ϕ_0, let $\tilde{\phi} = \phi - \phi_0$ and wrap it within $[-\pi,\ \pi]$, then the pdf of $\tilde{\phi}$ is symmetric around zero. For simple notation, ϕ will be used instead of $\tilde{\phi}$ in subsequent analyses and $f(\phi)$ shall refer to the translated zero-centered pdf. After some simple derivations, the mutual information (5.3) becomes

$$\begin{aligned} \mathcal{I} &= E\log(1 + \gamma \tilde{\mathbf{h}} \mathbf{Q} \tilde{\mathbf{h}}^*) \\ &= \int_{-\pi}^{\pi} \log\left[\gamma(1-\alpha^2)\eta + \gamma\alpha\varrho\cos(\phi + \psi_0) + \gamma\alpha^2 + 1\right] f(\phi)\, d\phi \,, \end{aligned} \tag{5.8}$$

where $\psi_0 = \psi + \phi_0$. The capacity maximization problem (5.4) now becomes equivalent to maximizing (5.8) by choosing η, ψ, and ϱ subject to the constraints (5.6) as

$$\begin{aligned} \max \quad & \int_{-\pi}^{\pi} \log\left[\gamma(1-\alpha^2)\eta + \gamma\alpha\varrho\cos(\phi+\psi_0) + \gamma\alpha^2 + 1\right] f(\phi)\, d\phi \qquad (5.9) \\ & 0 \;\le\; \eta \;\le\; 1 \\ \text{subject to} \quad & -\pi \;\le\; \psi \;\le\; \pi \\ & 0 \;\le\; \varrho \;\le\; 2\sqrt{\eta(1-\eta)}\,. \end{aligned}$$

Since problem (5.4) is convex, this problem is also convex and hence can be solved exactly.

5.1.2 Summary of results

The optimal transmission scheme is defined by the transmit covariance matrix $\mathbf{Q}$, which in turn is defined by η, ψ, and ϱ. These parameters are found based on the CSIT, which includes the antenna gain ratio α, the channel phase-shift distribution $f(\phi)$, and the SNR γ. The main results can be summarized as follows.

- The optimal signal phase-shift is the negative of the mean of the channel phase-shift: $\psi^\star = -\phi_0$, or that plus π, depending on the specific channel phase-shift pdf $f(\phi)$. In other words, the phase shift of the optimal transmit signal must offset the average phase shift in the channel. The $\psi^\star$ value is independent of α and γ. This result is established in Section 5.2.

- When the antenna gains are unequal ($\alpha < 1$), the optimal transmission scheme is always single-mode beamforming with unequal power allocation at the two transmit antennas. The optimal signal correlation $\varrho^\star$ is a function of the optimal signal power allocation $\eta^\star$, and $\eta^\star$ is specified by the phase-shift pdf $f(\phi)$, the antenna gain ratio α, and the SNR γ. This result is derived in Section 5.3.1.

- When the antenna gains are equal ($\alpha = 1$), the optimal transmission can either be beamforming, or space-time coding with correlated signals. In this case, the power allocation η has no effect on the average mutual information (5.8). The optimal signal correlation $\varrho^\star$ is determined by $f(\phi)$ and γ. The transmit power can then

be arbitrarily divided between the two antenna, within the range specified by the upper bound on $\varrho^\star$ in (5.6). This result is analyzed in Section 5.3.2.

5.2 The optimal signal phase-shift

The optimal signal phase-shift $\psi^\star$ is independent of the antenna gain ratio α and the SNR γ, and hence, is treated separately in this section.

Theorem 7. *The optimal phase-shift $\psi^\star$ between the signals transmitted from the two antennas is the negative of the mean of the channel phase-shift ϕ_0, or that plus π, depending on the channel phase-shift pdf $f(\phi)$. That is,*

$$\psi^\star = -\phi_0 \quad or \quad \psi^\star = \pi - \phi_0 \; . \tag{5.10}$$

Proof. The original problem (5.4) is convex and hence has a unique optimal solution, which leads to a unique value of $\psi^\star$. Due to symmetry of the phase-shift pdf, $f(\phi) = f(-\phi)$, the average mutual information in (5.8) can be rewritten as

$$\mathcal{I} = \int_0^\pi \log\left[p^2 + 2p\gamma\alpha\varrho\cos\psi_0\cos\phi + \gamma^2\alpha^2\varrho^2\left(\cos^2\psi_0 + \cos^2\phi - 1\right)\right] f(\phi)\, d\phi \; ,$$

where $p = \gamma\left(1-\alpha^2\right)\eta + \gamma\alpha^2 + 1$. The goal is to find the optimal value of $\psi_0 = \psi + \phi_0$ that maximizes $\mathcal{I}$, subject to $-\pi \le \psi \le \pi$. Let $z = \cos\psi_0$, then the optimization can be performed in terms of z instead of ψ, then the optimal value $\psi^\star$ can be derived from $z^\star$. If the optimal $z^\star$ is not 1 or -1, then there will be two different values of $\psi^\star$ within the range $[-\pi, \pi]$ that satisfy $\cos(\phi^\star + \phi_0) = z^\star$, since cosine is an even function. But this finding violates the uniqueness of $\psi^\star$. Therefore, $z^\star$ must be either 1 or -1, which leads to $\psi^\star = -\phi_0$ or $\psi^\star = \pi - \phi_0$, respectively. This optimal $\psi^\star$ is a result of the symmetry of the channel phase-shift pdf. □

The choice between $\psi = -\phi_0$ and $\psi = \pi - \phi_0$ that makes $\mathcal{I}$ larger is the optimal $\psi^\star$. It depends on the phase-shift pdf $f(\phi)$. More simply, if the translated phase-shift pdf $f(\phi)$ is monotonic within the range $0 \le \phi \le \pi$, then the choice between $\phi = 0$ and $\phi = \pi$ that makes $f(\phi)$ larger determines the optimal $\psi^\star$ as $-\phi_0$ or $\pi - \phi_0$, respectively (see the

analysis in Appendix A.8). This monotonicity applies to the Rician phase distribution used in simulations in Section 5.4. Since $f(\phi)$ is circular within $[-\pi\ \pi]$, it can be rotated so that $f(0) > f(\pi)$. Therefore, without loss of generality, the optimal signal phase-shift is assumed to be $\psi^\star = -\phi_0$ subsequently.

5.3 The optimal signal power and correlation

This section establishes the optimal set of η and ϱ. The cases of unequal antenna gains ($\alpha < 1$) and equal antenna gains ($\alpha = 1$) have significantly different impacts on the optimal $\eta^\star$ and $\varrho^\star$. While the solution for unequal antenna gains can be applied to the equal-gain case, the latter has a larger solution space. Therefore, these two cases are analyzed separately.

5.3.1 Unequal antenna gains

Without loss of generality, assume the first antenna always has higher gain than the second, thus α is strictly less than 1. With the optimal signal phase-shift $\psi^\star = -\phi_0$, the optimization problem (5.9) now becomes

$$\begin{aligned} \max \quad & \int_0^\pi \log\left[\gamma\left(1-\alpha^2\right)\eta + \alpha\varrho\gamma\cos\phi + \gamma\alpha^2 + 1\right] f(\phi)\, d\phi \qquad (5.11) \\ \text{subject to} \quad & 0 \ \leq\ \eta \ \leq\ 1 \\ & 0 \ \leq\ \varrho \ \leq\ 2\sqrt{\eta(1-\eta)}\,. \end{aligned}$$

The optimal $\eta^\star$ and $\varrho^\star$ are related as in the following theorem.

The optimal signal correlation $\varrho^\star$

Theorem 8. *With $\alpha < 1$, the optimal correlation between signals transmitted from the two antennas has the magnitude*

$$\varrho^\star = 2\sqrt{\eta(1-\eta)}\,. \qquad (5.12)$$

The transmit signals then has the form

$$x_2 = \zeta e^{-j\phi_0} x_1 \ , \tag{5.13}$$

with ζ given by

$$\zeta = \sqrt{\frac{1-\eta}{\eta}} \ . \tag{5.14}$$

In other words, the optimal transmission scheme reduces to simple single-mode beamforming with unequal power at each antenna.

Proof. Problem (5.11) is a convex optimization problem. Form the Lagrangian as

$$\mathcal{L}(\eta, \varrho, \lambda) = E \log \left[\gamma \left(1-\alpha^2\right) \eta + \alpha\varrho\gamma \cos\phi + \gamma\alpha^2 + 1\right] - \lambda \left[\varrho - 2\sqrt{\eta(1-\eta)}\right] \ ,$$

where $\lambda \geq 0$ is the Lagrange multiplier associated with the upper constraint on ϱ. Then the optimal $\eta^\star$ and $\varrho^\star$ are obtained by setting the partial derivatives of $\mathcal{L}(\eta, \varrho, \lambda)$ to zero. In particular, setting the partial derivative with respect to η to zero leads to

$$E\left[\frac{\gamma\left(1-\alpha^2\right)}{\gamma\left(1-\alpha^2\right)\eta + \alpha\varrho\gamma\cos\phi + 1 + \gamma\alpha^2}\right] = \lambda \frac{2\eta - 1}{\sqrt{\eta\left(1-\eta\right)}} \ .$$

With $\alpha < 1$, the expression under the expectation is always positive, hence the left-hand-side of the above expression is strictly greater than 0 for all distributions of ϕ. Since $\lambda \geq 0$, the optimal values must satisfy $\lambda^\star > 0$ and $\eta^\star > \frac{1}{2}$. Now $\lambda^\star$ strictly positive implies that the upper constraint on ϱ is tight (by complementary slackness [54]), hence $\varrho^\star = 2\sqrt{\eta(1-\eta)}$.

Another way to arrive at this result is by equating the partial derivative of $\mathcal{L}(\eta, \varrho, \lambda)$ with respect to ϱ to zero to get

$$\frac{\partial \mathcal{I}}{\partial \varrho} = E\left[\frac{\alpha\gamma\cos\phi}{\gamma\left(1-\alpha^2\right)\eta + \alpha\varrho\gamma\cos\phi + 1 + \gamma\alpha^2}\right] = \lambda > 0 \ .$$

Therefore, $\mathcal{I}$ is increasing in ϱ at the optimal point. This property leads to the optimal $\varrho^\star$ achieved at its maximum value, $\varrho^\star = 2\sqrt{\eta(1-\eta)}$.

This maximum correlation magnitude can be reached only when the signal sent from one antenna is a scaled version of the signal from the other, following the equality condition in (5.7). Applying the phase shift result of Theorem 7, the optimal transmit signals must satisfy $x_2 = \zeta e^{-j\phi_0} x_1$ for some real constant ζ. The correlation magnitude becomes $\varrho^\star = |2E[x_1 x_2^*]| = 2\zeta\eta$, and since $\varrho^\star = 2\sqrt{\eta(1-\eta)}$, the ζ value is established as (5.14). □

For $\alpha < 1$, the optimal covariance matrix $\mathbf{Q}$ always has rank one. The optimal transmit strategy is to always do *single-mode beamforming*, with the power at each antenna adjusted according to the CSIT, as discussed next.

The optimal power allocation $\eta^\star$

Replacing the optimal $\varrho^\star$ into the average mutual information in (5.11), the problem then becomes finding $\eta \in [0,\ 1]$ to maximize the following expression:

$$\tilde{\mathcal{I}}(\eta) = E\left[\log\left(\left(1-\alpha^2\right)\eta + 2\alpha\sqrt{\eta(1-\eta)}\cos\phi + \alpha^2 + \frac{1}{\gamma}\right)\right] , \tag{5.15}$$

where the expectation is performed on the distribution of ϕ. Since the above expression is concave in η, the optimal $\eta^\star$ is the solution of

$$E\left[\frac{1-\alpha^2 + \frac{1-2\eta}{\sqrt{\eta(1-\eta)}}\alpha\cos\phi}{\left(1-\alpha^2\right)\eta + 2\alpha\sqrt{\eta(1-\eta)}\cos\phi + \alpha^2 + \frac{1}{\gamma}}\right] = 0 . \tag{5.16}$$

This optimal $\eta^\star$ is unique and is a function of $f(\phi)$, α, γ. Depending on the pdf $f(\phi)$, the above equation may require numerical solution. Once $\eta^\star$ is found, beamforming transmission can be established according to Theorems 7 and 8.

Now consider two special cases of the channel phase-shift pdf: uniform and delta-function. In each case, the optimal $\eta^\star$ can be found precisely as follows.

Corollary 1. *With $\alpha < 1$, for uniform channel phase-shift, the optimal power allocation is $\eta^\star = 1$, implying using a single antenna. For exact channel phase-shift knowledge with a delta-function pdf, the optimal power allocation is transmit maximal-ratio-combining*

given by

$$\eta_{MRC} = \frac{1}{1+\alpha^2} \; . \tag{5.17}$$

Proof. First consider uniform channel phase-shift pdf. After some simple derivation, expression (5.15) can be written as

$$\tilde{\mathcal{I}}(\eta) \;\; = \;\; \frac{1}{\pi}\int_0^{\pi/2} \log\left[\left(\left(1-\alpha^2\right)\eta + \alpha^2 + \frac{1}{\gamma}\right)^2 - 4\alpha^2\eta(1-\eta)\cos^2\phi\right] d\phi \; .$$

Maximizing this expression is equivalent to maximizing the logarithm. Given $0 \leq \eta \leq 1$, the optimal $\eta^\star$ that maximizes this logarithm must satisfy $\eta^\star \geq 0.5$, since otherwise, using $1-\eta$ will achieve a higher value as the second term inside the logarithm remains unchanged. For $0.5 \leq \eta \leq 1$, both terms inside this logarithm are monotonic and reach the maximum simultaneously at $\eta = 1$. Hence without channel phase-shift knowledge, the optimal power allocation is $\eta^\star = 1$.

Next consider exact channel phase-shift knowledge with the delta-function pdf. Expression (5.15) now becomes

$$\begin{aligned}\tilde{\mathcal{I}}(\eta) &= \log\left(\left(1-\alpha^2\right)\eta + 2\alpha\sqrt{\eta(1-\eta)} + \alpha^2 + \frac{1}{\gamma}\right) \\ &= \log\left(\left(\sqrt{\eta} + \alpha\sqrt{1-\eta}\right)^2 + \frac{1}{\gamma}\right) \; .\end{aligned}$$

To find the optimal η that maximizes $\tilde{\mathcal{I}}(\eta)$, subject to $0 \leq \eta \leq 1$, set the derivative with respect to η of the expression inside the logarithm to zero. Solving that equation leads to (5.17). □

5.3.2 Equal antenna gains

This section treats the case $\alpha = 1$. The average mutual information in (5.9) now becomes

$$\mathcal{I} = 2\int_0^{\pi} \log\bigl(\varrho\gamma\cos\phi + \gamma + 1\bigr) f(\phi)\, d\phi \; .$$

The signal power allocation η does not appear in this expression as a result of the equal antenna gains. Therefore, in this case, the correlation magnitude ϱ can be found independently of η, and $\mathcal{I}$ can be maximized over $0 \leq \varrho \leq 1$.

The optimal signal correlation $\varrho^\star$

Since the above expression for $\mathcal{I}$ is concave in ϱ, the optimal $\varrho^\star$ is the solution of

$$\frac{\partial \mathcal{I}}{\partial \varrho} = 2 \int_0^\pi \frac{\gamma \cos\phi}{\varrho\gamma\cos\phi + \gamma + 1} f(\phi)\, d\phi = 0 \,. \tag{5.18}$$

The optimal $\varrho^\star$ depends on the specific phase distribution $f(\phi)$ and the SNR γ.

The optimal power allocation $\eta^\star$

The optimal $\varrho^\star$ and $\eta^\star$ are now only related to each other through the inequality

$$\varrho^\star \leq 2\sqrt{\eta^\star(1-\eta^\star)} \,. \tag{5.19}$$

Hence any power allocation η that satisfies this relation is optimal. The signal is then designed according to the obtained optimal $\mathbf{Q}$. The rank of this covariance matrix is not restricted to be 1 as in the unequal-antenna-gain case. The choice of $\eta^\star$, which influences the rank of $\mathbf{Q}$, can be divided into two general categories:

- *Rank-one* $\mathbf{Q}$ – *Beamforming:* Here the power allocation $\eta^\star$ is chosen to satisfy with equality the bound (5.19) as

$$\eta^\star = \frac{1}{2}\left(1 \pm \sqrt{1-(\varrho^\star)^2}\right) \,. \tag{5.20}$$

  This solution is the same as the optimal scheme for unequal-antenna-gain case (5.12). The optimal signal then satisfies $x_2 = \zeta e^{-j\phi_0} x_1$, where ζ is now given by

$$\zeta = \frac{\varrho^\star}{1 \pm \sqrt{1-(\varrho^\star)^2}} \,.$$

  This transmission scheme is again simple single-mode beamforming.

- *Full-rank* $\mathbf{Q}$*:* This solution can be obtained by assigning to η a value that strictly satisfies the inequality (5.19). Signal design now becomes finding a coding scheme for the given covariance matrix $\mathbf{Q}$. A specific choice is $\eta = \frac{1}{2}$, which makes the signals from the two antennas have equal power. The optimal signals x_1 and x_2 then are identically Gaussian-distributed and are correlated with a correlation factor equal to $\varrho^\star/2$.

As a special case for both categories, when the phase-shift pdf $f(\phi)$ is uniform, equivalent to *no phase knowledge*, then the optimal solution is $\varrho^\star = 0$. The optimal scheme becomes sending independent zero-mean Gaussian signals from the two antennas, with the only constraint being that their powers add up to one. Using a single antenna and putting all transmit power there ($\eta^\star = 1$) also achieves the capacity without randomness, hence single antenna transmission is preferred for uniform channel phase-shift.

5.4 Design examples

The Rician distribution is used for the channel phase-shift pdf in the simulations. This distribution arises from the phase of a constant phasor perturbed by additive, random zero-mean complex Gaussian noise with equal variance on the real and imaginary parts [28, 45]. The *phase estimate quality* can be conveniently described by the Rician factor β. Assuming a mean ϕ_0 and a given quality β, and denoting $\tilde{\phi} = \phi - \phi_0$, the phase-shift pdf is

$$f_{\mathbf{\Phi}}(\phi) = \frac{e^{-\beta^2}}{2\pi}\Big\{1 + \sqrt{\pi}\beta\cos\tilde{\phi}e^{\beta^2\cos^2\tilde{\phi}}\left[1 + \operatorname{erf}\left(\beta\cos\tilde{\phi}\right)\right]\Big\}. \tag{5.21}$$

If $\beta = 0$, the phase distribution is uniform, corresponding to no phase knowledge. When $\beta \to \infty$, the distribution converges to the Dirac delta-function, which means the phase-shift is exactly ϕ_0. A plot of the phase-shift pdf with mean $\phi_0 = 0$ at various values of β is given in Figure 2.6.

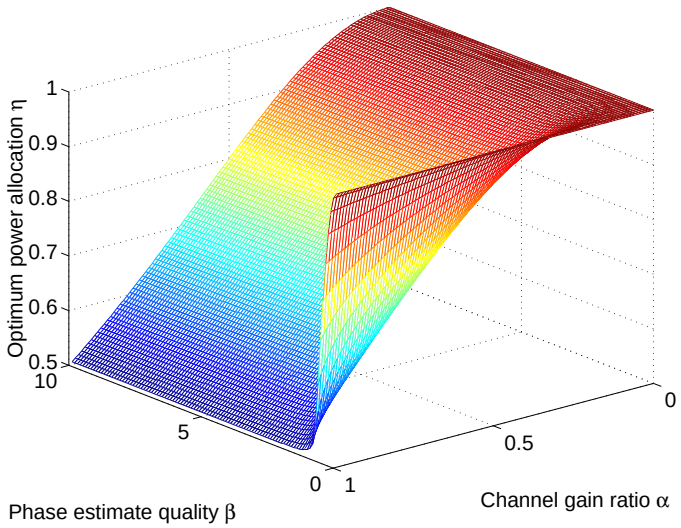

Figure 5.2: The optimal power allocation $\eta^\star$ with unequal antenna gains (SNR = 10dB).

5.4.1 Unequal antenna gains

Equation (5.16) is solved numerically to find $\eta^\star$. The SNR γ has a very little effect on $\eta^\star$, which can be inferred from this equation as $1/\gamma$ can be ignored for reasonably large γ values. Simulation results show that $\eta^\star$ is practically the same for all $\gamma \geq -20$dB. Figure 5.2 shows the optimal power allocation $\eta^\star$ as a function of the antenna gain ratio α and the phase estimates quality β, at SNR $\gamma = 10$dB.

When $\eta = 1$, it means only one antenna is used. This solution is optimal when no phase estimate exists ($\beta = 0$). In this case, using only the stronger antenna to transmit is optimal regardless of the actual α value ($\alpha \neq 1$ here). As the phase estimate quality increases, the power is distributed to both antennas unequally. The scheme approaches transmit maximum-ratio-combining (MRC) beamforming (5.17), which is optimal when the channel is known perfectly at the transmitter.

Simulation suggests that MRC beamforming can be close to optimal for a range of imperfect phase estimates. Figure 5.3 shows slices of the optimal power allocation versus the phase estimate quality and the antenna gain ratio. In the power versus phase estimate quality plot, the power allocation η levels off at approximately $\beta \geq 3$ for all antenna gain ratios. These levels are the MRC power allocations at the corresponding antenna gain

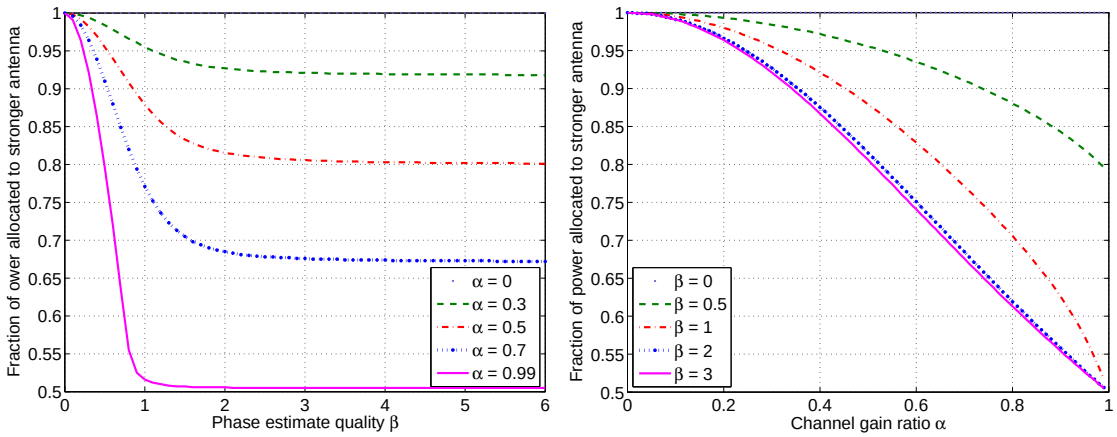

(a) Power versus the phase estimate quality. (b) Power versus the antenna gain ratio.

Figure 5.3: Slices of the optimal $\eta^\star$ with unequal antenna gains.

ratio α. The same effect is reflected in the power versus antenna gain ratio plot. The power allocation curves at $\beta \geq 3$ are almost indistinguishable, and correspond to a plot of the MRC power allocation (5.17) versus α.

5.4.2 Equal antenna gains

Solving equation (5.18) with the Rician phase pdf numerically leads to the optimal $\varrho^\star$ shown in Figure 5.4. The value $\varrho = 1$ means beamforming, in which the signal sent from one antenna is a scaled version of the signal sent from the other, whereas $\varrho = 0$ means independent signals from the two antennas.

For a beamforming solution ($\mathbf{Q}$ rank one), the power split between the two antennas (5.20) is regulated according to the phase estimate quality β and the SNR γ, as shown in Figure 5.5(a). Since the roles of the two antennas now are symmetric, the figures only shows $\eta^\star \geq 0.5$. The lines in this plot correspond to the edge of the surface in Figure 5.2 at $\alpha = 1$ for different SNRs. At this edge, $\eta^\star$ depends quite significantly on the SNR at low β, but then levels out to 0.5 at higher β for all SNRs.

If the phase estimate quality β is *above* a certain threshold, which is a function of the SNR γ, then the integral in (5.18) is always non-negative for $0 \leq \varrho \leq 1$, which leads to *only beamforming* being optimal. In this case, the beamforming corresponds to $\varrho^\star = 1$ and $\eta^\star = \frac{1}{2}$, that is, both antennas transmit the same symbol with equal power (with a

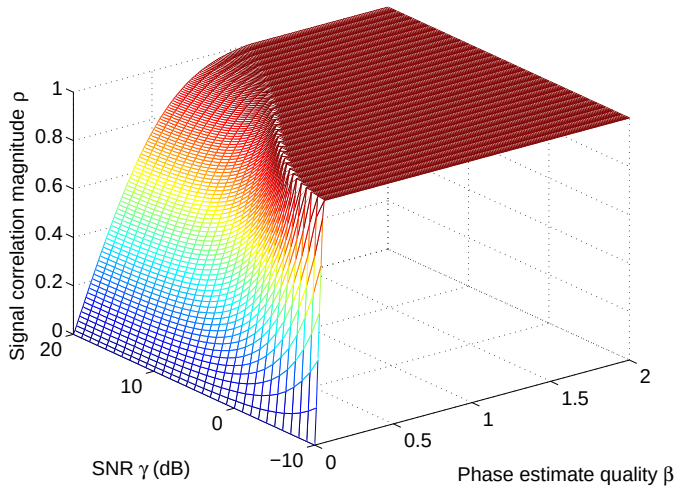

Figure 5.4: The optimal signal correlation $\varrho^\star$ with equal antenna gains.

phase shift between them). This threshold is plotted in Figure 5.5(b).

5.5 Benefits of high-K variable-phase CSIT

Having derived the optimal transmission scheme that maximizes the channel capacity, this section quantifies the capacity gain and summarizes the benefits of high-K variable-phase CSIT.

5.5.1 The capacity gain

The capacity gain with this CSIT obviously depends on the quality of the channel phase-shift knowledge. Without any phase-shift estimate, for any α (either unequal or equal antenna gains), the optimal transmission scheme uses only a single antenna and the channel ergodic-capacity is

$$\mathcal{C}_0 = \log(1+\gamma) \ .$$

With perfect phase-shift estimate, the optimal scheme is MRC transmit beamforming (5.17), and the capacity becomes

$$\mathcal{C}_1 = \log\left(1+\left(1+\alpha^2\right)\gamma\right) \ .$$

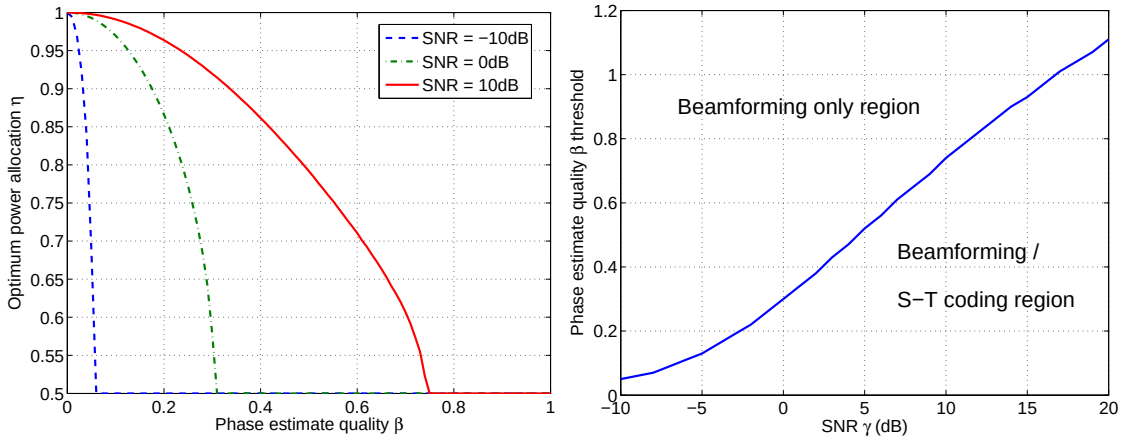

(a) Portion of the total power allocated to the first antenna in beamforming.

(b) Phase estimate quality threshold above which only beamforming is optimal.

Figure 5.5: The optimal power allocation $\eta^\star$ with equal antenna gains.

If there is no CSIT, including no channel amplitude information, however, the transmitter sends independent Gaussian signals with equal power from the two antennas and obtains an average mutual information as

$$\mathcal{I}_{\text{eq}} = \log\left(1 + \frac{1+\alpha^2}{2}\gamma\right) .$$

The capacity gain from CSIT therefore has a range of

$$\mathcal{C}_0 - \mathcal{I}_{\text{eq}} \leq \Delta\mathcal{C} \leq \mathcal{C}_1 - \mathcal{I}_{\text{eq}} .$$

At high SNRs, the gain becomes an additive constant and has the range simplified to

$$1 - \log(1+\alpha^2) \leq \Delta\mathcal{C} \leq 1 \quad \text{(bps/Hz)} .$$

This gain can also be transfered to an SNR advantage at the same transmission rate as

$$10\log_{10}\left(\frac{1+\alpha^2}{2}\right) \leq \text{SNR}_{\text{gain}} \leq 3 \ \ \text{(dB)} .$$

This analysis shows that, when the antennas have unequal gains, knowledge of these gains is valuable, even when the antenna phase-shift is unknown. Power allocation to the

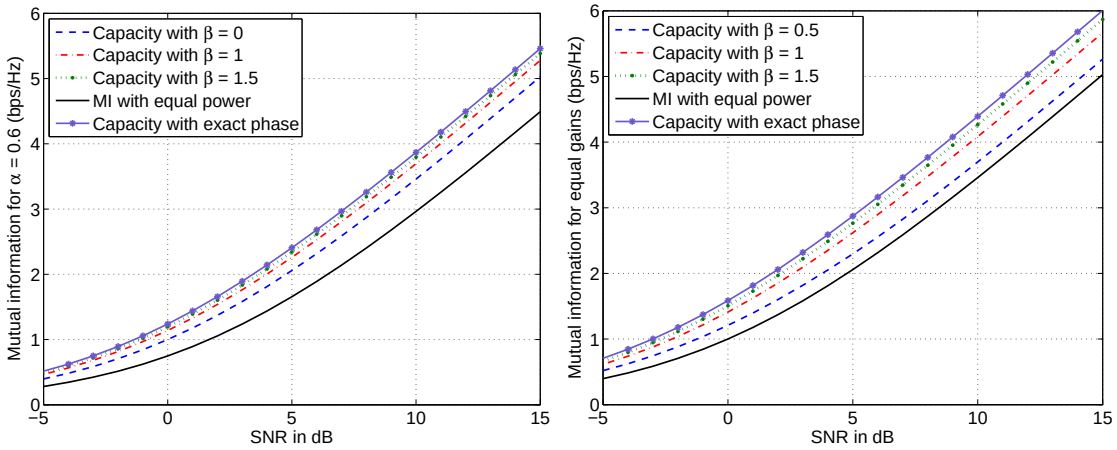

(a) Capacity for unequal antenna gain with $\alpha = 0.6$.

(b) Capacity for equal antenna gain ($\alpha = 1$).

Figure 5.6: Capacity with various channel knowledge.

two antennas can be regulated according to the known antenna-gain-ratio to achieve a higher capacity than that obtained by independent and equal power transmission. With equal antenna gains, however, some phase-shift knowledge is required to gain spectral efficiency. Figure 5.6 provides examples of the capacity gain at various channel knowledge for both cases of $\alpha < 1$ and $\alpha = 1$, using the Rician phase-shift pdf.

5.5.2 The simple transmission scheme

More profound than the capacity gain is the simplicity of the optimal transmission scheme with CSIT. With any antenna gain ratio, single-mode beamforming is optimal. The two antennas can thus send the same symbol, with a phase shift based on the known mean of the channel phase-shift. The power transmitted from these antennas is regulated according to the quality of the phase-shift knowledge. More accurate knowledge brings the power allocation toward the well-known maximal-ratio-combining solution. As the phase-shift knowledge becomes more uncertain, the power allocated to the antenna with weaker gain, or to a chosen one between two equal-gain antennas, should be reduced accordingly. Eventually, when the phase-shift is completely unknown, this antenna power reduces to zero, and only one antenna is then used.

5.6 Chapter summary

This chapter has considered the 2×1 channel with partial CSIT consisting of the channel amplitude and phase-shift pdf. The capacity-optimal transmission scheme is simple single-mode beamforming on the mean of the channel phase shift. The two antennas then send the same symbol, with per-antenna power adjusted according to the CSIT. If the antenna gains are equal, the optimal scheme can also send different but correlated signals from the two antennas. In all cases, when the channel phase-shift is known perfectly, the scheme coincides with maximal-ratio-combining transmit beamforming. When the channel phase-shift is completely unknown, the scheme reduces to single antenna transmission. This partial CSIT thus helps simplify the transmission scheme significantly as single-mode beamforming. At the same time, it provides a spectral efficiency gain of up to 1 bps/Hz or an SNR advantage of up to 3dB for a MISO system with two transmit antennas.

Chapter 6

CONCLUSION

The main conclusion of this thesis is that intelligent use of transmit channel side information in MIMO wireless is beneficial. The thesis has focused on studying two forms of side information, namely dynamic CSIT and high-K variable-phase CSIT, and illustrated the benefits by detailed capacity analysis and practical precoding designs. Results show that even partial CSIT can help improve system performance in terms of the transmission rate or reliability at a given transmit power. Naturally, the performance gain increases with higher CSIT quality.

This chapter concludes the thesis. The chapter begins with a summary of the thesis main results, follows by a brief overview of the deployment of precoding in emerging wireless standards, and ends with a discussion of future research directions in exploiting transmit channel information.

6.1 Thesis summary

This thesis has focused on exploiting channel side information at the transmitter (CSIT) in a single-user MIMO wireless system. CSIT can increase MIMO capacity and enhance system reliability. The time-varying nature of wireless channels, however, often degrades the CSIT quality, posing challenges in system analysis and signal design.

The thesis contribution has been three fold: modeling dynamic CSIT, analyzing the capacity gain and optimal input given a CSIT, and designing linear precoders to realize

the gain. The dynamic CSIT model takes into account the channel temporal variation by using an initial, potentially outdated channel measurement and the channel statistics, including the mean, covariance, and temporal correlation [18]. The model consists of a channel estimate and its error covariance, which function as an effective channel mean and an effective channel covariance, respectively. Both parameters are functions of the channel temporal correlation factor ρ, which indicates the CSIT quality. Depending on this quality, the model covers smoothly from perfect ($\rho = 1$) to statistical ($\rho = 0$) CSIT [18, 19] (Chapter 2).

Second, the thesis analyzes the capacity gain and the optimal input with dynamic CSIT asymptotically at low and high SNRs [20], and develops a convex optimization program to find the capacity non-asymptotically [22]. The program helps to assess the tightness of a simple capacity lower-bound, based on the Jensen optimal input. Results differ with SNR and the relative number of antennas. At low SNRs, the capacity lower-bound is tight for all systems. The capacity gain here is multiplicative, and the optimal input is typically simple single-mode beamforming. At high SNRs, for systems with equal or fewer transmit than receive antennas, the capacity bound is also tight, but the capacity gain diminishes to zero due to equi-power optimal input. For other systems, the bound becomes loose at high SNRs, but the capacity gain is additive and the optimal input may drop modes, if the channel mean or transmit antenna correlation is strong (Chapter 3).

Third, linear precoders exploiting CSIT are designed, using convex analysis and matrix algebra. Optimal from an information theoretic viewpoint, a linear precoder functions as a multi-mode beamformer. It decouples the transmit signal into orthogonal eigen-beams and assigns higher power to the directions where the channel is strong, but reduced or no power to the weak. For dynamic CSIT, an optimal precoder is constructed using a dynamic water-filling process [23]. The design obtains a range of significant and robust precoding gains, depending on the CSIT quality [18] (Chapter 4). Another precoder is designed for high-K variable-phase CSIT, which reduces to simple single-mode beamforming with variable antenna power allocation, depending on the channel phase-shift information [24] (Chapter 5).

For dynamic CSIT, a common observation emerging from the capacity and precoding

results is that, the performance gain becomes sensitive to the CSIT quality only at relatively high quality, approximately $\rho \geq 0.6$. Otherwise, it is similar to the gain obtained from statistical CSIT at $\rho = 0$. This observation suggests that, in dynamic CSIT, the initial channel measurement is useful only when its correlation with the current channel is relatively strong; otherwise, using the channel statistics alone achieves most of the performance gain.

6.2 Precoding deployment in wireless standards

Precoding has been successfully incorporated in the IEEE 802.16e standard for broadband wireless metropolitan networks [3]. The standard supports both closed- and open-loop precoding for the downlink. In the closed-loop method, the precoder is based on either an initial channel measurement or the channel statistics, corresponding to CSIT quality $\rho = 1$ or $\rho = 0$, respectively. The user-unit measures the channel and the fading rate, using the forward-link preambles or pilots. Based on the channel measurement, it picks a short-term precoding matrix from a codebook of unitary precoders, containing the beam directions. The fading rate is used to calculate a time-to-live parameter, which is fed back to the basestation along with the short-term precoding index. The basestation uses this short-term precoding matrix until the time-to-live expires. Thereafter, it precodes using channel statistics information, which is updated at a much slower rate and is always valid. In the open-loop method, a subset of users is scheduled to transmit a sounding signal. The base station then estimates the channels for these users and determines the CSIT based on reciprocity after transmit-receive RF calibration.

MIMO is entering the IEEE 802.11n standard for wireless local area networks (WLANs). The standard supports both space-time coding and spatial multiplexing. The current precoding proposals use an open-loop method, relying on the reciprocity principle that the best beam on reception must be the best beam for transmission. The access point thus uses pre-formed beams for receiving and transmitting, and records the beam(s) with the best signal strength on reception for each user, then uses the same beam(s) during transmission.

The 3GPP standard uses a closed-loop beamforming technique, based on feedback of the channel phase and amplitude information. Precoding is under discussion in High-Speed Downlink Packet Access (HSDPA) for mobile communication. Channel-sounding techniques appear to be preferred.

6.3 Future directions

Exploiting CSIT is a current research area with still many open problems in both single- and multi-user domains. In single-user, for examples, an analytical solution for the optimal precoder with statistical CSIT (both mean and covariance) under the capacity criterion remains unsolved. Precoding with a more general channel covariance structure, such as a non-Kronecker model, has hardly been studied. Extension to frequency selective channels increases the complexity in acquiring and modeling partial CSIT and requires efficient precoding techniques [82]. Codebook design and its application in compressing channel information efficiently for closed-loop systems is also a rich research area [38, 40]. Another practical question is the tradeoff between overheads in CSIT acquisition and performance gains from the CSIT.

In multi-user communication, exploiting partial CSIT is an important open problem. Recent results have established the capacity regions for the Gaussian multiple access and broadcast channels [46, 83]. Dirty-paper coding [84], for example, is a capacity-optimal precoding scheme for the broadcast channel. These results, however, require full channel information at all transmitters and receivers, which is quite impractical in wireless, where obtaining CSIT usually demands substantial resources. Initial research has shown that the loss of degrees of freedom due to the lack of CSIT reduces the capacity region of an isotropic vector broadcast-channel to that of a scalar one [85]. Imperfect CSIT also severely reduces the growth of the sum-rate broadcast capacity at high SNRs [86]. Further research are required to characterize multi-user partial CSIT and their impacts on the channel capacity, and to design signal processing schemes given the CSIT.

Opportunistic scheduling is a scheme exploiting multi-user diversity by serving the users with the best channels each time. It achieves an optimal throughput growth-rate

with a large number of users [87, 88]. This growth, however, assumes arbitrary delay and accurate instantaneous CSIT, both are unrealistic in practical wireless systems. A study of hard delay constraints has revealed drop in system throughput for an increasing number of users [89]. Erroneous CSIT, likewise, will reduce the system throughput. Understanding this effect requires further research.

Appendix A

Derivations and Proofs

A.1 K-factor threshold for mode-dropping at all SNRs

This section provides the derivation for (3.20). In problem (3.19), replacing λ_2 as a function of λ_1, noting that the optimal $\lambda_1 \geq \lambda_2$, the problem becomes equivalent to

$$\begin{aligned} \max_{\lambda_1} \quad & g(\lambda_1) = E_{\tilde{\mathbf{h}}_j}\left[\log\det\left(\mathbf{I}_M + \lambda_1\gamma\sum_{j=1}^{M}\breve{\mathbf{h}}_j\breve{\mathbf{h}}_j^* + \frac{1-M\lambda_1}{N-M}\gamma\sum_{j=M+1}^{N}\tilde{\mathbf{h}}_j\tilde{\mathbf{h}}_j^*\right)\right] \\ \text{subject to} \quad & \frac{1}{N} \leq \lambda_1 \leq \frac{1}{M}\,, \end{aligned}$$

where $\breve{\mathbf{h}}_j = \left(\beta\mathbf{e}_j + \tilde{\mathbf{h}}_j\right)$. Since problem (3.19) is convex, this problem is convex. Thus, to have the optimal $\lambda_1^\star = 1/M$, it is sufficient and necessary that $\frac{dg(\lambda_1)}{d\lambda_1}\Big|_{\lambda_1=1/M} \geq 0$, which translates to

$$\begin{aligned} 0 \quad &\leq \quad E_{\tilde{\mathbf{h}}_j}\left[\mathrm{tr}\left[\left(\mathbf{I}_M + \frac{\gamma}{M}\sum_{j=1}^{M}\breve{\mathbf{h}}_j\breve{\mathbf{h}}_i^*\right)^{-1}\left(\gamma\sum_{j=1}^{M}\breve{\mathbf{h}}_j\breve{\mathbf{h}}_i^* - \frac{\gamma M}{N-M}\sum_{j=M+1}^{N}\tilde{\mathbf{h}}_j\tilde{\mathbf{h}}_j^*\right)\right]\right] \\ &\overset{(a)}{=} \quad M^2 - ME_{\tilde{\mathbf{h}}_j}\left[\mathrm{tr}\left[\left(\mathbf{I}_M + \frac{\gamma}{M}\sum_{j=1}^{M}\breve{\mathbf{h}}_j\breve{\mathbf{h}}_i^*\right)^{-1}\left(\mathbf{I}_M + \frac{\gamma}{N-M}\sum_{j=M+1}^{N}\tilde{\mathbf{h}}_j\tilde{\mathbf{h}}_j^*\right)\right]\right]\,, \end{aligned}$$

where (a) follows from adding and subtracting $M\mathbf{I}_M$ in the second parenthetic factor inside the trace expression, and $\tilde{\mathbf{h}}_j$ and $\breve{\mathbf{h}}_j$ are independent. Due to this independence,

and noting that $\tilde{\mathbf{h}}_j \sim \mathcal{N}\left(\mathbf{0}, (1-\beta^2)\mathbf{I}_M\right)$, the above inequality leads to

$$\begin{aligned} M &\geq \operatorname{tr}\left(E_{\tilde{\mathbf{h}}_j}\left[\left(\mathbf{I}_M + \frac{\gamma}{M}\sum_{j=1}^{M}\breve{\mathbf{h}}_j\breve{\mathbf{h}}_i^*\right)^{-1}\right] E_{\tilde{\mathbf{h}}_j}\left[\mathbf{I}_M + \frac{\gamma}{N-M}\sum_{j=M+1}^{N}\tilde{\mathbf{h}}_j\tilde{\mathbf{h}}_j^*\right]\right) \\ &= \operatorname{tr}\left(E_{\tilde{\mathbf{h}}_j}\left[\left(\mathbf{I}_M + \frac{\gamma}{M}\sum_{j=1}^{M}\breve{\mathbf{h}}_j\breve{\mathbf{h}}_i^*\right)^{-1}\right]\left[1+\gamma\left(1-\beta^2\right)\right]\right) . \end{aligned}$$

This expression results in (3.20).

A.2 $\mathbf{R}_t$ condition-number threshold for mode-dropping at all SNRs

This section provides the derivation for (3.25). In problem (3.24), replacing λ_1 as a function of λ_2 and noting that $\lambda_1 \geq \lambda_2$, the problem becomes equivalent to

$$\begin{aligned} \max_{\lambda_2} f(\lambda_2) &= E_{\tilde{\mathbf{h}}_i}\left[\log\det\left(\mathbf{I}_M + \gamma\frac{1-(N-L)\lambda_2}{L}\xi_1\sum_{i=1}^{L}\tilde{\mathbf{h}}_i\tilde{\mathbf{h}}_i^* + \gamma\lambda_2\xi_2\sum_{j=L+1}^{N}\tilde{\mathbf{h}}_j\tilde{\mathbf{h}}_j^*\right)\right] \\ \text{subject to} \quad & 0 \leq \lambda_2 \leq \frac{1}{N} , \end{aligned}$$

where $\tilde{\mathbf{h}}_i \sim \mathcal{N}(\mathbf{0}, \mathbf{I}_M)$. The condition for the optimal $\lambda_2^\star = 0$ is $\frac{\partial f}{\partial \lambda_2}\Big|_{\lambda_2=0} \leq 0$, which translates to

$$\begin{aligned} 0 &\geq E_{\tilde{\mathbf{h}}_i}\left[\operatorname{tr}\left[\left(\mathbf{I}_M + \frac{\gamma\xi_1}{L}\sum_{j=1}^{L}\tilde{\mathbf{h}}_i\tilde{\mathbf{h}}_i^*\right)^{-1}\left(\gamma\xi_2\sum_{j=L+1}^{N}\tilde{\mathbf{h}}_j\tilde{\mathbf{h}}_j^* - \gamma\xi_1\frac{N-L}{L}\sum_{i=1}^{L}\tilde{\mathbf{h}}_i\tilde{\mathbf{h}}_i^*\right)\right]\right] \\ &\overset{(a)}{=} \operatorname{tr}\left(E_{\tilde{\mathbf{h}}_i}\left[\left(\mathbf{I}_M + \frac{\gamma\xi_1}{L}\sum_{j=1}^{L}\tilde{\mathbf{h}}_i\tilde{\mathbf{h}}_i^*\right)^{-1}\left(\gamma\xi_2\mathbf{I}_M - \frac{\gamma\xi_1}{L}\sum_{j=1}^{L}\tilde{\mathbf{h}}_i\tilde{\mathbf{h}}_i^*\right)(N-L)\right]\right) \\ &= \operatorname{tr}\left(E_{\tilde{\mathbf{h}}_i}\left[\left(\mathbf{I}_M + \frac{\gamma\xi_1}{L}\sum_{j=1}^{L}\tilde{\mathbf{h}}_i\tilde{\mathbf{h}}_i^*\right)^{-1}\left[(\gamma\xi_2+1)\mathbf{I}_M - \left(\mathbf{I}_M + \frac{\gamma\xi_1}{L}\sum_{j=1}^{L}\tilde{\mathbf{h}}_i\tilde{\mathbf{h}}_i^*\right)\right]\right]\right) \\ &\quad \times (N-L) \\ &= \left[\operatorname{tr}\left(E_{\tilde{\mathbf{h}}_i}\left[\left(\mathbf{I}_M + \frac{\gamma\xi_1}{L}\sum_{j=1}^{L}\tilde{\mathbf{h}}_i\tilde{\mathbf{h}}_i^*\right)^{-1}(\gamma\xi_2+1)\right]\right) - M\right](N-L) , \end{aligned}$$

where (a) follows from the mutually exclusive, independent sums and $E\left[\sum_{j=L+1}^{N}\tilde{\mathbf{h}}_j\tilde{\mathbf{h}}_j^*\right] = (N-L)\mathbf{I}_M$. The above inequality leads to (3.25).

A.3 Solving a quadratic matrix equation

This section solves the quadratic matrix equation (4.23). Rewrite this equation by multiplying left and right with $\mathbf{W}$ as

$$\nu\mathbf{W}\mathbf{R}_t^{-2}\mathbf{W} - M\mathbf{W} - \mathbf{H}_m^*\mathbf{H}_m = \mathbf{0}\,. \tag{A.1}$$

This is a matrix quadratic equation in $\mathbf{W}$, which can be solved similarly to a scalar equation. Recall that the scalar quadratic equation

$$ax^2 + bx + c = 0$$

has the solution as

$$x = \frac{1}{2a}\left(-b \pm \sqrt{\Delta}\right)$$

where $\Delta = b^2 - 4ac$. In the matrix equation (A.1),

$$\begin{aligned} a &\sim \nu\mathbf{R}_t^{-2} \\ b &\sim -M\mathbf{I}_N \\ c &\sim -\mathbf{H}_m^*\mathbf{H}_m. \end{aligned}$$

Form the matrix equivalence of Δ as in (4.25)

$$\mathbf{\Psi} = M^2\mathbf{I}_N + 4\nu\mathbf{R}_t^{-1}\mathbf{H}_m^*\mathbf{H}_m\mathbf{R}_t^{-1}\,,$$

in which a is split around c to ensure symmetry. The solutions then follow as

$$\mathbf{W} = \frac{1}{2\nu}\mathbf{R}_t\left(M\mathbf{I}_N \pm \mathbf{\Psi}^{\frac{1}{2}}\right)\mathbf{R}_t\,,$$

in which a^{-1} is again split on two sides. The positive semidefinite value of $\mathbf{W}$ is chosen as in (4.24).

A quick check to verify the answer can be carried out by plugging the solutions into (A.1) as

$$\begin{aligned}
& \nu\mathbf{W}\mathbf{R}_t^{-2}\mathbf{W} - M\mathbf{W} - \mathbf{H}_m^*\mathbf{H}_m \\
= \;& \frac{1}{4\nu}\mathbf{R}_t\left(M\mathbf{I}_N \pm \mathbf{\Psi}^{\frac{1}{2}}\right)^2\mathbf{R}_t - \frac{M}{2\nu}\mathbf{R}_t\left(M\mathbf{I}_N \pm \mathbf{\Psi}^{\frac{1}{2}}\right)\mathbf{R}_t - \mathbf{H}_m^*\mathbf{H}_m \\
= \;& \frac{1}{4\nu}\mathbf{R}_t\left(M^2\mathbf{I}_N \pm 2M\mathbf{\Psi}^{\frac{1}{2}} + \mathbf{\Psi}\right)\mathbf{R}_t - \frac{M}{2\nu}\mathbf{R}_t\left(M\mathbf{I}_N \pm \mathbf{\Psi}^{\frac{1}{2}}\right)\mathbf{R}_t - \mathbf{H}_m^*\mathbf{H}_m \\
= \;& -\frac{M^2}{4\nu}\mathbf{R}_t^2 + \frac{1}{4\nu}\mathbf{R}_t\mathbf{\Psi}\mathbf{R}_t - \mathbf{H}_m^*\mathbf{H}_m \\
= \;& -\frac{M^2}{4\nu}\mathbf{R}_t^2 + \frac{1}{4\nu}\mathbf{R}_t\left(M^2\mathbf{I}_N + 4\nu\mathbf{R}_t^{-1}\mathbf{H}_m^*\mathbf{H}_m\mathbf{R}_t^{-1}\right)\mathbf{R}_t - \mathbf{H}_m^*\mathbf{H}_m \\
= \;& \mathbf{0}.
\end{aligned}$$

A.4 Deriving the bounds on ν in the outer algorithm

To derive the bounds in (4.30), apply Weyl's theorem [72] $\lambda_1(A) + \lambda_k(B) \leq \lambda_k(A+B) \leq \lambda_N(A) + \lambda_k(B)$ to the left-hand-side expression in (4.29). The following bounds on this expression, with k modes dropped ($1 \leq k \leq N-1$), are obtained:

$$\begin{aligned}
f_{\text{upper}} &= \frac{M(N-k)}{2\nu} + (N-k)\frac{\sqrt{M^2+4\nu\lambda_N}}{2\nu} - \sum_{i=k+1}^{N}\frac{1}{\lambda_i(\mathbf{R}_t)} \\
f_{\text{lower}} &= \frac{M(N-k)}{2\nu} + (N-k)\frac{\sqrt{M^2+4\nu\lambda_1}}{2\nu} - \sum_{i=k+1}^{N}\frac{1}{\lambda_i(\mathbf{R}_t)}\,.
\end{aligned}$$

Equating each bound to η_0 results in a quadratic equation, from which the corresponding value for ν in (4.30) is derived.

A.5 Solving the trace relaxation problem

To solve (4.37), again form the Lagrangian and differentiate with respect to $\mathbf{W}$ to obtain

$$-\mathbf{W}^{-1}\mathbf{H}_m^*\mathbf{H}_m\mathbf{W}^{-1} - M\mathbf{W}^{-1} + \nu\mathbf{R}_t^{-1}\mathbf{\Lambda}_{\mathbf{A}}^{-1}\mathbf{R}_t^{-1} = 0\,,$$

where ν is the Lagrange multiplier associated with the equality constraint. Let $\mathbf{G}$ be the Hermitian matrix such that $\mathbf{R}_t\mathbf{\Lambda_A}\mathbf{R}_t = \mathbf{G}^2$, then the above quadratic matrix equation has the solution

$$\mathbf{W} = \frac{1}{2\nu}\mathbf{G}\left(M\mathbf{I}_N + \mathbf{\Psi}^{\frac{1}{2}}\right)\mathbf{G}\,,$$

where

$$\mathbf{\Psi} = M^2\mathbf{I}_N + 4\nu\mathbf{G}^{-1}\mathbf{H}_m^*\mathbf{H}_m\mathbf{G}^{-1}\,.$$

Now $\mathbf{B}$ can be written as

$$\mathbf{B} = \frac{4}{\rho}\left[\frac{1}{2\nu}\mathbf{R}_t^{-1}\mathbf{G}\left(M\mathbf{I}_N + \mathbf{\Psi}(\nu)^{\frac{1}{2}}\right)\mathbf{G}\mathbf{R}_t^{-1} - \mathbf{R}_t^{-1}\right]\,,$$

and the product $\mathbf{\Lambda_A^{-1}B}$ becomes

$$\mathbf{\Lambda_A^{-1}B} = \frac{4}{\rho}\left(\frac{M}{2\nu}\mathbf{I}_N + \frac{1}{2\nu}\mathbf{\Lambda_A^{-1}}\mathbf{R}_t^{-1}\mathbf{G}\mathbf{\Psi}^{\frac{1}{2}}\mathbf{G}\mathbf{R}_t^{-1} - \mathbf{\Lambda_A^{-1}}\mathbf{R}_t^{-1}\right).$$

The Lagrange multiplier ν must satisfy the equality constraint in (4.37), or equivalently, $\mathrm{tr}\left(\mathbf{\Lambda}_A^{-1}\mathbf{B}\right) = 1$, while ensuring $\mathbf{B} \succcurlyeq \mathbf{0}$. Similar to the orthogonal STBC case, ν is solved in two steps. First, assume that $\mathbf{B}$ is full-rank and solve the equation $\mathrm{tr}\left(\mathbf{\Lambda_A^{-1}B}\right) = 1$. If the resulting $\mathbf{B}$ is not PSD, then drop the weakest eigen-mode of $\mathbf{B}$ and resolve for ν, using the equation

$$\sum_{i=k+1}^{N}\lambda_i\left(\mathbf{\Lambda_A^{-1}B}\right) = 1\,,$$

where k is the number of dropped modes, and keep dropping modes until $\mathbf{B}$ is PSD. In this case, the eigenvalues of $\mathbf{\Lambda_A^{-1}B}$ cannot be written explicitly as functions of ν to obtain an equation similar to (4.27). Nevertheless, since the eigenvalue sum is monotonic in ν, similarly, ν can be found by performing an one-dimensional binary search in each step. The bounds on ν for the equation with k modes dropped ($0 \le k \le N-1$) are given by

$$\nu_{\text{bound}} = \frac{\alpha}{\beta^2} + \frac{M}{\beta}\,, \tag{A.2}$$

where for the upper bound

$$\begin{aligned}\alpha &= \lambda_{\max}\left(\mathbf{G}^{-1}\mathbf{H}_m^*\mathbf{H}_m\mathbf{G}^{-1}\right)\\ \beta &= \lambda_{\min}\left(\mathbf{\Lambda}_{\mathbf{A}}^{-1}\mathbf{R}_t^{-1}\right)+\frac{\rho}{4(N-k)}\,,\end{aligned}$$

and for the lower bound

$$\begin{aligned}\alpha &= \lambda_{\min}\left(\mathbf{G}^{-1}\mathbf{H}_m^*\mathbf{H}_m\mathbf{G}^{-1}\right)\\ \beta &= \lambda_{\max}\left(\mathbf{\Lambda}_{\mathbf{A}}^{-1}\mathbf{R}_t^{-1}\right)+\frac{\rho}{4(N-k)}\,.\end{aligned}$$

To derive the upper bound, use the inequality $\sum_{k+1}^{N}\lambda_i(\mathbf{\Lambda}_{\mathbf{A}}^{-1}\mathbf{B}) \le (N-k)\lambda_{\max}(\mathbf{\Lambda}_{\mathbf{A}}^{-1}\mathbf{B})$ and further obtain an upper bound on $\lambda_{\max}(\mathbf{\Lambda}_{\mathbf{A}}^{-1}\mathbf{B})$ as

$$\lambda_{\max}(\mathbf{\Lambda}_{\mathbf{A}}^{-1}\mathbf{B}) \le \frac{4}{\rho}\left[\frac{M}{2\nu}+\frac{1}{2\nu}\lambda_{\max}\left(\mathbf{\Lambda}_{\mathbf{A}}^{-1}\mathbf{R}_t^{-1}\mathbf{G}\mathbf{\Psi}^{\frac{1}{2}}\mathbf{G}\mathbf{R}_t^{-1}\right)-\lambda_{\min}\left(\mathbf{\Lambda}_{\mathbf{A}}^{-1}\mathbf{R}_t^{-1}\right)\right]\,,$$

invoking the inequality $\lambda_{\max}(A+B) \le \lambda_{\max}(A)+\lambda_{\max}(B)$ for Hermitian matrices [73]. The following chain holds:

$$\begin{aligned}\lambda_{\max}\left(\mathbf{\Lambda}_{\mathbf{A}}^{-1}\mathbf{R}_t^{-1}\mathbf{G}\mathbf{\Psi}^{\frac{1}{2}}\mathbf{G}\mathbf{R}_t^{-1}\right) &\overset{(a)}{=} \lambda_{\max}\left(\mathbf{G}\mathbf{R}_t^{-1}\mathbf{\Lambda}_{\mathbf{A}}^{-1}\mathbf{R}_t^{-1}\mathbf{G}\mathbf{\Psi}^{\frac{1}{2}}\right)\\ &\overset{(b)}{\le} \lambda_{\max}\left(\mathbf{G}\mathbf{R}_t^{-1}\mathbf{\Lambda}_{\mathbf{A}}^{-1}\mathbf{R}_t^{-1}\mathbf{G}\right)\lambda_{\max}\left(\mathbf{\Psi}^{\frac{1}{2}}\right)\\ &\overset{(c)}{=} \lambda_{\max}\left(\mathbf{\Lambda}_{\mathbf{A}}^{-1/2}\mathbf{R}_t^{-1}\mathbf{G}^2\mathbf{R}_t^{-1}\mathbf{\Lambda}_{\mathbf{A}}^{-1/2}\right)\lambda_{\max}\left(\mathbf{\Psi}^{\frac{1}{2}}\right)\\ &\overset{(d)}{=} \lambda_{\max}\left(\mathbf{\Psi}^{\frac{1}{2}}\right)\\ &\overset{(e)}{=} \sqrt{M^2+4\nu\lambda_{\max}\left(\mathbf{G}^{-1}\mathbf{H}_m^*\mathbf{H}_m\mathbf{G}^{-1}\right)}\,,\end{aligned}$$

where (a) and (c) follow from $\lambda(AB)=\lambda(BA)$ [72], (b) follows from $\lambda_{\max}(AB) \le \lambda_{\max}(A)\lambda_{\max}(B)$ for Hermitian matrices [73], (d) follows from the definition for $\mathbf{G}$, and (e) follows from $\lambda(\mathbf{I}+A)=1+\lambda(A)$. The upper bound on ν can then be found by solving

$$\frac{M}{2\nu}+\frac{1}{2\nu}\sqrt{M^2+4\nu\alpha}-\beta=0$$

with α and β specified above. The lower bound is derived similarly.

A.6 Optimal precoder with mean CSIT and non-identity A

This section provides the derivation for the optimal precoder with mean CSIT given a non-identity **A** in (4.53) and (4.54). From problem (4.52), form the Lagrangian as

$$\mathcal{L}\left(\nu, \lambda_i(\mathbf{B})\right) = \sum_i \left(1 + \frac{\gamma}{4}\lambda_i(\mathbf{B})\right)^{-1} \lambda_{m,i} - M \sum_i \log\left(1 + \frac{\gamma}{4}\lambda_i(\mathbf{B})\right) - \nu\left(\sum_i \xi_i \lambda_i(\mathbf{B}) - 1\right) .$$

where ν is the Lagrange multiplier associated with the equality constraint. Take the derivative of $\mathcal{L}\left(\nu, \lambda_i(\mathbf{B})\right)$ with respect to $\lambda_i(\mathbf{B})$ and set it to zero to get

$$\frac{\gamma\lambda_{m,i}}{4\left(1 + \frac{\gamma}{4}\lambda_i(\mathbf{B})\right)^2} - \frac{M\gamma}{4\left(1 + \frac{\gamma}{4}\lambda_i(\mathbf{B})\right)} - \nu\xi_i = 0$$

Let $z = 1 + \frac{\gamma}{4}\lambda_i(\mathbf{B})$, the above equation is equivalent to

$$4\nu\xi_i z^2 + M\gamma z - \gamma\lambda_{m,i} = 0 ,$$

which leads to

$$z = \frac{1}{8\nu\xi_i}\left(M\gamma \pm \sqrt{M^2\gamma^2 + 16\nu\xi_i\gamma\lambda_{m,i}}\right) .$$

Replacing this result into $\lambda_i(\mathbf{B}) = 4(z-1)/\gamma$, noting that $\lambda_i(\mathbf{B}) \geq 0$ and that $\xi_i = 1/\lambda_i(\mathbf{A})$, expression (4.53) then follows.

To find the Lagrange multiplier ν, solve the equality constraint, which now becomes

$$\sum_{i=1}^{N}\left[\frac{1}{2\nu}\left(M + \sqrt{M^2 + 16\nu\frac{\lambda_{m,i}}{\gamma\lambda_i(\mathbf{A})}}\right) - \frac{4}{\gamma\lambda_i(\mathbf{A})}\right]_+ = 1 .$$

The upper- and lower-bounds on the solution for ν can be established by replacing $\lambda_{m,i}/\lambda_i(\mathbf{A})$ with its largest and smallest values, $\tilde{\lambda}_N$ and $\tilde{\lambda}_1$, respectively. With k dropped modes, the equation for the upper bound becomes

$$\frac{(N-k)}{2\nu}\left(M + \sqrt{M^2 + 16\nu\frac{\tilde{\lambda}_N}{\gamma}}\right) - \sum_{i=k+1}^{N}\frac{4}{\gamma\lambda_i(\mathbf{A})} = 1 .$$

With ζ_k defined in (4.55), the above equation can be rewritten as

$$\sqrt{M^2 + 16\nu\frac{\tilde{\lambda}_N}{\gamma}} = 2\zeta_k\nu - M \ .$$

Solving this equation leads to the upper bound for ν in (4.54). The lower bound is derived similarly.

A.7 Optimal beam directions with transmit covariance CSIT

This sections proves (4.61) as the optimal beam directions for problem (4.60). Consider the following more constrained problem

$$\begin{aligned} \max \quad & E_{\mathbf{H}_w}\left[f\left(\mathbf{I} + a\rho\mathbf{H}_w\mathbf{R}_t^{\frac{1}{2}}\mathbf{F}\mathbf{Q}\mathbf{F}^*\mathbf{R}_t^{\frac{1}{2}}\mathbf{H}_w^*\right)\right] \\ \text{subject to} \quad & \mathrm{tr}\left(\mathbf{F}\mathbf{F}^*\right) = 1 \\ & \mathrm{tr}\left(\mathbf{R}_t^{\frac{1}{2}}\mathbf{F}\mathbf{Q}\mathbf{F}^*\mathbf{R}_t^{\frac{1}{2}}\right) = \xi \ , \end{aligned} \tag{A.3}$$

where ξ is equal to that resulted from the optimal solution of (4.60). Due to the setup, the two problems are equivalent: the second formulation is more constrained and hence has a smaller or equal optimal value compared to the first formulation; and the choice of ξ makes the two optimal values the same.

Now consider the second problem (A.3) by itself, the chosen ξ must be the largest feasible value. The reason is that, if a feasible ξ_2 is larger than ξ_1, then the objective function in the problem with ξ_2 can be chosen to be larger than that with ξ_1, hence causing contradiction. Based on the inequality $\mathcal{R}\mathrm{tr}(A_1\cdots A_m) \leq \sum_i \sigma_i(A_1)\cdots\sigma_i(A_m)$ for complex matrices [73], without affecting the singular values of $\mathbf{F}$ and hence the power constraint, the value ξ is largest when the right and left singular vectors of $\mathbf{F}$ are the same as the eigenvectors of $\mathbf{Q}$ and $\mathbf{R}_t$, respectively. In other words, the optimal conditions for the precoder singular vectors are

$$\begin{aligned} \mathbf{U}_\mathbf{F} &= \mathbf{U}_t \\ \mathbf{V}_\mathbf{F} &= \mathbf{U}_\mathbf{Q} \ , \end{aligned}$$

which proves (4.61), and concurrently (4.57).

A.8 Optimal phase-shift with high-K variable-phase CSIT

This section analyzes the two choices for the optimal signal phase-shift in (5.10). With $\psi = -\phi_0$, the average mutual information (5.8) becomes

$$\mathcal{I}|_{\psi=-\phi_0} = 2\int_0^{\pi} \log\left(p + \gamma\alpha\rho\cos\phi\right) f(\phi) d\phi \ .$$

For $\psi = \pi - \phi_0$, a similar expression is obtained but with the plus sign replaced by a minus sign. The difference between $\mathcal{I}$ at the two candidates for $\phi^\star$ is

$$\begin{aligned} \Delta\mathcal{I} &= \mathcal{I}|_{\psi=-\phi_0} - \mathcal{I}|_{\psi=\pi-\phi_0} \\ &= 2\int_0^{\pi} \log\left(\frac{p + \gamma\alpha\rho\cos\phi}{p - \gamma\alpha\rho\cos\phi}\right) f(\phi)\, d\phi \ . \end{aligned}$$

The logarithmic expression is anti-symmetric around $\pi/2$, therefore the above difference can be rewritten as

$$\Delta\mathcal{I} = 2\int_0^{\pi/2} \log\left(\frac{2p}{p - \gamma\alpha\rho\cos\phi} - 1\right)\left[f(\phi) - f\left(\phi + \frac{\pi}{2}\right)\right] d\phi \ .$$

Since the logarithmic expression in the above integral is non-negative within the integral range, if $f(\phi) - f\left(\phi + \frac{\pi}{2}\right)$ has only one sign within this range, then the sign of $\Delta\mathcal{I}$ can be simply determined without having to evaluate the integral explicitly. Specifically, if the translated phase-shift pdf $f(\phi)$ is monotonous within the range $0 \le \phi \le \pi$, then the choice between $\phi = 0$ and $\phi = \pi$ that makes $f(\phi)$ larger determines the optimal $\psi^\star$ to be $-\phi_0$ or $\pi - \phi_0$, respectively.

Appendix B

Simulation Parameters

B.1 Channel parameter normalization

This section discusses the channel normalization used in simulations. Consider a frequency-flat quasi-static block fading MIMO wireless channel with N transmit and M receive antennas. For simulations, the channel is normalized for a constant average power gain of MN, such that $E[\mathrm{tr}(\mathbf{H}^*\mathbf{H})] = MN$. The transmit signal power is assumed to have been adjusted accordingly. The normalization ensures a fair performance comparison between systems operating on channels with different mean or covariance matrices and, therefore, allows an objective gain measure (otherwise, a stronger channel power-gain will likely result in a better precoding or capacity gain).

With normalization, the channel mean (2.19) and covariance (2.16) can be written as

$$\begin{aligned} \mathbf{H}_m &= \sqrt{\frac{K}{K+1}}\dot{\mathbf{H}}_m \\ \mathbf{R}_0 &= \frac{1}{K+1}\dot{\mathbf{R}}_0\,, \end{aligned} \tag{B.1}$$

where $\dot{\mathbf{H}}_m$ and $\dot{\mathbf{R}}_0$ are the normalized channel mean and covariance, such that

$$\begin{aligned} ||\dot{\mathbf{H}}_m||_F^2 &= MN \\ \mathrm{tr}(\dot{\mathbf{R}}_0) &= MN\,. \end{aligned}$$

For the Kronecker antenna correlation model (2.17), the normalized channel covariance can be written as

$$\dot{\mathbf{R}}_0 = \dot{\mathbf{R}}_{t,0}^T \otimes \dot{\mathbf{R}}_{r,0} \ ,$$

where

$$\begin{aligned} \mathrm{tr}(\dot{\mathbf{R}}_{t,0}) &= N \\ \mathrm{tr}(\dot{\mathbf{R}}_{r,0}) &= M \ . \end{aligned}$$

When transmit antenna correlation alone exists, it can be written as

$$\mathbf{R}_t = \frac{1}{K+1}\dot{\mathbf{R}}_{t,0} \ ,$$

while $\mathbf{R}_r = \mathbf{I}$. Consequently, normalized CSIT parameters are specified.

B.2 Parameters for capacity optimization

This section lists the CSIT parameters for capacity optimization in Sections 3.4.2 and 3.5. All simulated channels have 4 transmit and either 2 or 4 receive antennas. The normalized transmit covariance matrix is

$$\dot{\mathbf{R}}_{t,0} = \begin{bmatrix} 0.8758 & -0.0993 - 0.0877i & -0.6648 - 0.0087i & 0.5256 - 0.4355i \\ -0.0993 + 0.0877i & 0.9318 & 0.0926 + 0.3776i & -0.5061 - 0.3478i \\ -0.6648 + 0.0087i & 0.0926 - 0.3776i & 1.0544 & -0.6219 + 0.5966i \\ 0.5256 + 0.4355i & -0.5061 + 0.3478i & -0.6219 - 0.5966i & 1.1379 \end{bmatrix} .$$

This matrix has the eigenvalues as $[2.717,\ 0.997,\ 0.237,\ 0.049]$ and a condition number of 55.5, representing strong antenna correlation. The normalized mean for the 4×2 channel is

$$\dot{\mathbf{H}}_m = \sqrt{10} \begin{bmatrix} 0.0749 - 0.1438i & 0.0208 + 0.3040i & -0.3356 + 0.0489i & 0.2573 - 0.0792i \\ 0.0173 - 0.2796i & -0.2336 - 0.2586i & 0.3157 + 0.4079i & 0.1183 + 0.1158i \end{bmatrix} .$$

The normalized mean for the 4×4 channel is

$$\dot{\mathbf{H}}_m = \sqrt{10} \begin{bmatrix} 0.2976 + 0.1177i & 0.1423 + 0.4518i & -0.0190 + 0.1650i & -0.0029 + 0.0634i \\ -0.1688 - 0.0012i & -0.0609 - 0.1267i & 0.2156 - 0.5733i & 0.2214 + 0.2942i \\ 0.0018 - 0.0670i & 0.1164 + 0.0251i & 0.5599 + 0.2400i & 0.0136 - 0.0666i \\ -0.1898 + 0.3095i & 0.1620 - 0.1958i & 0.1272 + 0.0531i & -0.2684 - 0.0323i \end{bmatrix}.$$

The simulated channels have $K = 0.1$.

The parameters used in the convex optimization programs are

Maximum number of iterations	MAXITER	$= 10$
Maximum number of line searches each step	MAXLINES	$= 50$
Initial barrier multiplying factor	barr_t	$= 100$
Barrier method update factor	μ	$= 100$
Tolerance ($\Delta x_{\text{nt}}^T \nabla^2 f(x) \Delta x_{\text{nt}} \leq \epsilon$)	ϵ	$= 10^{-5}$
Number of channel samples in Monte-Carlo simulations	NSAMPLE	$= 20000$.

B.3 Parameters for precoding with dynamic CSIT

The channel parameters used in the precoding simulations in Section 4.3.3 are as follows.

For the 2×1 channel

$$\begin{aligned} \dot{\mathbf{H}}_m &= \sqrt{10} \begin{bmatrix} +0.3805 + 0.1069i & -0.1845 - 0.0985i \end{bmatrix}, \\ \dot{\mathbf{R}}_{t,0} &= \begin{bmatrix} 1.1843 & -0.7537 + 0.5638i \\ -0.7537 - 0.5638i & 0.8157 \end{bmatrix}. \end{aligned}$$

For the 4×1 channel

$$\begin{aligned} \dot{\mathbf{H}}_m &= \sqrt{10} \begin{bmatrix} 0.2727 - 0.1675i & -0.0577 + 0.1771i & 0.1421 + 0.2523i & 0.3283 - 0.2670i \end{bmatrix}, \\ \dot{\mathbf{R}}_{t,0} &= \begin{bmatrix} 0.8611 & 0.2582 - 0.6041i & 0.2458 - 0.1377i & 0.1637 + 0.0991i \\ 0.2582 + 0.6041i & 1.0311 & 0.5159 + 0.0262i & -0.0935 - 0.0804i \\ 0.2458 + 0.1377i & 0.5159 - 0.0262i & 0.7158 & -0.5048 - 0.2518i \\ 0.1637 - 0.0991i & -0.0935 + 0.0804i & -0.5048 + 0.2518i & 1.3921 \end{bmatrix}. \end{aligned}$$

The simulated channels have $K = 0.1$, except for Figure 4.6, in which K varies.

B.4 Parameters for precoding comparison

The 4×2 channel parameters used in the precoding comparison in Section 4.6 are as follows. The transmit covariance matrix is

$$\dot{\mathbf{R}}_{t,0} = \begin{bmatrix} 0.8758 & -0.0993 - 0.0877i & -0.6648 - 0.0087i & 0.5256 - 0.4355i \\ -0.0993 + 0.0877i & 0.9318 & 0.0926 + 0.3776i & -0.5061 - 0.3478i \\ -0.6648 + 0.0087i & 0.0926 - 0.3776i & 1.0544 & -0.6219 + 0.5966i \\ 0.5256 + 0.4355i & -0.5061 + 0.3478i & -0.6219 - 0.5966i & 1.1379 \end{bmatrix}.$$

The channel mean matrix used in dynamic CSIT is

$$\dot{\mathbf{H}}_m = \sqrt{10} \begin{bmatrix} 0.0749 - 0.1438i & 0.0208 + 0.3040i & -0.3356 + 0.0489i & 0.2573 - 0.0792i \\ 0.0173 - 0.2796i & -0.2336 - 0.2586i & 0.3157 + 0.4079i & 0.1183 + 0.1158i \end{bmatrix}.$$

Again, the simulated channels have $K = 0.1$, except for Figure 4.11, in which K varies.

Notation

Acronyms

BER	Bit error rate.
CSIR	Channel side information at the receiver.
CSIT	Channel side information at the transmitter.
EVD	Eigenvalue decomposition.
FDD	Frequency-division duplex.
IEEE	Institute of Electrical and Electronic Engineers.
MIMO	Multiple-input multiple-output.
MISO	Multiple-input single-output.
MMSE	Minimum mean squared-error.
MSE	Mean squared-error.
PEP	Pair-wise error probability.
QSTBC	Quasi-orthogonal STBC.
RF	Radio frequency.
SNR	Signal to noise ratio.
ST	Space-Time.
STBC	Space-time block code.
SVD	Singular value decomposition.
TDD	Time-division duplex.

Operations

$E[.]$	Expected value.
$\otimes$	Kronecker product.
$\Pr(.)$	Probability.
$\exp(.)$	Exponential.
$\mathcal{R}e$	The real part.
$\mathcal{I}m$	The imaginary part.
$\ll$	Significantly less than.
$(.)^\star$	Optimal value.
$(x)_+$	$\max(x, 0)$, where x is real.

Vectors and Matrices

$\mathbf{X}$	Matrix $\mathbf{X}$ (bold-face capital letter).
$\mathbf{x}$	Vector $\mathbf{x}$ (bold-face lower-case letter).
$\mathbf{X}^T$	Transpose of $\mathbf{X}$.
$\mathbf{X}^*$	Conjugate transpose of $\mathbf{X}$.
$\det(\mathbf{X})$	Determinant of $\mathbf{X}$.
$\mathrm{tr}(\mathbf{X})$	Trace of $\mathbf{X}$.
$\|\|\mathbf{X}\|\|_F$	Frobenius norm of $\mathbf{X}$.
$\lambda_i(\mathbf{X})$	Eigenvalues of a Hermitian matrix $\mathbf{X}$.
$\sigma_i(\mathbf{X})$	Singular values of $\mathbf{X}$.
$\mathbf{\Lambda}_X$	The diagonal matrix of the eigenvalues of $\mathbf{X}$.
$\mathbf{\Sigma}_X$	The diagonal matrix of the singular values of $\mathbf{X}$.
$\mathbf{U}_X, \mathbf{V}_X$	The eigen- or singular-vector matrix of $\mathbf{X}$.
$\mathbf{X} \succcurlyeq \mathbf{0}$	$\mathbf{X}$ is positive semi-definite.
$\mathrm{vec}(\mathbf{X})$	Vectorize $\mathbf{X}$ by concatenating the columns of $\mathbf{X}$.
$\mathbf{I}$	An identity matrix.
$\mathcal{N}(\mathbf{H}_m, \mathbf{R}_0)$	Gaussian distribution with mean $\mathbf{H}_m$ and covariance $\mathbf{R}_0$.

Symbols

$\mathcal{C}$	Channel ergodic capacity.
$\mathcal{I}$	Mutual information.
N	The number of transmit antennas.
M	The number of receive antennas.
K_t	The rank of the transmit covariance matrix.
h	A scalar wireless channel.
$\mathbf{H}$	A MIMO flat-fading channel.
$\mathbf{H}_0$	A channel measurement (sample) at time 0.
$\mathbf{H}_w$	A random channel with i.i.d zero-mean unit-variance circular complex Gaussian elements.
$\mathbf{H}_m$	The channel mean.
$\mathbf{R}_0, \mathbf{R}$	The channel covariance and auto-covariance.
$\mathbf{R}_t$	Transmit covariance, also called transmit antenna correlation.
$\mathbf{R}_r$	Receive covariance, also called receive antenna correlation.
$\hat{\mathbf{H}}$	A channel estimate.
$\mathbf{E}$	Estimation error.
$\mathbf{R}_e$	The error or effective covariance.
ρ	The channel temporal correlation function.
K	The Rician K factor
T_c	The channel coherence time.
B_c	The channel coherence bandwidth.
t	Continuous time.
Δ_t	Delay.
n, m	Discrete time or delay.
$\mathbf{F}$	The precoding matrix.
$\mathbf{D}$	The diagonal matrix of the singular-values of $\mathbf{F}$.
p_i	Power loading on beam i.
$\mathbf{C}$	A codeword.
$\mathbf{Q}$	The codeword covariance matrix or input covariance.
$\mathbf{A}$	The codeword difference product matrix.
γ	The signal to noise ratio.
ν	The Lagrange multiplier.
δ	The Dirac delta function.
ϕ, ψ	Phase or phase-shift.
P_e	System error probability.
$X, \mathbf{X}$	The transmit signal.
$Y, \mathbf{Y}$	The receive signal.

Bibliography

[1] S. Nanda, R. Walton, J. Ketchum, M. Wallace, and S. Howard, "A high-performance MIMO OFDM wireless LAN," *IEEE Communications Magazine*, vol. 43, no. 2, pp. 101–109, Feb. 2005.

[2] I. S. 802.11n, "Part 11: Wireless LAN medium access control (MAC) and physical layer (PHY) specifications - High throughput," *Working IEEE Standards*, 2006.

[3] I. S. 802.16e, "Part 16: Air interface for fixed and mobile broadband wireless access systems," *IEEE Standards*, Oct 2005.

[4] E. S. Brown, "The selling of cell phone TV," *Technology Review*, Nov. 2004. [Online]. Available: http://www.technologyreview.com/read_article.aspx?id=13901&ch=infotech

[5] L. Yang and G. Giannakis, "Ultra-wideband communications: An idea whose time has come," *IEEE Signal Processing Magazine*, vol. 21, no. 6, pp. 26–54, Nov. 2004.

[6] I. Telatar, "Capacity of multi-antenna Gaussian channels," *Bell Laboratories Technical Memorandum,* http://mars.bell-labs.com/papers/proof/, Oct. 1995. [Online]. Available: http://mars.bell-labs.com/papers/proof/

[7] A. Paulraj, R. Nabar, and D. Gore, *Introduction to Space-Time Wireless Communications*. Cambridge, UK: Cambridge University Press, 2003.

[8] I. S. 802.20, "Part 20: Mobile broadband wireless access (MBWA)," *Working IEEE Standards*, 2006.

[9] A. Hottinen, O. Tirkkonen, and R. Wichman, *Multi-antenna transceiver techniques for 3G and beyond*. Wiley & Sons, Inc., 2003.

[10] A. Paulraj and C. Papadias, "Space-time processing for wireless communications," *IEEE Signal Processing Magazine*, vol. 14, no. 6, pp. 49–83, Nov. 1997.

[11] G. Caire and S. S. Shamai, "On the capacity of some channels with channel state information," *IEEE Trans. on Info. Theory*, vol. 45, no. 6, pp. 2007–2019, Sep. 1999.

[12] C. Shannon, "Channels with side information at the transmitter," *IBM J. of Research and Devel.*, vol. 2, no. 4, pp. 289–293, Oct. 1958.

[13] M. Skoglund and G. Jöngren, "On the capacity of a multiple-antenna communication link with channel side information," *IEEE J. on Selected Areas in Comm.*, vol. 21, no. 3, pp. 395–405, Apr. 2003.

[14] W. Jakes, *Microwave Mobile Communications*. IEEE Press, 1994.

[15] T. Rappaport, *Wireless Communications: Principles and Practice*. Prentice Hall PTR, 1996.

[16] A. Goldsmith and P. Varaiya, "Capacity of fading channels with channel side information," *IEEE Trans. Info. Theory*, vol. 43, no. 6, pp. 1986–1992, Nov. 1997.

[17] V. Tarokh, H. Jafarkhani, and R. Calderbank, "Space-time block codes from orthogonal designs," *IEEE Trans. on Info. Theory*, vol. 45, no. 5, pp. 1456–1467, July 1999.

[18] M. Vu and A. Paulraj, "A robust transmit CSI framework with applications in MIMO wireless precoding," *Proc. 39th Asilomar Conf. Sig., Sys. and Comp.*, Nov. 2005.

[19] ——, *MIMO Wireless Communications*. Cambridge University Press, 2006, ch. Precoding design.

[20] ——, "Characterizing the capacity for MIMO wireless channels with non-zero mean and transmit covariance," *Proc. Forty-Third Allerton Conf. on Comm., Control, and Comp.*, Sep. 2005.

[21] ——, "Some asymptotic capacity results for MIMO wireless with and without channel knowledge at the transmitter," *Proc. 37th Asilomar Conf. Sig., Sys. and Comp.*, vol. 1, pp. 258–262, Nov. 2003.

[22] ——, "Capacity optimization for Rician correlated MIMO wireless channels," *Proc. 39th Asilomar Conf. Sig., Sys. and Comp.*, Nov. 2005.

[23] ——, "Optimal linear precoders for MIMO wireless correlated channels with nonzero mean in space–time coded systems," *IEEE Trans. on Signal Processing*, vol. 54, no. 6, pp. 2318–2332, June 2006.

[24] ——, "Optimum space-time transmission for a high K factor wireless channel with partial channel knowledge," *Wiley Journal on Wireless Comm. and Mobile Computing*, vol. 4, pp. 807–816, Nov. 2004.

[25] J. Proakis, *Digital Communications*. McGraw-Hill, 1989.

[26] H. Hasemi, "The indoor radio propagation channel," *Proceedings of the IEEE*, vol. 8, no. 7, pp. 943–968, July 1993.

[27] A. Papoulis, *Probability, Random Variables, and Stochastic Processes*. McGraw-Hill Inc., 1991.

[28] S. Rice, "Statistical properties of a sine wave plus random noise," *Bell Systems Technical Journal*, vol. 27, pp. 109–157, Jan 1948.

[29] D. Shiu, G. Foschini, M. Gans, and J. Kahn, "Fading correlation and its effect on the capacity of multielement antenna systems," *IEEE Trans. on Comm.*, vol. 48, no. 3, pp. 502–513, Mar. 2000.

[30] A. Graham, *Kronecker Products and Matrix Calculus with Application*. Ellis Horwood Ltd., 1981.

[31] K. Yu, M. Bengtsson, B. Ottersten, D. McNamara, P. Karlsson, and M. Beach, "Second order statistics of NLOS indoor MIMO channels based on 5.2 GHz measurements," *Proc. IEEE Global Telecomm. Conf.*, vol. 1, pp. 25–29, Nov. 2001.

[32] J. Kermoal, L. Schumacher, K. Pedersen, P. Mogensen, and F. Frederiksen, "A stochastic MIMO radio channel model with experimental validation," *IEEE J. on Selected Areas in Comm.*, vol. 20, no. 6, pp. 1211–1226, Aug. 2002.

[33] D. Bliss, A. Chan, and N. Chang, "MIMO wireless communication channel phenomenology," *IEEE Trans. on Antennas and Propagation*, vol. 52, no. 8, pp. 2073–2082, Aug. 2004.

[34] A. Sayeed, "Deconstructing multiantenna fading channels," *IEEE Trans. on Signal Proc.*, vol. 50, no. 10, pp. 2563–2579, Oct. 2002.

[35] W. Weichselberger, M. Herdin, H. Özcelik, and E. Bonek, "A stochastic MIMO channel model with joint correlation of both link ends," *IEEE Trans. on Wireless Comm.*, vol. 5, no. 1, pp. 90–100, Jan. 2006.

[36] D. Baum, D. Gore, R. Nabar, S. Panchanathan, K. Hari, V. Erceg, and A. Paulraj, "Measurement and characterization of broadband MIMO fixed wireless channels at 2.5ghz," *Proc. Int'l Conf. Per. Wireless Comm.*, pp. 203–206, Dec. 2000.

[37] A. Bourdoux, B. Come, and N. Khaled, "Non-reciprocal transceivers in OFDM/SDMA systems: Impact and mitigation," *Proc. Radio and Wireless Conf.*, pp. 183–186, Aug. 2003.

[38] B. Hochwald, T. Marzetta, T. Richardson, W. Sweldens, and R. Urbanke, "Systematic design of unitary space-time constellations," *IEEE Trans. Info. Theory*, pp. 1962–1973, Sep. 2000.

[39] D. Love and R. Heath, Jr., "Limited feedback unitary precoding for spatial multiplexing," *IEEE Trans. Info. Theory*, vol. 51, no. 8, pp. 2967–2976, Aug. 2005.

[40] ——, "Limited feedback unitary precoding for orthogonal space-time block codes," *IEEE Trans. Signal Processing*, vol. 53, no. 1, pp. 64–73, Jan. 2005.

[41] A. Narula, M. Lopez, M. Trott, and G. Wornell, "Efficient use of side information in multiple-antenna data transmission over fading channels," *IEEE J. Sel. Areas Comm.*, vol. 16, no. 8, pp. 1423–1436, Oct. 1998.

[42] G. Jöngren, M. Skoglund, and B. Ottersten, "Combining beamforming and orthogonal space-time block coding," *IEEE Trans. on Info. Theory*, vol. 48, no. 3, pp. 611–627, Mar. 2002.

[43] T. Kailath, A. Sayed, and B. Hassibi, *Linear Estimation*. Prentice Hall, 2000.

[44] D. Goeckel, "Adaptive coding for time-varying channels using outdated fading estimates," *IEEE Trans. on Comm.*, vol. 47, no. 6, pp. 844–855, June 1999.

[45] J. P.Z.Peebles, *Probability, Random Variables, and Random Signal Principles*. McGraw-Hill, 1993.

[46] T. Cover and J. Thomas, *Elements of Information Theory*. John Wiley & Sons, Inc., 1991.

[47] G. Letac and H. Massam, "All invariant moments of the Wishart distribution," *Scandinavian Journal of Statistics*, vol. 31, no. 2, pp. 295–318, June 2004.

[48] E. Visotsky and U. Madhow, "Space-time transmit precoding with imperfect feedback," *IEEE Trans. on Info. Theory*, vol. 47, no. 6, pp. 2632–2639, Sep. 2001.

[49] S. Jafar and A. Goldsmith, "Transmitter optimization and optimality of beamforming for multiple antenna systems," *IEEE Trans. on Wireless Comm.*, vol. 3, no. 4, pp. 1165–1175, July 2004.

[50] S. Venkatesan, S. Simon, and R. Valenzuela, "Capacity of a Gaussian MIMO channel with nonzero mean," *Proc. IEEE Vehicular Tech. Conf.*, vol. 3, pp. 1767–1771, Oct. 2003.

[51] D. Hösli, Y.-H. Kim, and A. Lapidoth, "Monotonicity results for coherent MIMO Rician channels," *IEEE Trans. on Info. Theory*, vol. 51, no. 12, pp. 4334–4339, Dec. 2005.

[52] E. Jorswieck and H. Boche, "Optimal transmission strategies and impact of correlation in multiantenna systems with different types of channel state information," *IEEE Trans. on Signal Processing*, vol. 52, no. 13, pp. 3440–3453, Dec. 2004.

[53] A. Tulino, A. Lozano, and S. Verdu, "Impact of antenna correlation on the capacity of multiantenna channels," *IEEE Trans. on Info. Theory*, vol. 51, no. 7, pp. 2491–2509, July 2005.

[54] S. Boyd and L. Vandenberghe, *Convex Optimization*. Cambridge, UK: Cambridge University Press, 2003. [Online]. Available: http://www.stanford.edu/~boyd/cvxbook.html

[55] E. Jorswieck and H. Boche, "Channel capacity and capacity-range of beamforming in MIMO wireless systems under correlated fading with covariance feedback," *IEEE Trans. on Wireless Comm.*, vol. 3, no. 5, pp. 1543–1553, Sep. 2004.

[56] S. Verdú, "Spectral efficiency in the wideband regime," *IEEE Trans. on Info. Theory*, vol. 48, no. 6, pp. 1319–1343, June 2002.

[57] J. Silverstein, "The smallest eigenvalue of a large dimensional Wishart matrix," *Annals of Probability*, vol. 13, no. 4, pp. 1364–1368, Nov. 1985.

[58] S. Geman, "A limit theorem for the norm of random matrices," *Annals of Probability*, vol. 8, no. 2, pp. 252–261, Apr. 1980.

[59] D. Maiwald and D. Kraus, "Calculation of moments of complex Wishart and complex inverse Wishart distributed matrices," *IEE Proceedings Radar, Sonar and Navigation*, no. 4, pp. 162–168, Aug. 2000.

[60] H. Van Trees, *Optimum Array Processing, Part IV of Detection, Estimation and Modulation Theory*. Wiley & Sons, Inc., 2002.

[61] A. Tulino, A. Lozano, and S. Verdu, "Capacity-achieving input covariance for single-user multi-antenna channels," *IEEE Trans. on Wireless Comm.*, vol. 5, no. 3, pp. 662–671, Mar. 2006.

[62] H. Sampath, P. Stoica, and A. Paulraj, "Generalized linear precoder and decoder design for MIMO channels using the weighted MMSE criterion," *IEEE Transactions on Communications*, vol. 49, no. 12, pp. 2198–2206, Dec 2001.

[63] A. Scaglione, P. Stoica, S. Barbarossa, G. Giannakis, and H. Sampath, "Optimal designs for space-time linear precoders and decoders," *IEEE Trans. on Signal Processing*, vol. 50, no. 5, pp. 1051–1064, May 2002.

[64] D. Palomar, J. Cioffi, and M. Lagunas, "Joint Tx-Rx beamforming design for multicarrier MIMO channels: A unified framework for convex optimization," *IEEE Trans. on Signal Processing*, vol. 51, no. 9, pp. 2381– 2401, Sept. 2003.

[65] D. Hösli and A. Lapidoth, "The capacity of a MIMO Ricean channel is monotonic in the singular values of the mean," *Proc. 5th Int'l ITG Conf. on Source and Channel Coding*, Jan. 2004.

[66] L. Liu and H. Jafarkhani, "Application of quasi-orthogonal space-time block codes in beamforming," *IEEE Trans. on Signal Processing*, vol. 53, no. 1, pp. 54–63, Jan. 2005.

[67] S. Zhou and G. Giannakis, "Optimal transmitter eigen-beamforming and space-time block coding based on channel mean feedback," *IEEE Trans. on Signal Processing*, vol. 50, no. 10, pp. 2599–2613, Oct. 2002.

[68] H. Sampath and A. Paulraj, "Linear precoding for space-time coded systems with known fading correlations," *IEEE Comm. Lett.*, vol. 6, no. 6, pp. 239–241, June 2002.

[69] S. Zhou and G. Giannakis, "Optimal transmitter eigen-beamforming and space-time block coding based on channel correlations," *IEEE Trans. on Info. Theory*, vol. 49, no. 7, pp. 1673–1690, July. 2003.

[70] V. Tarokh, N. Seshadri, and R. Calderbank, "Space-time codes for high data rate wireless communication: Performance criterion and code construction," *IEEE Trans. on Info. Theory*, vol. 44, no. 2, pp. 744–765, Mar. 1998.

[71] L. Zheng and D. Tse, "Diversity and multiplexing: A fundamental tradeoff in multiple-antenna channels," *IEEE Trans. on Info. Theory*, vol. 49, no. 5, pp. 1073–1096, May 2003.

[72] R. Horn and C. Johnson, *Matrix Analysis*. Cambridge University Press, 1985.

[73] A. Marshall and I. Olkin, *Inequalities: Theory of Majorization and Its Applications*. Academic Press, 1979.

[74] S. Alamouti, "A simple transmit diversity technique for wireless communications," *IEEE J. Sel. Areas Comm.*, vol. 16, pp. 1451–1458, Oct. 1998.

[75] H. Jafarkhani, "A quasi-orthogonal space time block code," *IEEE Trans. on Comm.*, vol. 49, no. 1, pp. 1–4, Jan. 2001.

[76] O. Tirkkonen, A. Boariu, and A. Hottinen, "Minimal non-orthogonality rate 1 space-time block code for 3+ Tx antennas," *Proc. IEEE ISSSTA2000*, vol. 2, pp. 429–432, Sep. 2000.

[77] H. Gamal, G. Caire, and M. Damen, "Lattice coding and decoding achieve the optimal diversity-multiplexing tradeoff of MIMO channels," *IEEE Trans. on Info. Theory*, vol. 50, no. 6, pp. 968–985, June 2004.

[78] A. Khoshnevis and A. Sabharwa, "On diversity and multiplexing gain of multiple antenna systems with transmitter channel information," *Proc. Allerton Conf. on Comm., Control, and Comp.*, Oct. 2004.

[79] Y. Ding, T. Davidson, Z. Luo, and K. Wong, "Minimum ber block precoders for zero-forcing equalization," *IEEE Trans. on Signal Processing*, vol. 51, no. 9, pp. 2410–2423, Sept. 2003.

[80] T. Kim, G. Jöngren, and M. Skoglund, "Weighted space-time bit-interleaved coded modulation," *Proc IEEE Info. Theory Workshop*, pp. 375–380, Oct. 2004.

[81] I. S. 802.11a, "Part 11: Wireless LAN medium access control (MAC) and physical layer (PHY) specifications high-speed physical layer in the 5 GHz band," *IEEE Standards*, June 1999.

[82] R. Fischer, C. Stierstorfer, and J. Huber, "Precoding for point-to-multipoint transmission over MIMO ISI channels," *Proc. Int. Zurich Sem. Commun.*, pp. 208–211, Feb. 2004.

[83] H. Weingarten, Y. Steinberg, and S. Shamai, "The capacity region of the Gaussian MIMO broadcast channel," *Proc. Conf. on Information Sciences and Systems (CISS)*, Mar. 2004.

[84] M. Costa, "Writing on dirty paper," *IEEE Trans. on Information Theory*, vol. 29, no. 3, pp. 439–441, May 1983.

[85] S. Jafar and A. Goldsmith, "Isotropic fading vector broadcast channels: The scalar upperbound and loss in degrees of freedom," *IEEE Trans. on Information Theory*, vol. 51, no. 3, pp. 848–857, Mar. 2005.

[86] A. Lapidoth, S. Shamai, and M. Wigger, "On the capacity of fading MIMO broadcast channels with imperfect transmitter side-information," *Proc. 43rd Ann. Allerton Conf. on Communication, Control, and Computing*, Sept. 2005.

[87] P. Viswanath, D. Tse, and R. Laroia, "Opportunistic beamforming using dumb antennas," *IEEE Trans. on Information Theory*, vol. 48, no. 6, pp. 1277–1294, June 2002.

[88] M. Sharif and B. Hassibi, "On the capacity of MIMO broadcast channels with partial side information," *IEEE Trans. on Information Theory*, vol. 51, no. 2, pp. 506–522, Feb. 2005.

[89] A. Eryilmaz and R. Srikant, "Scheduling with QoS constraints over rayleigh fading channels," *Proc. 43rd IEEE Conf. on Decision and Control*, vol. 4, pp. 3447–3452, Dec. 2004.